


NOTE

This report is the result of a joint study carried out by Mr. D. M. DeVito of The Magnavox Company/Advanced Systems Analysis Office and Dr. M. M. Goutmann and Mr. R. C. Harper of General Atronics Corporation, a subsidiary of The Magnavox Company.

ACKNOWLEDGMENT

Magnavox wishes to acknowledge the help and cooperation received during the course of this contract. In particular, we wish to thank Mr. John Bryan of NASA/GSFC, Greenbelt, Maryland, for his technical and administrative guidance during the program. We also recognize the significant contributions by Mr. Clark Watterson of ESSA/Office of Telecommunication Sciences, Boulder, Colorado, and Dr. J. Neil Birch and Mr. Robert H. French both of Magnavox/Advanced Systems Analysis Office



D. M. DeVito
Program Manager

PREFACE

The objective of this program is to develop an optimum design for a propagation path simulator for the channel between the Tracking and Data Relay Satellite (TDRS) in geostationary orbit and a User spacecraft orbiting the earth at an altitude between 200 and 4000 kilometers. The simulator is required to duplicate the time varying parameters of the propagation channel.

The scope of the study encompasses:

- a) evaluation of the quantitative effects of various channel parameters on the TDRS/User link;
- b) establishment of performance requirements for the simulator including the limits of variation for each of the channel parameters, the required resolution in parameter adjustment, and the interrelationship between parameters;
- c) a comparative analysis of simulation techniques leading to the design of a realizable channel simulator.

The channel parameters which have been investigated can be grouped into six categories, namely:

- 1) Attenuation Effects
- 2) Atmospheric Refraction
- 3) Signal Phase Delay
- 4) Polarization Rotation
- 5) Frequency Effects
- 6) Noise and Radio Frequency Interference

A comparison of the relative magnitude of the propagation channel characteristics for the TDRS/User link is shown in Table 1.

Table 1 Comparison of the Relative Magnitude of the Propagation Channel Parameters for the TDRS/User Link

Description	VHF	S-band
<u>Attenuation Effects:</u>		
Free Space Attenuation	165-169 dB	189-192 dB
Direct Path Loss	167-170 dB	191-193 dB
Indirect Path Loss		
Ionospheric Absorption	<.1 dB	<.001 dB
Tropospheric Absorption	<.05 dB	<.3 dB
Losses due to Aurora	<.1 dB	<.1 dB
<u>Refraction:</u>		
Ionospheric Refraction	<10 ⁻³ radians	<10 ⁻⁵ radians
Tropospheric Refraction	negligible	negligible
<u>Signal Phase Delay:</u>		
Ionospheric Effects	≈10 ⁻⁸ sec	≈10 ⁻⁸ sec
Tropospheric Effects	≈10 ⁻⁶ sec	≈10 ⁻⁸ sec
Birefringence	<10 ⁻⁹ sec	<10 ⁻⁹ sec
Multipath Time Delay	.2-30 msec	.2-30 msec
<u>Polarization Rotation:</u>		
Chromatic Aberration	< 2°/MHz	< 2°/MHz
Faraday Rotation*	≈ 200 degrees	≈ 1 degree
<u>Frequency Effects:</u>		
Direct Path Doppler	0-4 KHz	0-68 KHz
Differential Doppler	0-2 KHz	0-34 KHz
Fading Bandwidth	0-2 KHz	0-34 KHz
Coherent Bandwidth	5-30 KHz	5-30 KHz
<u>Carrier-to-Noise Power Density:</u>		
At TDRS	44.6 dB-Hz	33.8 dB-Hz
At User	54.6 dB-Hz	44.9 dB-Hz
Radio Frequency Interference	problem	minimal

* For systems employing circularly polarized antennas such as the TDRS, Faraday rotation effects are not encountered.

It can be shown that the channel parameters having the most profound effect on the performance of the link are:

- 1) Free Space Attenuation
- 2) Multipath Time Delay
- 3) Direct Path Doppler
- 4) Differential Doppler
- 5) Fading Bandwidth
- 6) System Noise Power Density
- 7) Radio Frequency Interference

The primary factors considered in arriving at the selected simulator design approach are twofold. First, the ease and flexibility with which the simulator parameters could be changed by an external control unit. Second, the cost of implementation traded off against the accuracy to which parameters could be adjusted. The range of variation of the simulator parameters is shown in Table 2. In addition to those parameters in the table are the introduction of noise and RFI which are controlled externally.

Table 2
Summary of Simulator Parameters

PARAMETER	VHF (136-139 MHz)	S-BAND (2.3 GHz)
Differential time delay between Direct and Reflected Signals	0-30 ms	0-30 ms
Signalling Bandwidth	2 MHz	4 MHz
Maximum Differential Time Delay of Reflected Signal	256 μ sec	256 μ sec
Fading Bandwidth of Reflected Signal	\sim 0-2 kHz	\sim 0-34 kHz
Direct Path Doppler	\sim 0-4 kHz	\sim 0-68 kHz
Reflected Path Doppler	\sim 0-4 kHz	\sim 0-68 kHz

The simulator is a hybrid system in that it is comprised of a mixture of both analog and digital circuitry. Control of the simulator is digital and is provided through one of two modes of operation. The first is the AUTO MODE in which the control of the simulation is maintained by an on-line computer or computer-generated magnetic tapes. This "dynamic" controlled operation provides for:

- Complete orbit dynamics
- Preemptive resume control
- Preemptive repeat control
- On-line user interaction
- Programmable tests
- Real and virtual time

The second mode of operation, the MANUAL MODE, is referred to as the "static" operation and provides for:

- Independent operation
- Manual setting of controls
- Frozen orbit statistics
- Independent calibration

In general, the simulator operates with any class of input signal regardless of the modulation format, providing the signal bandwidth is confined to 2 MHz. The simulator subsystem components require, at most, present state-of-the-art hardware, and thus are essentially "off-the-shelf" items.

The estimated cost of hardware for the channel simulator is approximately \$50,000. It is estimated that to completely fabricate the system requires approximately a five man-year effort, distributed over a twelve or eighteen month period.

TABLE OF CONTENTS

<u>Section</u>	<u>Title</u>	<u>Page</u>
I	INTRODUCTION.	I-1
	A. TDRS SYSTEM DESCRIPTION AND OPERATION	I-2
	B. STUDY OBJECTIVES.	I-5
II	THE TDRS/USER PROPAGATION CHANNEL	II-1
	A. THE MULTIPATH SIGNAL.	II-1
	B. CHANNEL PARAMETERS.	II-11
	1. Doppler Effects	II-11
	2. Signal Multipath Delay.	II-17
	3. Coherent Bandwidth.	II-19
	C. THE EFFECTS OF THE ATMOSPHERE ON THE CHANNEL	II-21
	1. Attenuation Effects	II-23
	2. Atmospheric Refraction Effects.	II-26
	3. Polarization Rotation	II-34
	4. Aurora.	II-39
	D. RADIO FREQUENCY INTERFERENCE AND NOISE	II-39
	1. The Effects of RFI.	II-40
	2. The Effects of Noise.	II-44
	E. CONCLUSIONS	II-45
III	PRELIMINARY DESIGN OF THE TDRS CHANNEL SIMULATOR	III-1
	A. FUNCTIONAL FORM OF THE CHANNEL SIMULATOR	III-2
	B. OPERATION AND CONTROL OF THE SIMULATOR	III-5

<u>Section</u>	<u>Title</u>	<u>Page</u>
III	C. FUNCTIONAL DESIGN OF THE SIMULATOR	III-12
	1. Discussion of Overall System	III-12
	a. Baseband Frequency Selection	III-12
	b. Low Pass Filtering and AGC	III-14
	c. A/D Converter	III-15
	d. Generation of Direct Path Signal; Variable Gain and Doppler Spectrum Shift Units	III-16
	e. Digital Delay Lines for Generation of Multipath Components	III-17
	f. D/A Converter and Filtering of Aliasing Frequencies	III-17
	g. Fading Bandwidth Modulation	III-18
	h. Miscellaneous Considerations	III-18
	2. 0-30 Millisecond Variable Delay Line	III-18
	3. Implementation of Doppler Spectrum Shift Unit	III-22
	4. Generation of the Time-Dispersed Components of the Reflected Signal	III-35
	5. Technique for Introducing Fading Band- width onto the Time Dispersive Components	III-42
	6. Summary of Recommended (Major) System Components	III-60
	D.. PRELIMINARY ANALYSIS OF THE TDRS CHANNEL SIMULATOR	III-60
IV	CONCLUSIONS AND RECOMMENDATIONS	IV-1

LIST OF ILLUSTRATIONS

<u>Figure No.</u>	<u>Title</u>	<u>Page</u>
1.1	Tracking and Data Relay Satellite System	I-3
1.2	Geometric Configuration of TDRS/User Link	I-6
1.3	General Tapped Delay Line Channel Model.	I-10
2.1	User/TDRS Communications Link.	II-2
2.2	The Divergence Factor as a Function of Grazing Angle and Spacecraft Altitude.	II-4
2.3	Relative Specular and Diffuse Reflected Power vs Grazing Angle	II-5
2.4	Multipath/Direct Signal Ratio as a Function of Orbital Altitude	II-8
2.5	TDRS Multipath Geometry.	II-9
2.6	Direct Path Range Between the User Spacecraft and the TDRS.	II-10
2.7	Differential Path Length (Δ) Between the User Spacecraft and the TDRS	II-12
2.8	Doppler Frequency Along the Direct Path for 136 MHz Carrier	II-14
2.9	Direct and Indirect Channel Response in Frequency Domain.	II-15
2.10	Differential Doppler as a Function of User Spacecraft Position	II-16
2.11	Differential Time Delay as a Function of Spacecraft Position	II-18
2.12	Coherent Bandwidth (a) Frequency Definition (b) Time Definition	II-20
2.13	The Atmosphere and its Approximate Region	II-24

<u>Figure No.</u>	<u>Title</u>	<u>Page</u>
2.14	One-Way Tropospheric Attenuation	II-27
2.15	Tropospheric Refractivity as a Function of Altitude.	II-30
2.16	Index of Refraction of the Ionosphere.	II-32
2.17	An Electron Density Model in the Ionosphere	II-33
2.18	Typical One-Way Time Delays and Range Errors	II-35
2.19	Faraday Rotation Effects	II-37
2.20	Time Delay Between Phase Fronts of Ordinary and Extraordinary Rays.	II-37
2.21	RFI Regions.	II-41
3.1	Functional Block Diagram of the TDRS Channel Simulator	III-4
3.2	Simulator Control Panel.	III-6
3.3	Functional Block Diagram of TDRS Channel Simulator.	III-13
3.4	MOS Delay Line	III-23
3.5	Doppler Shift Unit	III-25
3.6	Major Spectra Produced by Mixer Operation.	III-27
3.7	Linear Phase Locked Loop Model	III-29
3.8	Alternative Method of Generating Doppler Spectrum Shift	III-33
3.9	RAM Configuration for Short (512 μ sec) Delay Line with 1/8 μ sec Access Intervals.	III-39
3.10	RAM Configuration for Short Delay Line (Accessing Scheme to generate 7 taps).	III-40
3.11	Fading Bandwidth Simulation Method I - SSB Technique	III-43

<u>Figure No.</u>	<u>Title</u>	<u>Page</u>
3.12	Symmetrical FET Characteristic	III-47
3.13	Symmetrical Single-Balanced FET Modulator.	III-47
3.14	Fading Bandwidth Simulation Method II - Gain Modulation.	III-52
3.15	Variable Q Multiplier Circuit.	III-54
3.16	Variable Cut-off Lowpass Filter.	III-59

LIST OF TABLES

<u>Table No.</u>	<u>Title</u>	<u>Page</u>
2.1	Ionospheric Absorption at 400-500 MHz.	II-25
2.2	Frequency Bands Covered by Interference Data for Region II	II-40
2.3	Effective Radiated Power Per Emitter in Watts	II-43
2.4	Expected Carrier-to-Noise Power Density Levels	II-44
2.5	Comparison of the Relative Magnitude of the Propagation Channel Parameters for the TDRS/User Link	II-46
3.1	Summary of Simulator Parameters.	III-2
3.2	Maximum Doppler Rate as a Function of User Altitude.	III-31
3.3	Catalog of Principal Components for TDRS Channel Simulator.	III-61
3.4	Cost Breakdown for Major Simulator Hardware	III-64
3.5	Cost Breakdown for 0-512 msec Delay Line	III-66
3.6	Cost Breakdown for Fading Bandwidth Modulator.	III-67
3.7	Cost Breakdown for Doppler Shift Unit	III-68
3.8	Cost Breakdown for Timing and Bookkeeping Hardware	III-69

I. INTRODUCTION

In the evaluation of any new communication system, experimental measurement of the system's performance characteristics over actual propagation paths is required, more often than not, to verify the analytical data governing the channel's performance. Test and evaluation of this type are oftentimes made simultaneously with several competing systems so that a comparative analysis of their relative performance may be obtained. For space communications systems, however, comparative tests of this type can be highly expensive. Over the past several years an alternative has emerged in the development of laboratory-type channel simulators for the evaluation of new communication techniques.

The use of a propagation path simulator offers many important advantages in the evaluation and design of information transmission systems. The outstanding advantage is the economic one. An effective simulator can save months of field testing and the relatively large expense of maintaining and staffing field sites. A simulator, by providing reproducible propagation distortions, can allow a valid comparative test of two or more modulation/-demodulation equipments at different times and places. It allows the comparison to be performed locally, (i.e., transmitter and receiver can be in the same physical location) allowing a far greater flexibility of operation with fewer personnel. The formidable "order wire" communication problem between remote sites can be eliminated; furthermore, testing of systems is not time-limited by the vagaries of the propagation path. Propagation conditions covering the full range of quality of transmission may be carried out without waiting for the natural occurrence of a desired condition. Various propagation conditions may

1-1

be simulated completely under the operator's control. Testing may be carried on without regard to other users of the radio channel.

In some respects the use of a simulator can provide more information about a communication system than actual "on-the-air" propagation tests. The various parameters of the propagation can be simulated independently of one another. The sensitivity of various systems can be evaluated with respect to each of the transmission parameters. As an example, it may be found that some systems are more vulnerable to the actual time dispersion of the medium than to the time-varying characteristics, a distinction which can be easily made with an effective simulator.

The overall objective of this study is to develop a design for the most practical simulator configuration for simulation of the propagation path between the Tracking and Data Relay Satellite (TDRS) and a user spacecraft.

A. TDRS SYSTEM DESCRIPTION AND OPERATION

The Tracking and Data Relay Satellite (TDRS) System is comprised of a number of mission control centers, ground stations, tracking and data relay satellites (TDRS), and users, as shown in Figure 1.1. The users consist of two basic types: unmanned scientific satellites and manned spacecraft.

During system operation, a minimum of two (2) manned spacecraft and forty (40) unmanned scientific satellites are required to have the capability of continuous two-way data and voice communication with a mission control center via specific ground stations. The specific ground stations will have the function of initially establishing the communication link to the user spacecraft through one (1) of either two (2) or three (3) TDRS. In addition

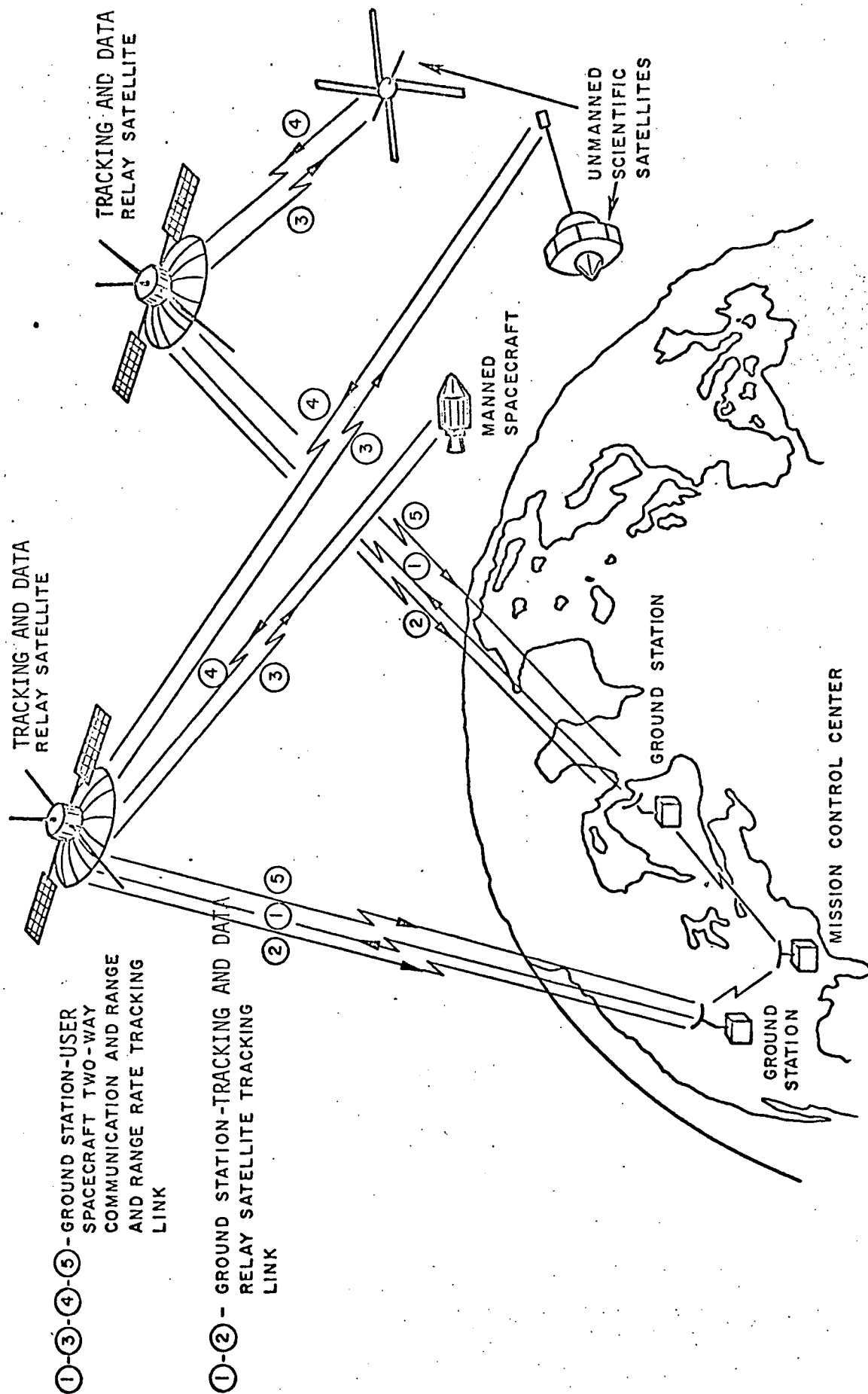


Fig. 1.1 TRACKING AND DATA RELAY SATELLITE SYSTEM

to the communications function, information regarding the range and range rate between TDRS and user spacecraft must be collected by the ground station and transmitted to a mission control center for the purpose of accurately predicting the orbits of the user spacecraft.

The figure illustrates the essentials of range and range rate tracking in the Tracking and Data Relay Satellite System configuration. It is assumed that a composite RF signal, denoted by (1), is transmitted continuously from a ground station. The signal structure contains voice and digital command information (for the TDRS and user spacecraft). At the TDRS the received signal is processed by a transponder and retransmitted. The signal (2) received by the ground station, which contains TDRS telemetry data, is processed by receiving equipment and range and range rate extraction and measurement instrumentation to yield periodic samples of raw range and range rate. The range and range rate information obtained are estimates of range and range rate between the ground station and the TDRS. The signal (3) received by a user spacecraft, containing command and voice information (in the case of a manned spacecraft), is processed and retransmitted back to the TDRS as signal (4) which contains user spacecraft telemetry and voice (in case of a manned user). The received signal at the TDRS is combined with the signals received from the other user spacecraft and a composite signal (5) is transmitted by the TDRS back to the ground station. The received signal (5) is processed by the receiving equipment and range and range rate extraction and measurement instrumentation to yield periodic samples of raw range and range rate data. These data are estimates of range and range rate between ground station and TDRS plus that between TDRS and user spacecraft. Depending on the frequency with which range and range rate data is deemed necessary, the extraction and measurement

instrumentation may be designed to accommodate all user spacecraft simultaneously (separate instrumentation for each user), each user spacecraft sequentially on a time-shared basis (one set of instrumentation for all users), or some hybrid arrangement (e.g., two (2) or three (3) users at one time). The raw range and range rate data is then transmitted via a ground communication link to a mission control center where it is processed (using least-squares smoothing techniques) to give smoothed estimates of range and range rate between TDRS and user spacecraft. The resulting smooth data is then used as an input to a digital computer which generates user spacecraft orbits.

The TDRS is located in a geostationary orbit and the user spacecraft orbiting earth at an altitude between 200 and 4000 kilometers. The geometric configuration of the TDRS/user link is shown in Figure 1.2. It consists essentially of two paths, one the direct path between the TDRS and user and the other, the indirect path which results from secondary reflection of the transmitted signal off the earth's surface. The communications link between the user spacecraft and TDRS may be described in terms of a multiplicity of parameters affecting both the direct and indirect (multipath) signals.

B. STUDY OBJECTIVES

The goal in this design effort is to take a completely objective approach in considering simulation techniques. The channel simulator is required to simulate the time varying parameters of the propagation channel between the TDRS and the user spacecraft. The channel parameters which have been investigated in this report are:

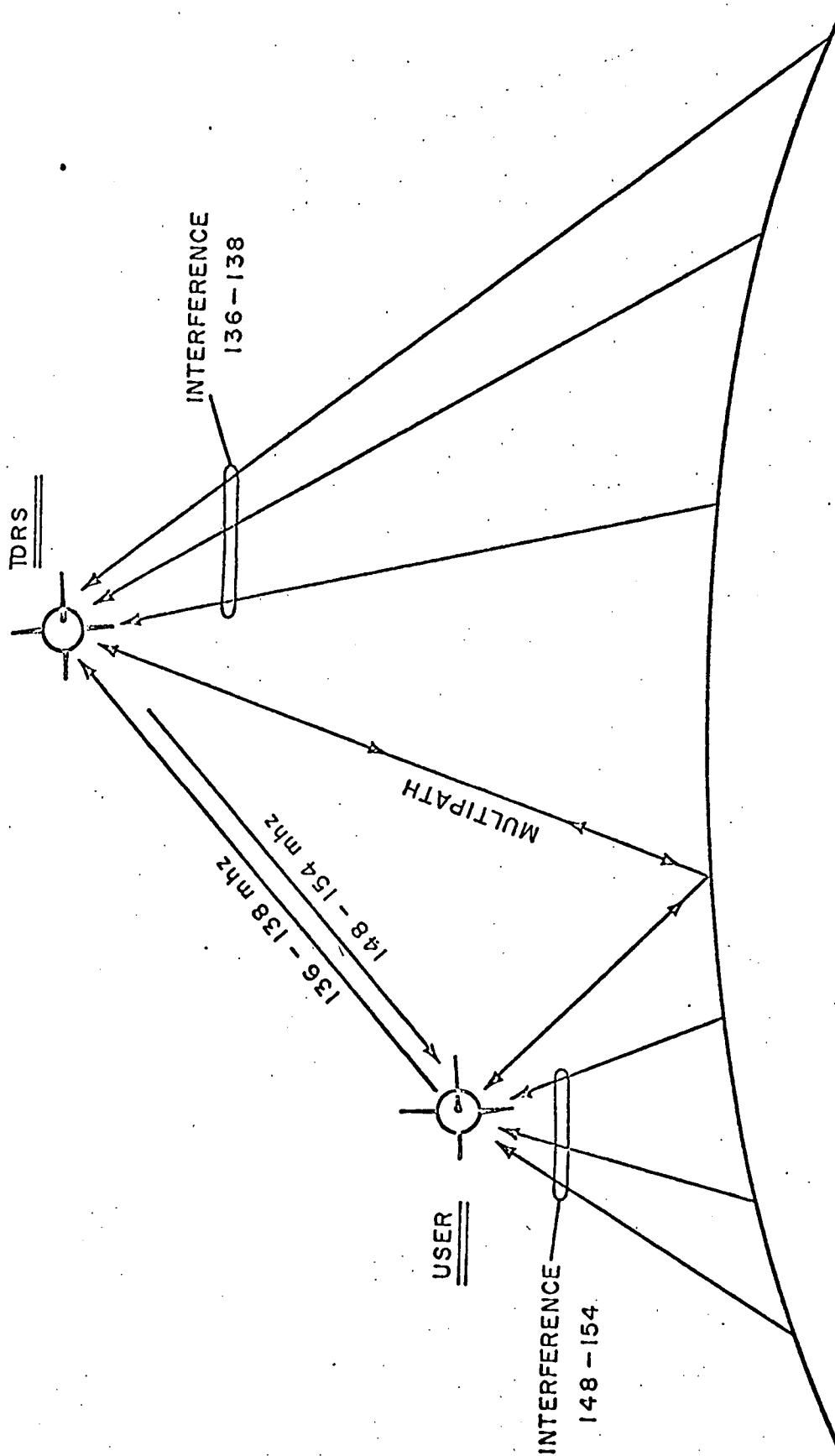


Figure 1.2 Geometric Configuration of TDRS/User Link

(1) Attenuation - including the spreading loss along each of the two paths.

(2) Signal delay - accounting for the time required for the signal to traverse each of the paths between the satellites.

(3) Differential delay - representing the difference in time of arrival of signals along the direct path and the reflected paths.

(4) Doppler - including the frequency offset of each component of the transmitted frequency spectrum caused by the relative motion between the two spacecraft.

(5) Doppler spread - accounting for the scattering of a CW signal as it strikes the nonspecular reflecting earth.

(6) Ionospheric effects - As a VHF radio signal traverses the ionosphere the wave is distorted. Included in the ionospheric effects are Faraday rotation which is in reality a polarization shift, refraction of the ionosphere, and phase delay in the ionosphere.

(7) Atmospheric effects - including effects of the earth's atmosphere such as refraction, medium discontinuities, weather, etc.

(8) Signal phase - the phase shift in each transmission path is a function of the path length, the transmission medium, and the path medium discontinuities.

(9) Amplitude effect - There are transmission factors which will also contribute to attenuation on each of the paths. Such items as earth absorption in the reflection area, antenna patterns, ionosphere, atmosphere, and so forth must be given consideration.

(10) Interference and noise - There are earth-based sources of interference which can be readily identified. These sources will act on both the TDRS and the user receivers. Thermal noise will consist not only of the receiver noise (KTB) but also the earth and other warm bodies in the antenna beam.

(11) Signal structure - The type of signal to be transmitted will vary. Two frequency bands must be considered. The first is a VHF channel (narrow band data) between 136 and 150 MHz; the second is an S-band channel between 2.2 and 2.3 GHz. The channel bandwidths are 2 MHz at VHF and 4 MHz at S-band.

An effective channel simulator has the potential of providing many advantages, namely:

- ° It provides a sufficiently accurate simulation of actual propagation conditions to allow valid absolute performance measurements to be made for a given system as well as relative performance evaluations of two or more equipments.
- ° The simulator provides controlled and calibrated distortions of the test signal in order to allow repeatable and meaningful data to be taken. It has sufficiently low residual distortion so as to have negligible effect on the transmitted signal. The levels of residual distortions such as additive noise, frequency perturbations, and spurious multipath response are sufficiently low as to allow predictable simulation over a wide range of propagation parameters.
- ° The simulator provides the ability to independently measure the effect of the various propagation distortions. This is accomplished by providing independent controls over the various additive and multiplicative distortion provisions of the simulator.
- ° The simulator provides a true analog channel in the sense that it will handle any signal format which occupies the proper spectrum independent of the modulation form. It is a linear system, permitting its use with modulation techniques which require amplitude linearity in the transmission circuit, exclusive of the satellite repeater.

- The simulator is a reliable and dependable device, comparable to standard laboratory test equipment.
- The simulator is expandable to meet future needs in terms of additional functions which may be provided for a more accurate representation of actual propagation in the light of future knowledge. This expansion is possible at moderate cost without obsoleting existing equipment.

In general a model for dispersive time-varying media is the tapped delay line model shown in Figure 1.3 . This model has been used by Kailath^{*} and others and is the model upon which the design of the channel simulator for the TDRS/user link will be based. Kailath has shown that this model is the most general model for a time varying dispersive channel, therefore there is good basis for the design study to be based on this general approach. The time dispersion of the medium is provided by the delay line tapped at discrete points. The maximum time interval allowable between taps is determined by the input signal bandwidth. Where the input signal is confined to a bandwidth of W , the maximum time interval between taps is $1/W$ (when the delay line is a bandpass element). This tap spacing in effect provides a sufficiently high sampling rate of the input signal to allow the synthesis of any arbitrary time dispersion characteristic within the resolution limitations set by the input filter. Each delay tap of the model feeds a signal to a time-varying gain function. These time-varying gains are complex-valued; i.e., they affect both the amplitude and phase of the signals coming from the delay line. The outputs of the time varying gain functions are summed to form the representation of the signal as it would be received.

^{*} T. Kailath, "Channel Characterization of Time Variant Dispersive Channels," Lectures on Communication System Theory, E. J. Baghdady, ed., McGraw-Hill Book Co., New York, 1961.

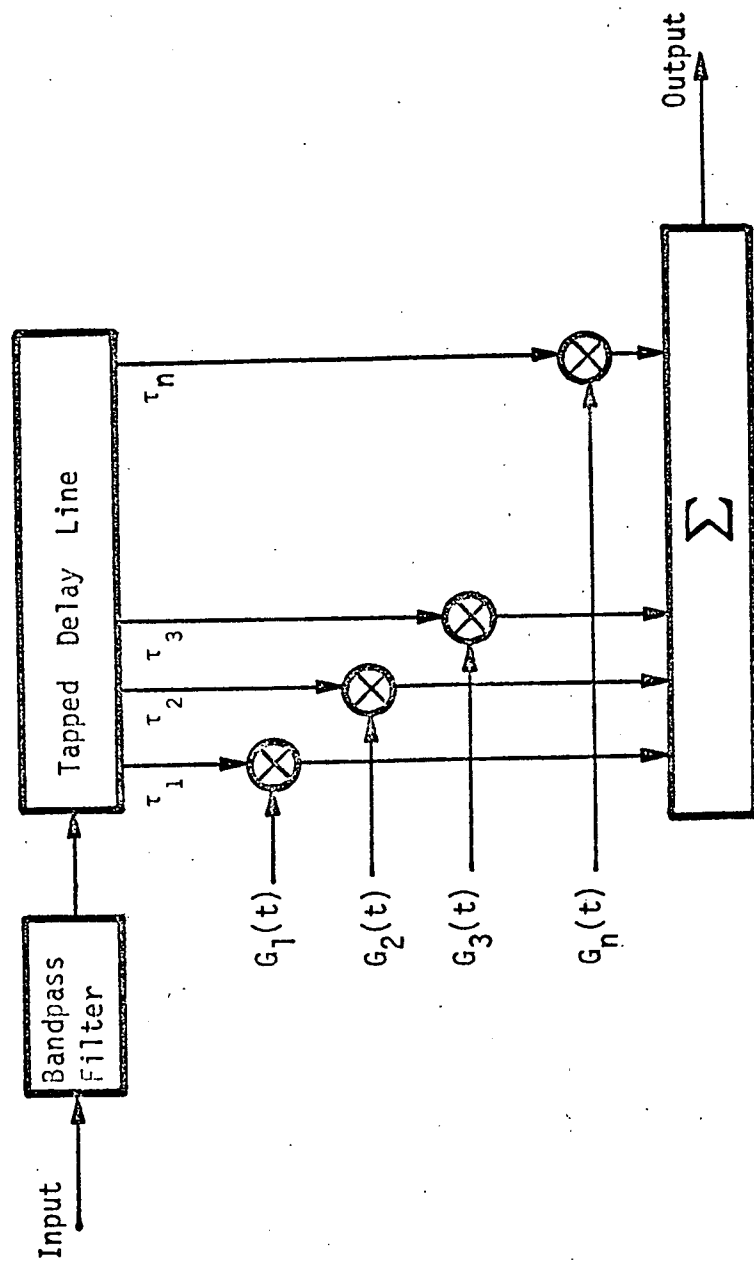


Figure 1.3 General Tapped Delay Line Channel Model

There are two general methods of simulating a propagation channel once the parameters of the channel have been defined. The first of these methods is to construct special purpose equipment from elements which provide the combination of propagation parameters exhibited by the real channel. The special purpose simulator, or "hardware" approach, usually has the advantages of operating in real time and of providing convenient system interfaces to equipment under test.

The second general method of channel simulation is the use of a computer which is primarily a general purpose machine to provide the simulation of the channel under the control of special simulation programs. This approach may be termed the "software" approach to channel simulation. The advantages of the software simulator may be in its economy, especially where an already existing general purpose computer may be used, and in its ability to operate upon mathematical descriptions of system waveforms which make it especially suitable for the evaluation of systems which have not been built and exist as mathematical abstractions. The software approach is likely not to operate in real time and where existing hardware systems are to be evaluated will probably require special buffering and translation functions to interface the real equipment with the computer-simulated propagation channel.

There is of course a wide spectrum of combinations of hardware and software possible in designing a channel simulation system. For example, it is likely that the number of adjustments required of a hardware simulator would be unwieldy from a human factors standpoint. It therefore seems attractive to make use of a small computer which can be programmed to set a large number of control functions within the hardware simulator corresponding to an

operator choice of channel parameters. The computer control of the hardware simulator could also be programmed to provide realistic time variation of the simulated channel parameters to correspond with the actual time history of the channel. In essence, this is the approach which Magnavox has chosen for the TDRS channel simulator.

In summary, the primary objectives of this study are:

- (1) Evaluation of the quantitative effects of the various channel parameters on the link.
- (2) Establishment of performance requirements for the simulator, such as
 - (a) the limits of variation for each of the channel parameters
 - (b) the required resolution in parameter adjustment
 - (c) the interrelationship between parameters.
- (3) Comparative analysis of simulation techniques leading to the design of a realizable channel simulator.

II. THE TDRS/USER PROPAGATION CHANNEL

In order to select a channel simulator to describe the communications link between a Tracking and Data Relay Satellite (TDRS) in geostationary orbit and a user satellite in a low altitude (200 to 4000 kilometers), it is necessary to define the parameters in the communications channel between the two spacecraft. Figure 2.1 is a representative illustration of user to TDRS link. A signal transmitted from either TDRS or user satellite will arrive at the other satellite by direct and indirect (reflection off a non-smooth earth) channels. This indirect path, commonly referred to as the multipath signal must be understood in order to predict the operation of the communication link. Therefore, it is necessary to define and analyze the parameters in both the direct and multipath channels.

A. THE MULTIPATH SIGNAL

The multipath signal is characterized by a time varying process which is statistically nonstationary because of the changing velocities and geometry between a user and the TDRS; however, the short-term statistics of this link can be considered stationary. This reflected signal will consist of a diffuse and specular component. The degree of diffuseness or specularity of the reflected signal will depend upon such factors as the grazing angle ψ , the roughness σ of the earth near the point of reflection, and the correlation length L across the surface of the earth. Roughness factor σ is a measure of the RMS height variations along the surface of the earth, and the correlation length L is a measure of the degree of correlation between points along the surface of the earth. The reflected power can consist of both specular

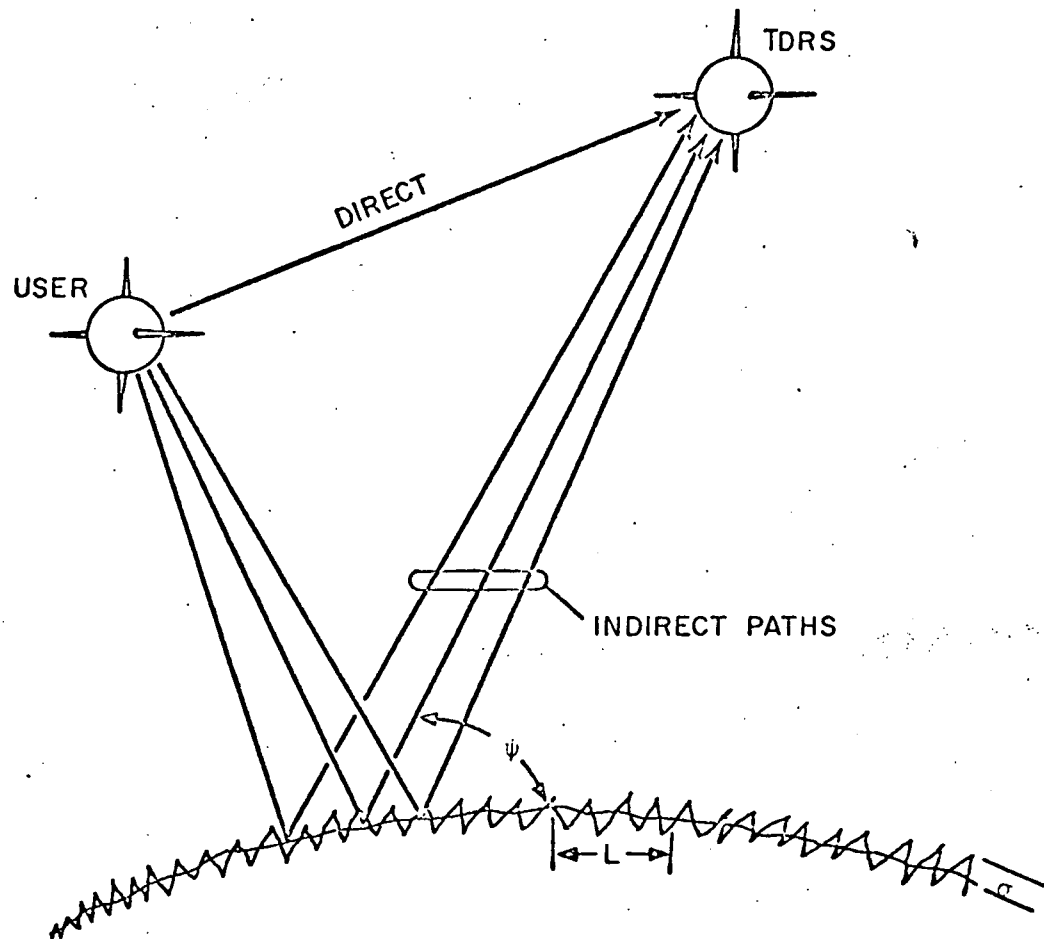


FIGURE 2-1 USER/TDRS COMMUNICATIONS LINK

and diffuse components. The specular component is essentially a delayed replica of the transmitted signal, whereas the diffuse component is noise like.

In general the amount of reflected specular power can be expressed by the following equation.

$$P_{\text{specular}} = \langle \rho_s^2 \rangle D^2 |R_0|^2 P_d$$

$$\langle \rho_s^2 \rangle = e^{-\left(\frac{4\pi\sigma}{\lambda} \sin \psi\right)^2}$$

P_d = the direct power

λ = the wavelength; $\langle \rho_s^2 \rangle$ = the scattering coefficient

σ = rms height of the reflecting surface

D = the average divergence factor associated with the spherical earth

$|R_0|^2$ is the mean squared reflection coefficient; ψ = the grazing angle.

The amount of diffuse power can be expressed by the equation derived by Duranni and Starras* and has the following form.

$$P_{\text{diffuse}} = D^2 |R_0|^2 F(\psi, h) P_d$$

h = the user height above the earth

$F(\psi, h) \leq 1$

The divergence factor is shown in Figure 2.2 as a function of the grazing angle for circular orbits of 200, 600, and 2000 kilometers. The relative expected specular and diffuse reflected power are illustrated in Figure 2.3, as a function of the grazing angle ψ for 136 mc and an average earth roughness and

* RCA Review - March 1968, pp. 77-105.

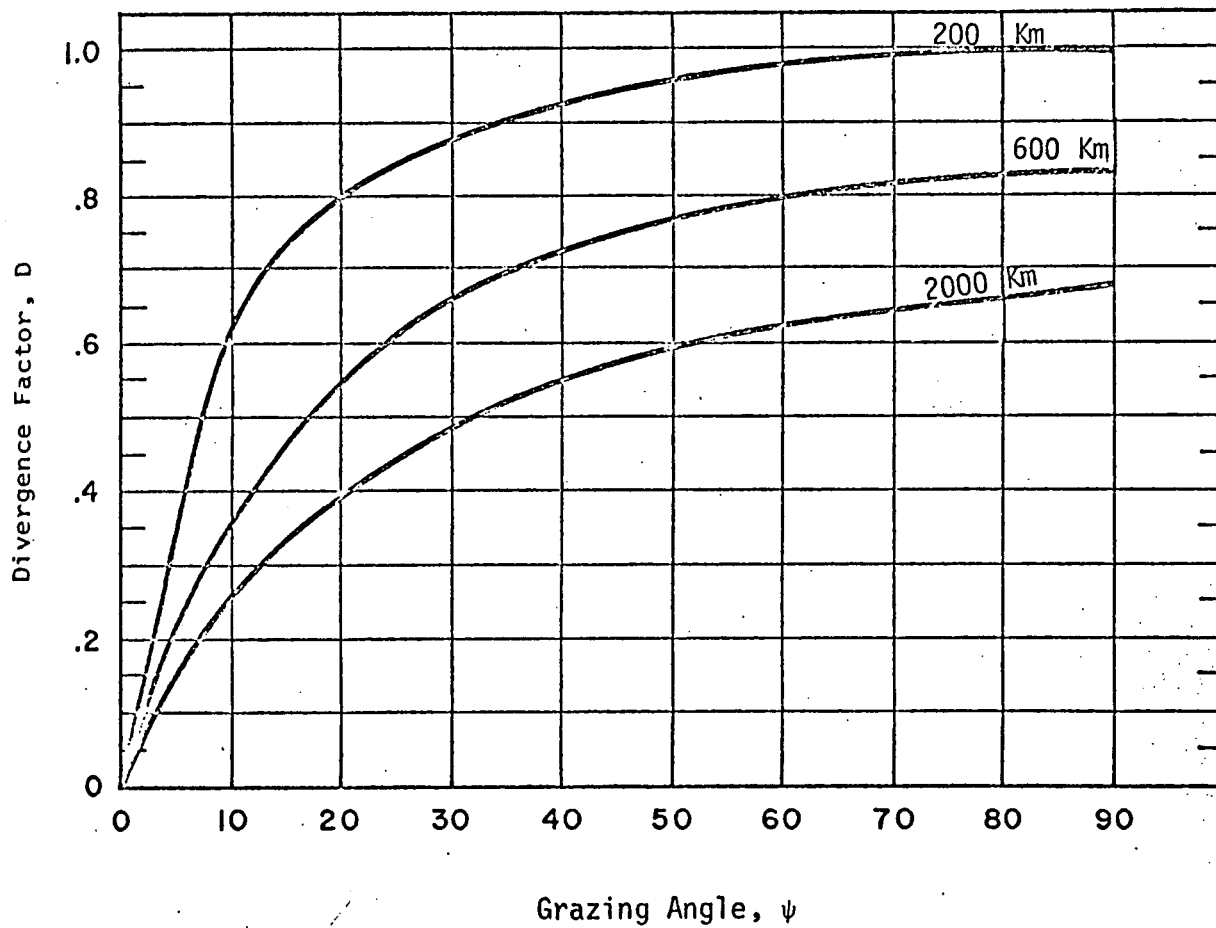


Figure 2.2 The Divergence Factor as a Function of Grazing Angle and Spacecraft Altitude

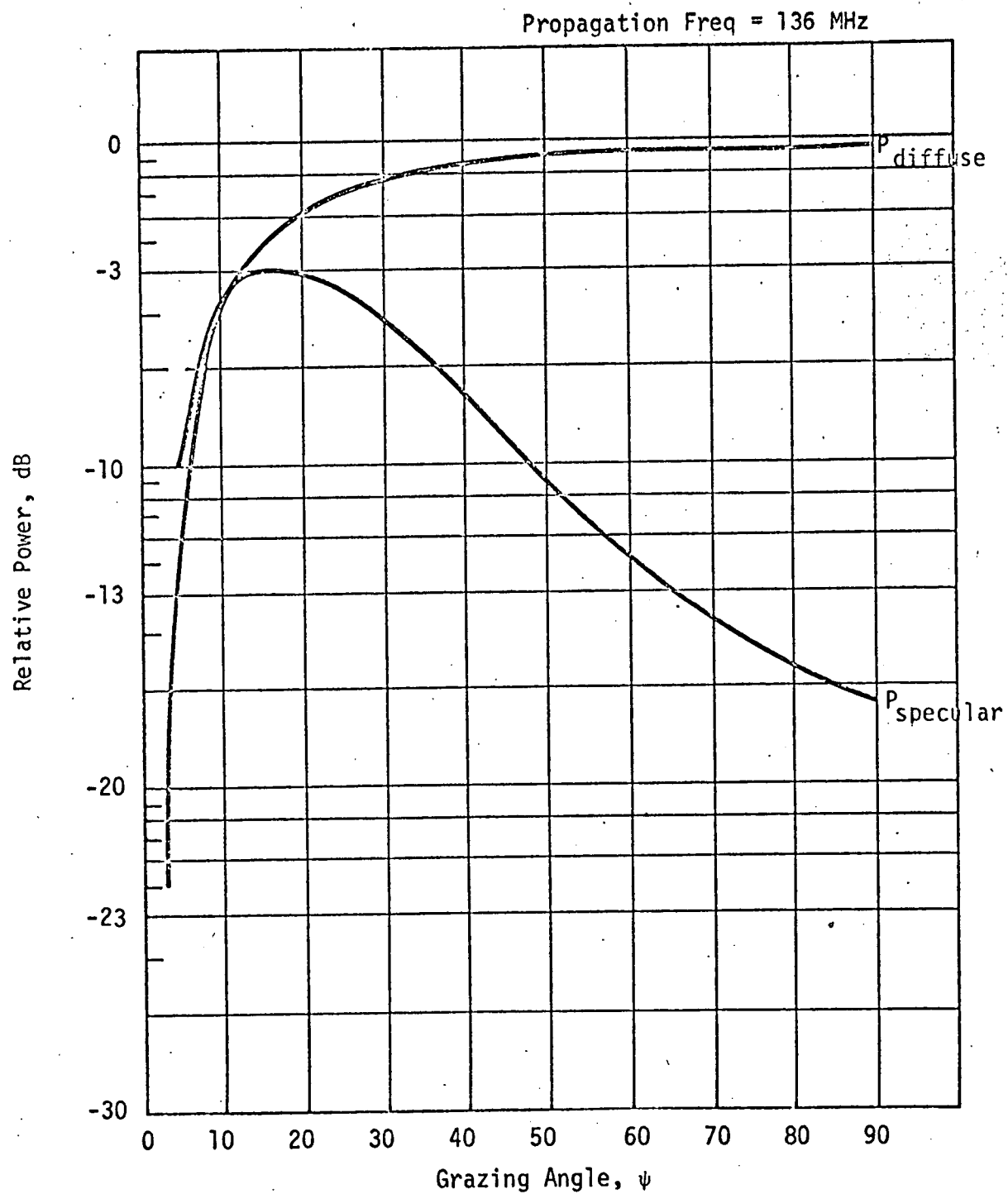


Figure 2.3 Relative Specular and Diffuse Reflected Power vs Grazing Angle

correlation distance. It can be noted that the specular power decreases with frequency and the diffuse power is essentially independent of frequency. At S-band, all the indirect power is essentially diffuse. It can be seen that at low-grazing angles the divergence factor serves to diminish the multipath signal, while at high grazing angles the primary reflected energy is diffuse. Furthermore, for reasonable roughness factors and correlation lengths, the primary source of reflected power will be diffuse for grazing angles in excess of 20° at VHF and practically always diffuse at S-band.

The composite multipath or indirect signal power will normally be equal to or less than the direct path signal when reflection coefficients of the earth are essentially unity and the grazing angles are in excess of 20°.

If we were able to separate the direct and the indirect signal paths at the TDRS when a CW signal is transmitted from a user we would observe that the envelope statistics associated with the indirect or reflected path would be Rician. This is true since the specular and diffuse components associated with the reflected path would constitute a fading signal consisting of a CW component and a diffuse component. Thus, the probability density governing the envelope would be Rician and is given by the following equation.

$$P(r_{\text{indirect}}) = \frac{r}{P_{\text{diffuse}}} \exp - \left(\frac{r^2 + 2P_{\text{specular}}}{2P_{\text{diffuse}}} \right) I_0 \left(\frac{r \sqrt{2P_{\text{spec}}}}{P_{\text{diffuse}}} \right)$$

$$P_{\text{scatter}} = P_{\text{diffuse}} + P_{\text{specular}}$$

As the grazing angle is increased, it was shown in Figure 2.3 how the specular component decreases rapidly and the above probability density of the received signal from the indirect path is essentially Raleigh.

Figure 2.4 provides an indication of the multipath signal level as a function of orbital altitude of the user satellite.

Prior to defining the parameters in the channel, the dynamic geometry of the TDRS system must be analyzed to quantitatively identify each of the channel parameters. Each of the user satellites will present a unique time varying multipath geometry as illustrated in Figure 2.5. In that figure R is the direct path between the TDRS and user spacecraft, the multipath would consist of two components S_2 from TDRS to earth, and S_1 from earth to user spacecraft.

Assuming a smooth spherical earth and without considering the effects of the ionosphere and troposphere on such factors as polarization, attenuation, and path length, curves for several of the critical channel parameters have been plotted.* These curves are representative of data that must be analyzed for the channel between the TDRS and user spacecraft. The use of these curves will be apparent after the various parameters of the channel are defined.

By referring to Figure 2.5, trigonometric functions can be found defining selected geometric parameters as a function of user satellite location. Direct path length between TDRS and the user spacecraft are shown in Figure 2.6. Cutoff in the curve is due to obscuration of the user spacecraft by the earth. The angle where this occurs varies with altitude of the user. Differential path length or the difference in path length between the direct and reflected paths is shown in Figure 2.7. From the curves for direct path length and differential path length between the TDRS and the user spacecraft, the free space propagation attenuation can be computed for both VHF and S-band. In

* These curves were obtained from GSFC Document No. X-520-69-38 "Range and Velocity Components of TDRS Multipath Signals", by T. Golden, Feb. 1969.

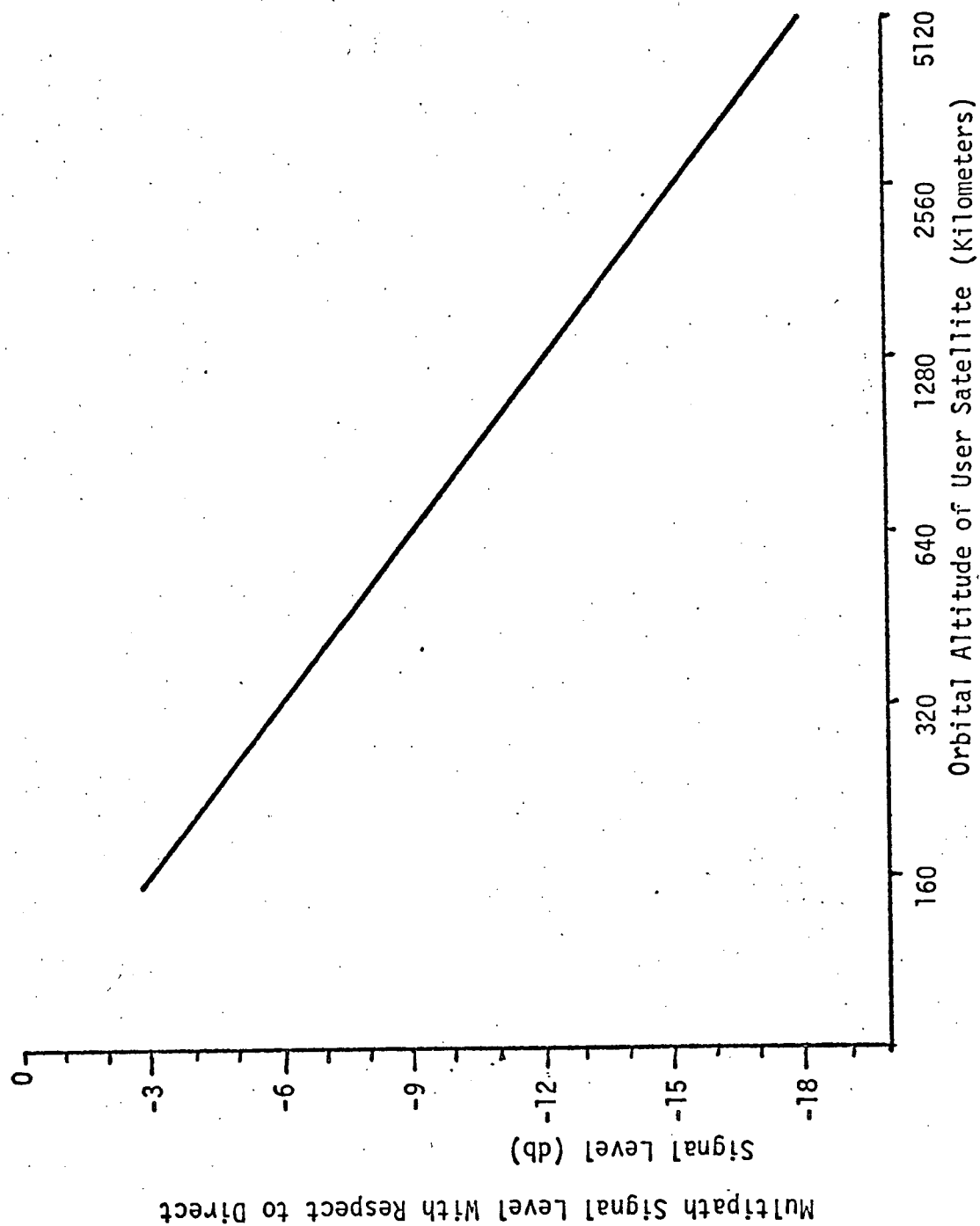


FIGURE 2.4 MULTIPATH/DIRECT SIGNAL RATIO AS A FUNCTION OF ORBITAL ALTITUDE

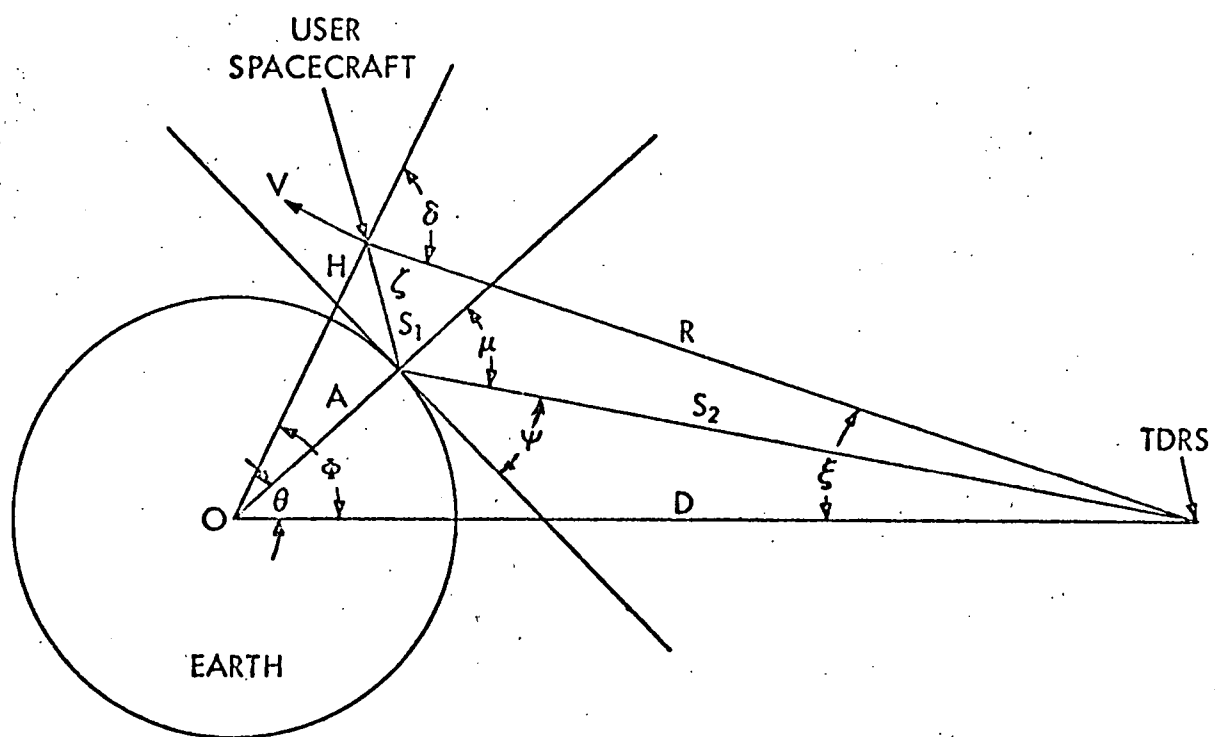


Figure 2.5 TDRS Multipath Geometry

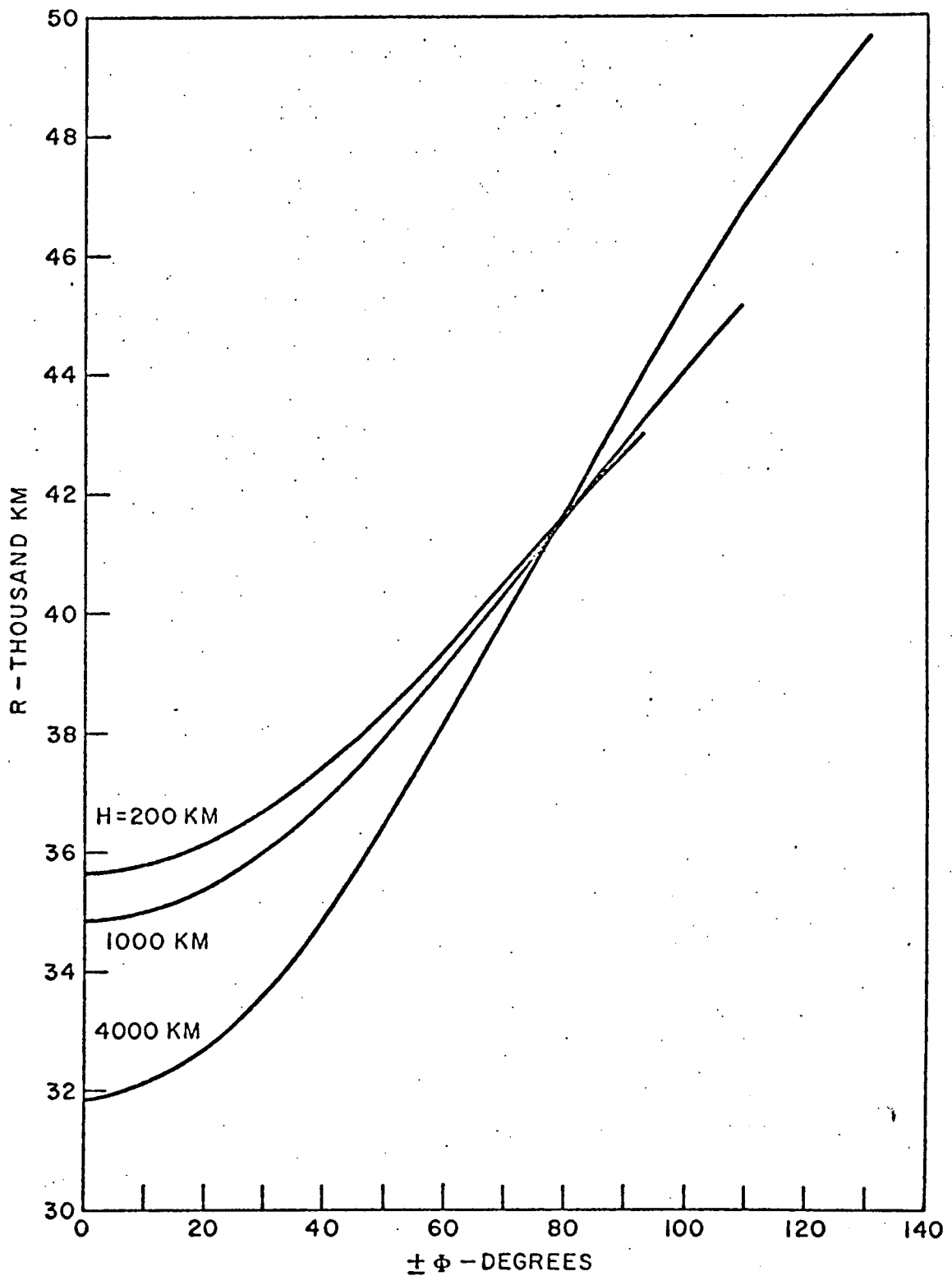


FIGURE 2.6 — DIRECT PATH RANGE BETWEEN THE USER SPACECRAFT AND THE TDRS

REPRODUCED FROM GSFC DOC. X-520-69-38 BY T. GOLDEN

addition, from the path length difference the differential time delay between the direct and reflected signal can be derived.

B. CHANNEL PARAMETERS

The parameters which control the channel between a TDRS and user satellite are defined below.

1. Doppler Effects

Doppler shift of the transmitted signal over all paths is of importance because it is a factor in determining the total bandwidth required for a signal. Usually the direct path Doppler must be added to the known or expected instabilities in the carrier frequency to determine the total required bandwidth.

a. Direct Path Doppler

The direct path signal between the TDRS and low-orbiting user can be considered to encounter a frequency shift, or Doppler shift due to the relative velocity between the user and TDRS. This Doppler frequency is varying due to the changing geometry between the two spacecraft. The Doppler rate of change is proportional to the time rate of change of the angle between the TDRS and the user (for a circular orbit).

The direct path Doppler frequency shift for three user satellite orbital altitudes are shown in Figure 2.8. These are a set of curves for 136 MHz showing that at the maximum Doppler shift is approximately 4000 Hz. Although curves are not shown at S-band, it can be calculated that for 2.3 GHz the maximum Doppler shift will be $2300 \times 3800/136$ or approximately 68 KHz. The expected Doppler frequency range then is 0 to 4 KHz and 0 to 68 KHz for VHF and S-band respectively, depending naturally on the height of the orbit.

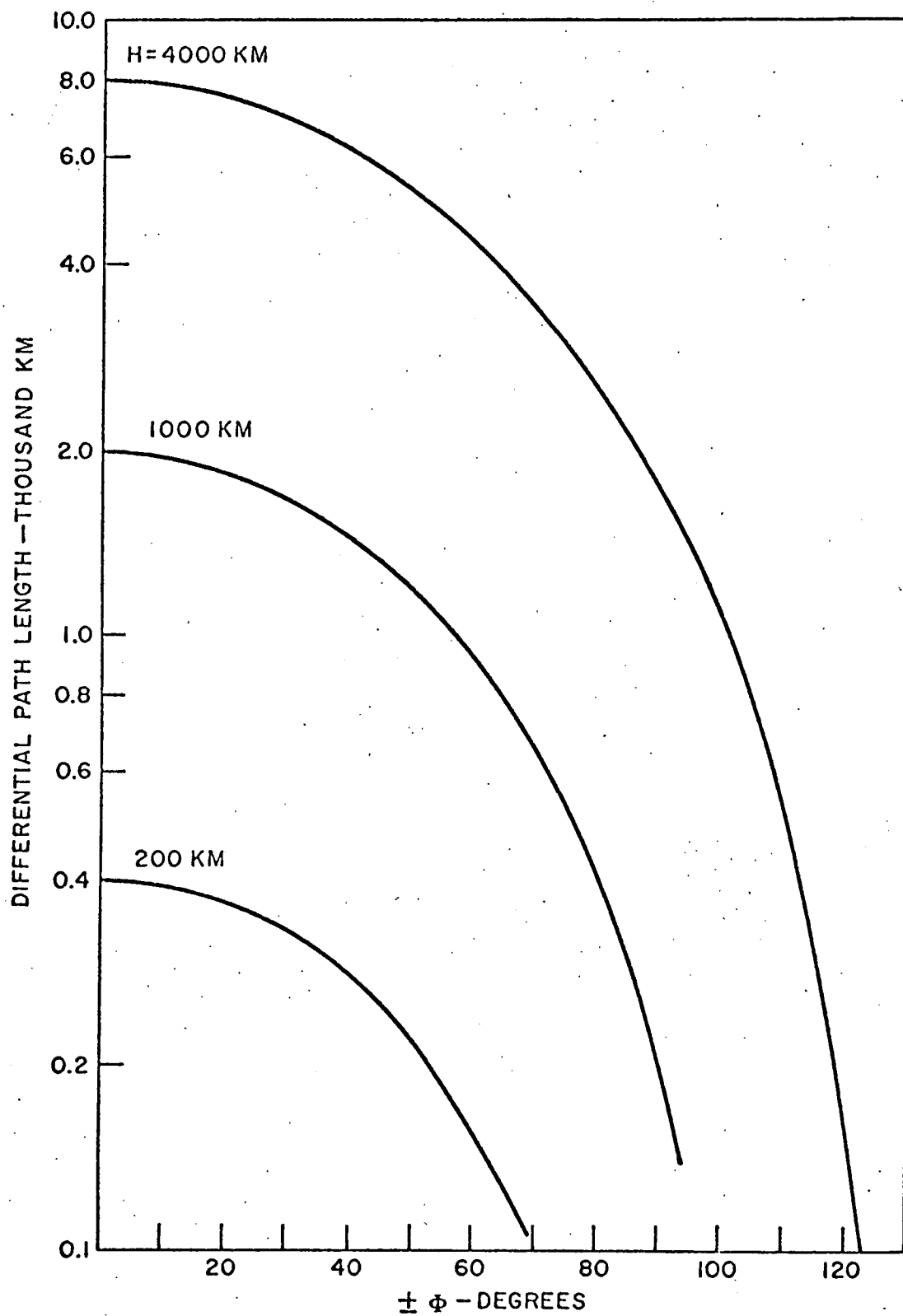


FIGURE 2.7 — DIFFERENTIAL PATH LENGTH (Δ) BETWEEN THE USER SPACECRAFT AND THE TDRS

b. Indirect Path Doppler Effect

The indirect signal reflects off the earth at some angle. This implies that there is some relative non-zero angle between the direct signal and the reflected signal at the earth's surface. Thus, a Doppler shifted signal is obtained from the multipath signal which is not equal to the Doppler signal from the direct path. This Doppler component due to specular reflection at the earth's surface is characterized in Figure 2.9. As explained previously, due to irregularities in the surface of the earth, there is a diffuse component to the multipath signal, and this produces a Doppler spectrum (fading bandwidth) which is also shown in Figure 2.9. For reasonable roughness factors and correlation lengths, the primary source of reflected power is diffuse for grazing angles greater than 20° . This situation prevails during most of the TDRS mission.

Figure 2.10 shows the differential Doppler between the reflected and direct paths for the 136 MHz carrier frequency. This figure is based on the assumption the Doppler shift results from reflections off a smooth spherical earth and is a good representation of the Doppler shift for the specular component of the reflected wave. It can be seen from Figure 2.10 that the differential Doppler will vary from about 0 to 2 KHz. This differential Doppler for S-band varies from 0 to 34 KHz; however, the specular component, because of the relationship between the rms height of the reflecting surface and the wavelength at S-band, should have relatively low power.

The indirect path doppler is always less (for circular orbits) than the direct path doppler (in magnitude), and as such the differential doppler will always be on the low frequency side of the direct path doppler.

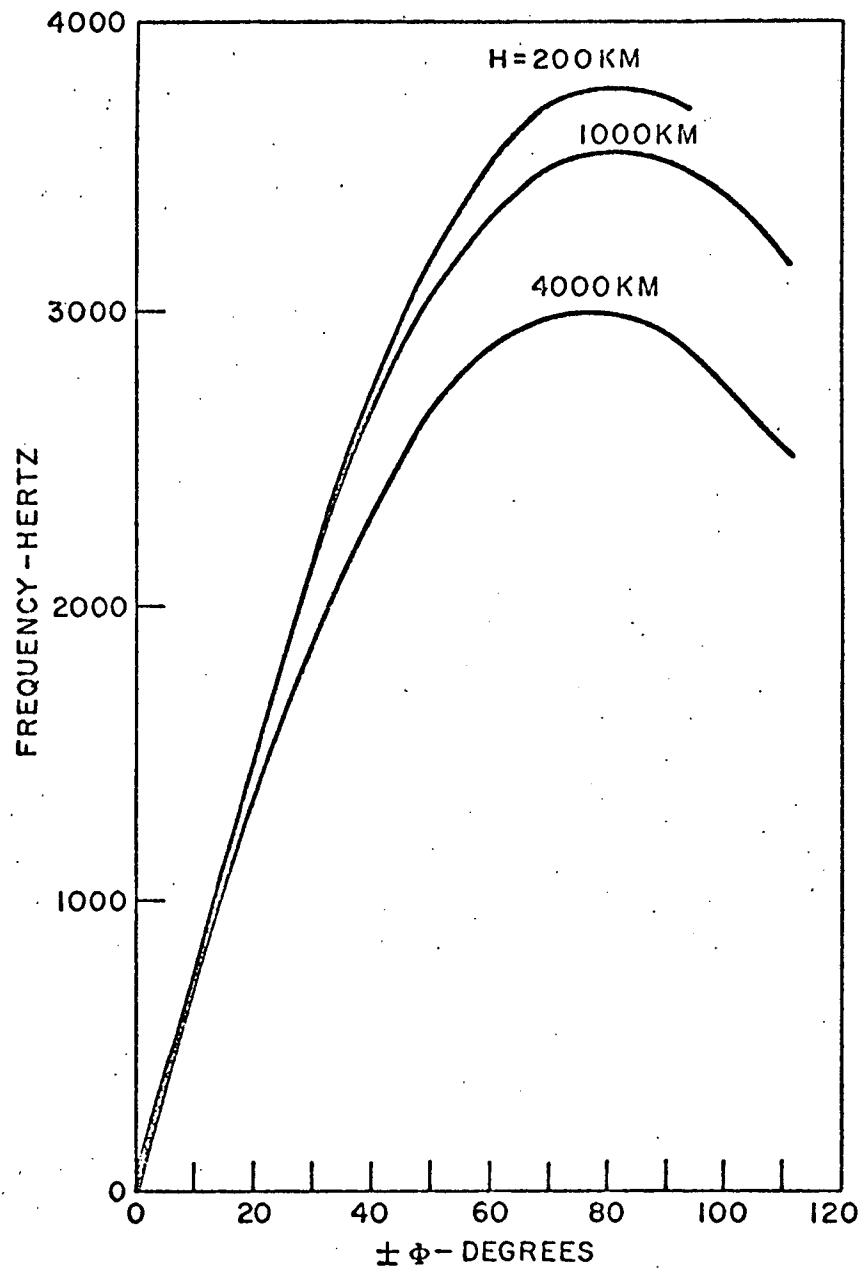


FIGURE 2-8 DOPPLER FREQUENCY ALONG THE DIRECT PATH FOR 136 MHz CARRIER

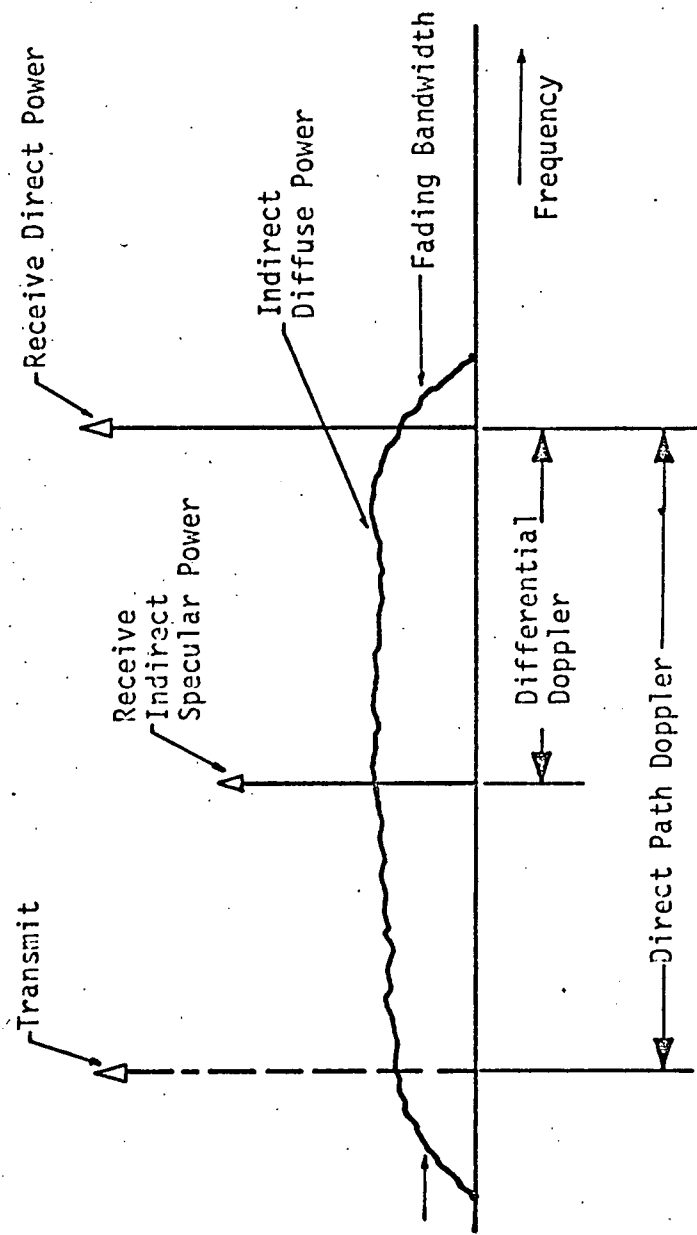


Figure 2.9 Direct and Indirect Channel Response in the Frequency Domain

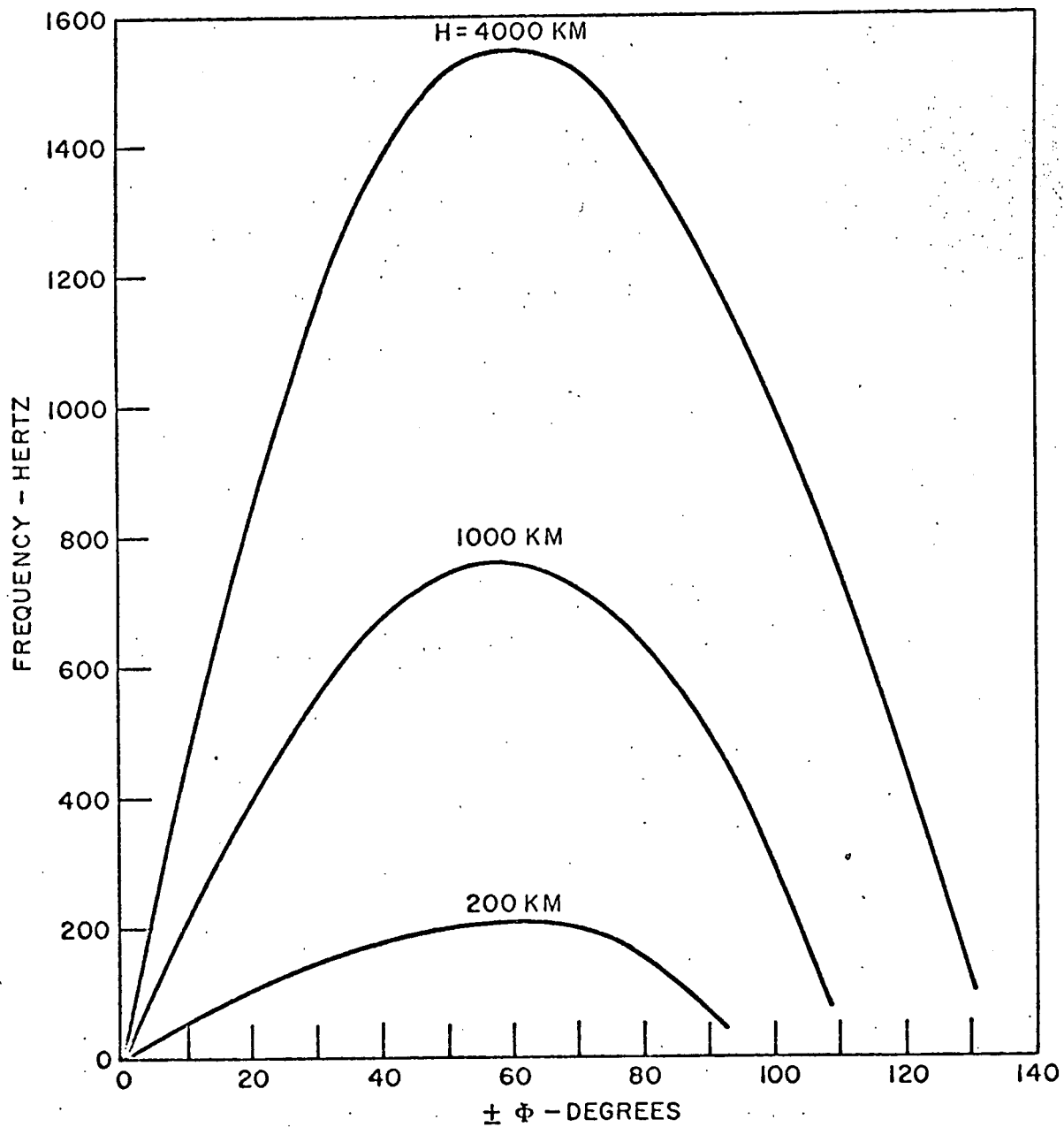


FIGURE 2.10 DIFFERENTIAL DOPPLER AS A FUNCTION OF USER SPACECRAFT POSITION

Another factor which can be attributed to the velocity of the user spacecraft is commonly referred to as the fading bandwidth B_F (Figure 2.9). Such fading is associated with the reflected signal and can be expressed analytically as:

$$B_F = \frac{v}{\lambda} \sqrt{2} \frac{\sigma}{L} \sin \psi$$

where v = the velocity of the user spacecraft

λ = wavelength of the propagation frequency

σ = the rms height variation of surface irregularities

L = the correlation length over the reflecting surface

ψ = the grazing angle

The fading bandwidth can be seen to be a function not only of the spacecraft velocity (relative to the earth) but also a function of the roughness of the earth's surface and the grazing angle, and is maximized for a grazing angle of 90° . At this point the reflected energy should be completely diffuse and the fading bandwidth is maximum. At VHF the fading bandwidth can be seen to vary from 0 to 2 KHz, while at S-band the fading bandwidth is increased by a factor of 17 over VHF to approximately 34 KHz. Fading bandwidth and differential Doppler combine to determine whether or not the multipath energy falls into the direct signal bandwidth, thus contributing to system degradation.

2. Signal Multipath Delay

Differential delay is a measure of the difference in time-of-arrival between signal traversing the direct and indirect path respectively. This differential delay is derived directly from the path length difference between the direct and indirect path. Figure 2.11 shows the differential path length delays, or the difference in arrival time between the direct and indirect

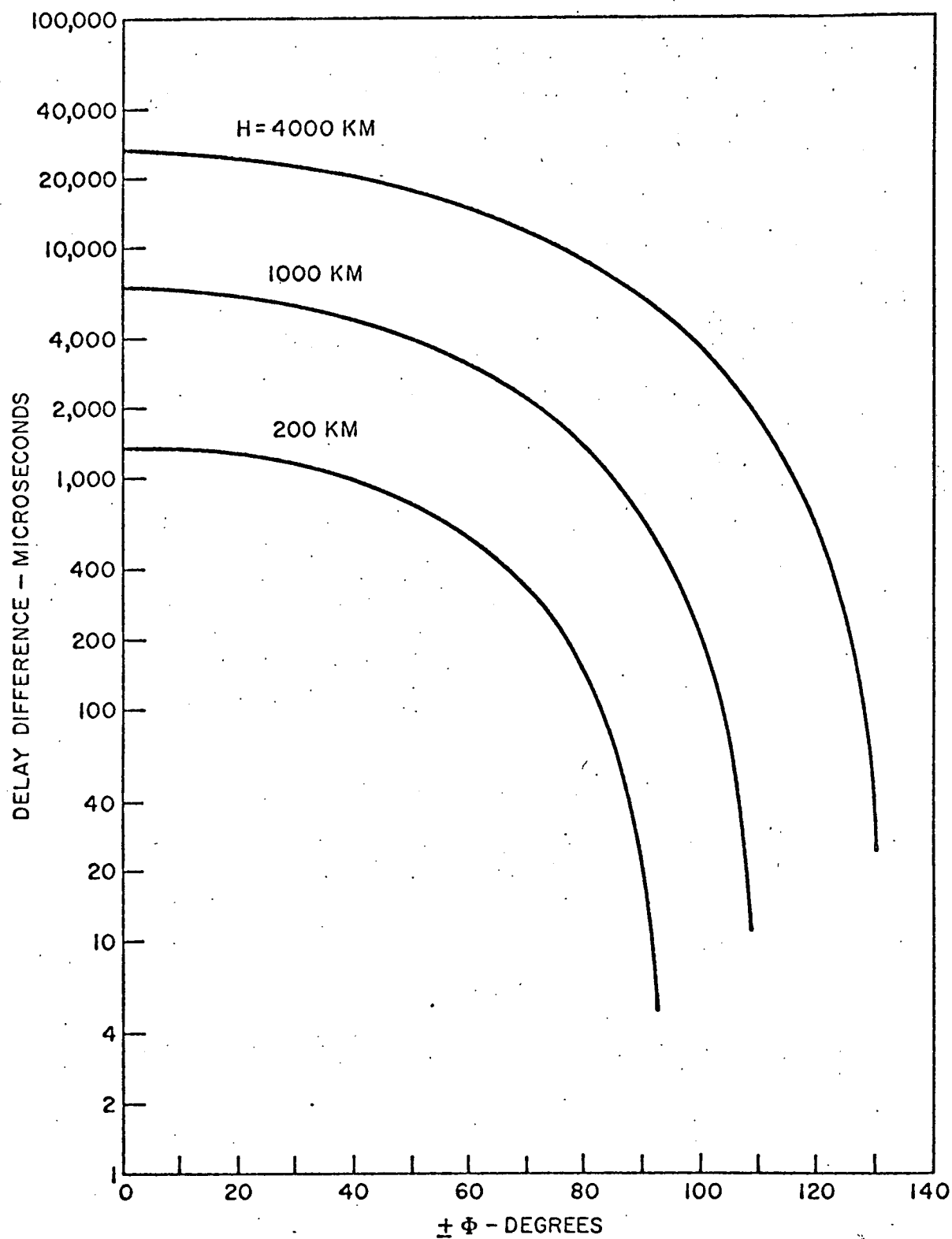


FIGURE 2.11 DIFFERENTIAL TIME DELAY AS A FUNCTION OF SPACECRAFT POSITION

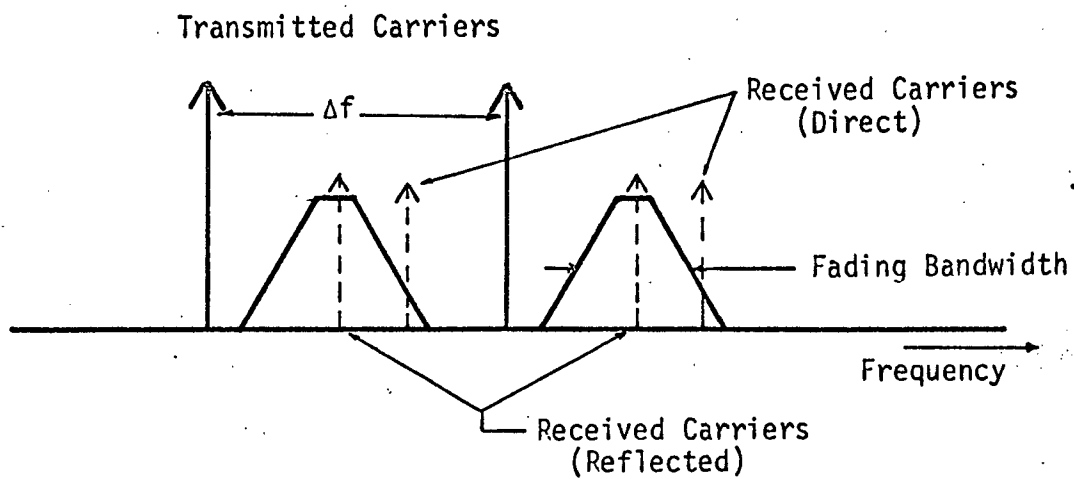
signals, as a function of user satellite altitude, and is shown to be approximately .2 milliseconds at 200 Km orbits ($\psi = 0^\circ$) and 30 milliseconds at 4000 Km orbit ($\psi = 90^\circ$). The absolute delay over the direct and indirect path is greater than 100 msec for each. Simulation of such delays is neither cost effective nor is it necessary since the relative delay between them (i.e., differential delay) is, in essence, what is seen at the satellite.

3. Coherent Bandwidth

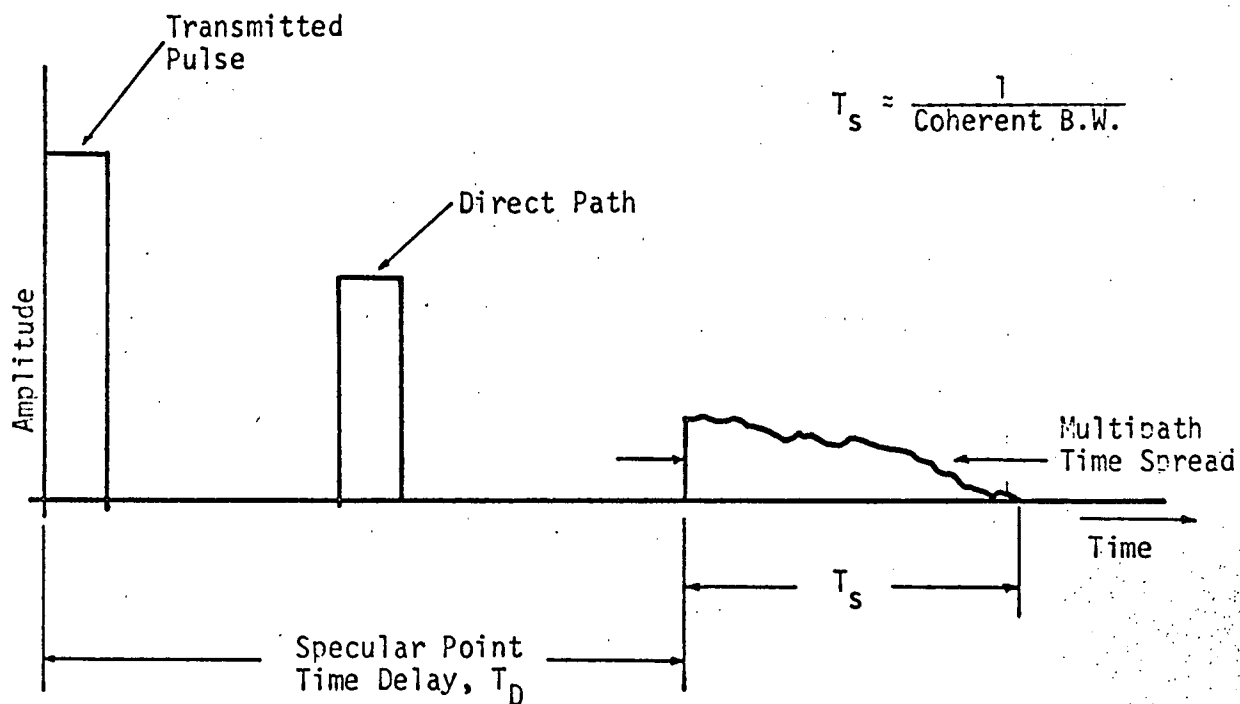
Coherent bandwidth of the fading channel is another parameter which is important in the evaluation of some systems exposed to multipath. It can be defined in several ways, but two methods are preferred.

The first is illustrated in Figure 2.12(a) which shows two transmitted carriers separated in frequency by ΔF received at the TDRS from a user craft via the direct and indirect paths. The coherent bandwidth B_c is defined as that value of ΔF required for the normalized correlation coefficient between the two reflected carriers to equal a value of 1/2. This definition is independent of the direct path received signals. Definition of coherent bandwidths based on the transmission of two CW signals separated in frequency is an accepted definition in the literature. The inverse time spread is related to coherence bandwidth through some constant factor which is usually a statistical parameter such as the rms spread in the time associated with the reflected signal. In the case of the TDRS, B_c does not necessarily limit the data capacity of the transmission link.

The second method is presented in Figure 2.12(b). If a pulse is transmitted by a user it will be received after some time via the direct path at the data relay satellite. At some time later, T_d (delay of the specular point), the multipath signal will arrive. The multipath signal will be time



a) Frequency Domain Definition



b) Time Domain Definition

Figure 2.12 Coherent Bandwidth

varying in amplitude and duration and will be characterized by an average multipath time spread T_s . The coherent bandwidth is related to the inverse of the multipath time spread through some constant factor. The value of B_c is important from a system point of view in that various signaling techniques such as frequency diversity require that the carriers be spaced in excess of the coherence bandwidth in order to provide full diversity action or maximum system performance. The time spread of a reflected signal is also of importance when time hopping pulse transmission techniques are used as the basis for signaling schemes.

Durrani and Starras^{*} in their formulation of the coherent bandwidth definition have shown that B_c is independent of propagation frequency and primarily dependent on the separation (ΔF) of the two CW components (Figure 2.12). Their results infer that the coherent bandwidth at S-band is essentially the same at VHF. Page and Chestnut^{**} have shown that a 1 μ sec transmitted pulse will exhibit between a 2 to 4 μ sec average time spread upon arrival at the satellite via the reflected path.

C. THE EFFECTS OF THE ATMOSPHERE ON THE CHANNEL

In addition to the free space path delay, a signal traversing the earth's atmosphere in an earth-space communications link is subjected to several effects, namely:

- (1) Tropospheric Attenuation
- (2) Ionospheric Attenuation
- (3) Tropospheric Refraction
- (4) Ionospheric Refraction

^{*} Op. cit.

^{**} Page, L. J., and Chestnut, P. C., "A Rough Earth Scattering Model for Multipath Prediction," Prepared under NASA Contract NAS5-20125 by ESL, Inc., June 1970.

- (5) Polarization Rotation
- (6) Birefringence
- (7) Chromatic Abberations
- (8) Aurora

The following sections discuss each of the aforementioned parameters and their relative effects on the link between the TDRS and the user spacecraft. It should be noted that wherever possible measured data has been used; however, there are many effects for which there exists only theoretical data, or data describing the gross effects of the various channel phenomena. In these instances, assumptions have been made to account for what is felt to be the realistic effects of the propagation channel. The analysis presented herein is for the general VHF/UHF range. For those channel parameters which exhibit more predominant effects in the frequency band of interest (i.e., 136-150 MHz and 2.2-2.3 GHz), the effects are so noted. It is not the intent of this section to establish the precise value of each of the channel parameters, except where it has been determined that they will have deleterious effects on the signal transmission.

Since low-orbiting satellites will fall within the ionospheric belt, some of the atmospheric effects will affect, in part, the direct path signal between the user and TDRS. The signal propagating along the indirect path will, for the most part (especially for user orbits of higher altitude), be subjected to the aforementioned atmospheric effects twice, once when propagating along the incident path to the earth, and again when propagating along the reflected path.

1. Attenuation Effects

Figure 2.13 shows the atmosphere and its regions. Due to density effects and diurnal effects the height of these layers in the ionosphere shift, but are essentially as shown in the figure. The troposphere remains essentially at the 30 Km height.

a. Spreading or Spatial Loss

The energy in a transmitted signal decreases due to the spatial spreading of the wave as it travels through the space. This is not a function of absorption or scattering of the signal, but strictly dependent on particle separation as it leaves a source, and is only a function of frequency and propagation distance. The spatial loss along the direct path can be computed to vary from 165 to 169 dB at VHF and from 189 to 192 dB at S-band. The free space loss of the reflected signal (assuming perfect reflection of the earth) varies from 167.2 to 169.5 dB and 191.4 to 193 dB for VHF and S-band respectively.

b. Ionospheric Absorption Losses

This loss can be attributed to the transfer of energy from the propagating electromagnetic wave to the motion of particles in the ionosphere. There are many factors to effect this loss and likewise the electron density to be encountered. These can be described as follows:

- (1) frequency utilization
- (2) time of day - absorption is much higher in the daytime than at night
- (3) season of the year
- (4) sunspot activity
- (5) path length through the ionization regions
- (6) latitude-longitude effects

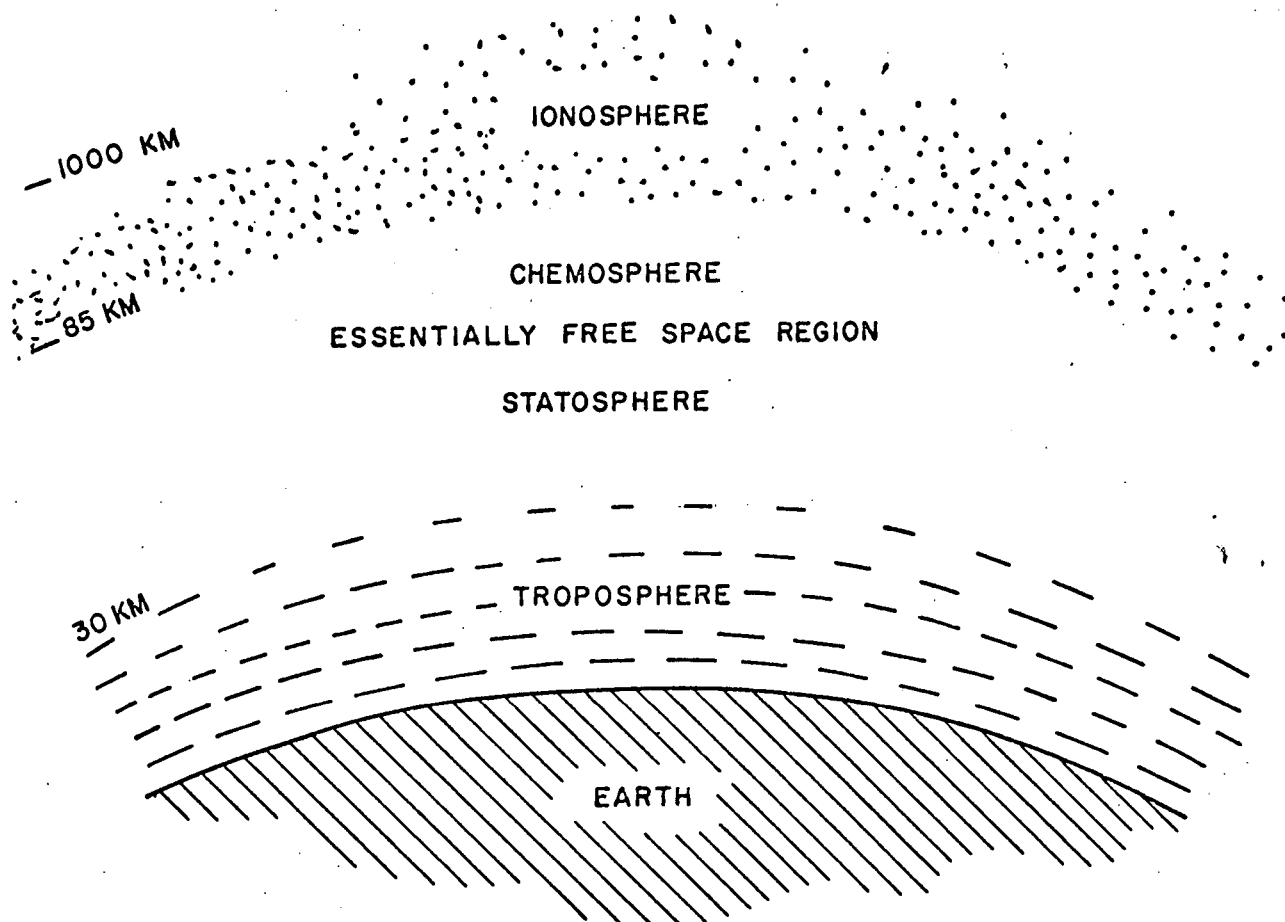


FIGURE 2.13 THE ATMOSPHERE AND ITS APPROXIMATE REGION

The absorption effect will be seen by the direct signal from a user to, (or from,) the TDRS, and the reflected signal is subject to this loss as well (the indirect path, for the most part will be subjected to this loss twice).

Approximate values for ionospheric absorption for 136-150 MHz and S-band are shown in Table 2.1. When compared to the free space path loss, this ionospheric loss is negligible.

Table 2.1
Ionospheric Absorption at 400-500 MHz

<u>Time of Day</u>	<u>VHF</u>	<u>S-band</u>
Nighttime	< .01 dB	< .0001 dB
Daytime	< .1 dB	< .001 dB

These results were derived from Lawrence, Little, and Chivers*, who developed a similar table for 100 MHz. The values in Table 2.1 have been approximated from those at 100 MHz based on the fact that absorption (in dB) varies inversely as the propagation frequency squared. For details concerning the propagation conditions the reader is referred to Lawrence's report.

c. Tropospheric Losses

Losses in the lower atmosphere are due almost entirely to molecular absorption by oxygen and uncondensed water vapor, and scattering by precipitation particles. Atmospheric models having loss characteristics similar to the actual troposphere have produced theoretical curves of the total molecular absorption for different propagation paths through the troposphere for signals traveling from the earth to outer space. Precipitation scattering

* IEEE Proceedings, January, 1964.

caused by rain, fog, snow, etc., can be considered single-particle scattering and this scattering becomes more of a factor as the size of the particles approach the wavelength of the signal. As can be seen in Figure 2.14 (a plot of single-path tropospheric attenuation), below 15 GHz the tropospheric absorption loss is essentially smooth and below 1 GHz is essentially constant. Furthermore, precipitation losses, except for extreme conditions, are not significant below 5 GHz. Here, once again the tropospheric absorption at VHF will be seen to be negligible when compared to the spatial or free path loss. At S-band the maximum atmospheric losses will be less than 0.3 dB for grazing angles greater than 10° .

2. Atmospheric Refraction Effects

Described previously were the absorption losses due essentially to the transfer of energy from the signal to the media. There are other effects which take place that contribute not only to the losses in the system but to distortion or changing of the signal as it propagates through the media. These factors will be discussed individually.

As signal passes through the atmosphere it is passing through a medium with continually changing properties, i.e., the temperature and moisture content are continually decreasing with height above the earth. The index of refraction is a function of the frequency, temperature, dielectric constant, pressure and moisture content in a medium and is found to decrease with height above the earth. Snell's law shows that if the index of refraction of the new medium is lower than the original medium there is a bending of the signal away from the perpendicular to the boundary surface. Similarly, there is a bending towards the vertical if the signal is entering a medium of higher index of

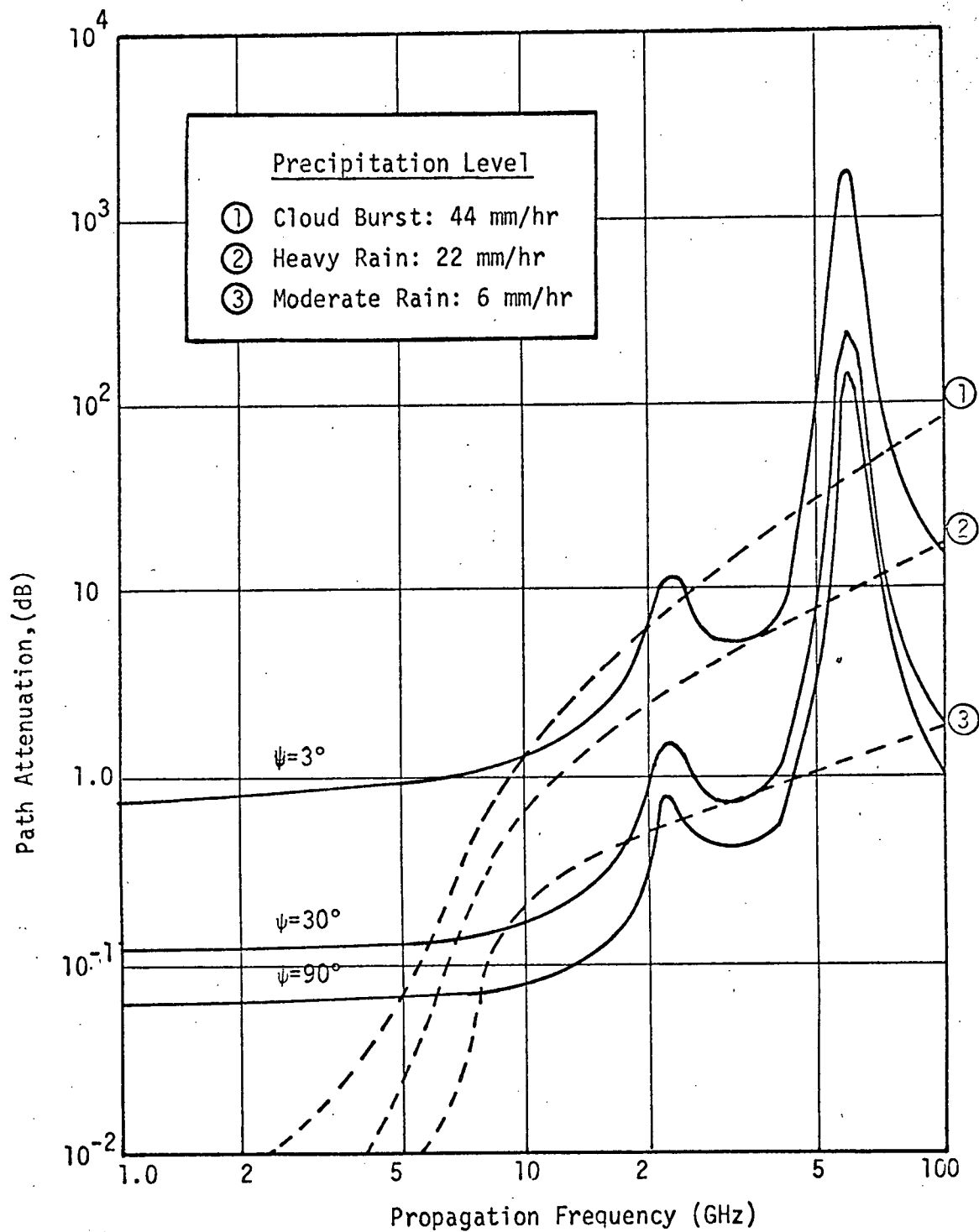


Figure 2.14 One Way Tropospheric Attenuation

refraction. Since the normal atmosphere has a gradual change in its physical properties, the change in the wave direction is gradual. This refraction at a boundary (whether discrete or continuous) is accompanied by some reflection of the incident signal. The result of this action is that the refracted wave as it is passing through the atmosphere is losing energy and encountering a constant direction and phase shift.

Abrupt changes in the atmosphere cause abrupt changes in the absorption qualities of the environment, the velocity of the signal in the environment, and the refraction of the signal in the environment. Causes of change in the electron density of the atmosphere, discontinuities, and abrupt changes caused by simultaneous sudden decreases in moisture (moisture lapse) and sudden increases in temperature (temperature inversion) with increasing altitude can result from the following:

- (1) When warm dry air flows from land out over cooler water, the evaporation of moisture from the water into the lower layer of air cools the air, increases the moisture lapse rate, and produces a temperature inversion, thus, producing a duct of abrupt physical difference than its immediate surroundings.

- (2) Nocturnal cooling of the surface of the earth causes ducts to appear. These appear due to:

- (a) A cloudy sky prevents much of the heat radiation from the earth to be dissipated smoothly into outer space.

- (b) Rapid temperature changes that appear from day to night over desert land.

- (c) Solar activity.

Since the magnitude of the dielectric constant is a function of parameters such as geographic location, weather, time of day, and season of the year, complete analysis of the propagation effect over all parametric variations would prove to be an extremely burdensome task. Generally, models of average atmospheric conditions are utilized.

a. Tropospheric Refraction

In the troposphere, the refractive index is dependent upon temperature, pressure, and partial pressure of water vapor. The index can be represented by

$$n = 1 + 10^6 \left[\frac{a}{T} \left(p + \frac{b\epsilon}{T} \right) \right]$$

where

n = refractive index

T = absolute temperature (degrees K)

p = total pressure in millibars

ϵ = water vapor partial pressure in millibars

a & b = experimental constants*

A more commonly used form of the refractive index is termed the refractivity, N , where

$$N = (n - 1) \times 10^6 = \frac{a}{T} \left(p + \frac{b\epsilon}{T} \right)$$

Figure 2.15 shows the effects of altitude on the tropospheric refractive index, and indicates that it is a function of the environment and dependent on factors such as relative humidity. In the figure N_d is the refractivity at zero percent relative humidity and N_w is the refractivity at 100 percent relative humidity.

* These constants vary according to author from between 74.4°K/mb and 79°K/mb, and 4800°K and 4973°K respectively.

In the 100-10,000 MHz range the refractive index is frequency insensitive. Tropospheric refraction at VHF and S-band is considered to be negligible.

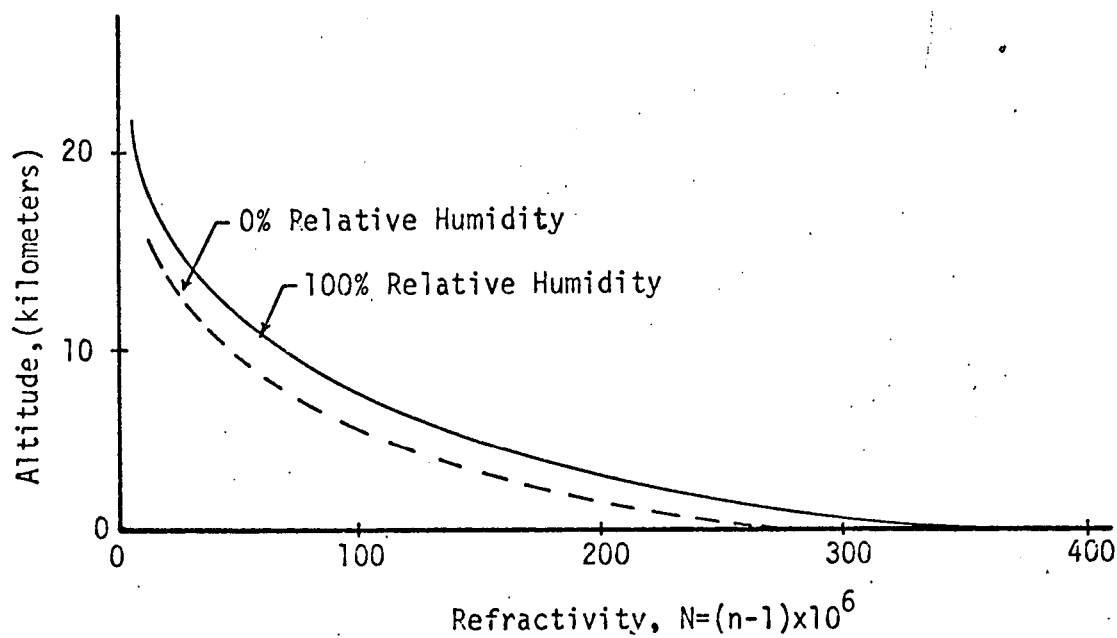


Figure 2.15 Tropospheric Refractivity

b. Ionospheric Refraction

The ionospheric refractive index, n , has been defined as

$$n = \sqrt{1 - \frac{4\pi N_e e^2}{m\omega^2}}$$

where

N_e = electron density (electrons/cm³)

e = electron charge (4.8×10^{-10} ESU)

m = electron mass (9.1×10^{-28} grams)

ω = angular frequency of the impressed signal

Because atmospheric ionization is mainly caused by solar radiation, maximum errors predominate on the day side, with appreciably less refraction occurring on the night side. The index of refraction of the ionosphere is shown in Figure 2.16 as a function of the electron density N_e and the frequency of the incident wave.

The distribution of electron density with height under equilibrium conditions is a function of the electron density at the level of greatest ionization and the normalized height. A typical electron density profile is presented in Figure 2.17. Extrapolating from Lawrence^{*} it can be shown that the ionospheric refraction at 136-150 MHz is (assuming a constant distribution of electron density) on the order of 10^{-3} radians. Ionospheric refraction effects decrease as the square of increasing frequency so that at S-band it will be on the order of 10^{-5} radians.

c. Atmosphere Induced Time Delay

Errors in time of arrival of a signal result due to refraction of the signal and the difference between the free space velocity and the actual velocity in the medium. Range errors corresponding to the delay time imposed by propagating through the ionosphere are inversely proportional to the ionospheric refractive index and grazing angle. Typical tropospheric one-way time

^{*}Op cit.

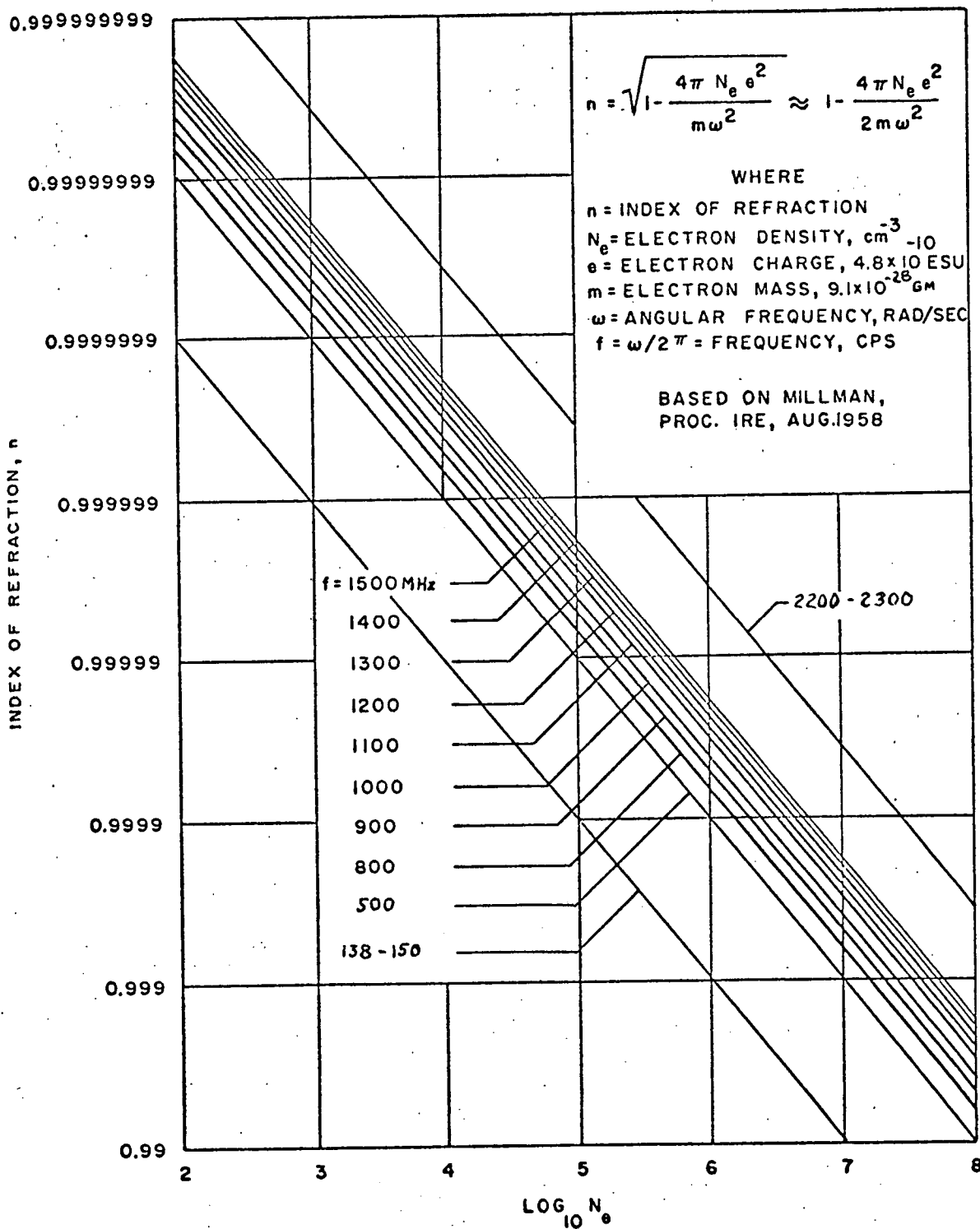


Fig. 2.16 Index of Refraction of the Ionosphere

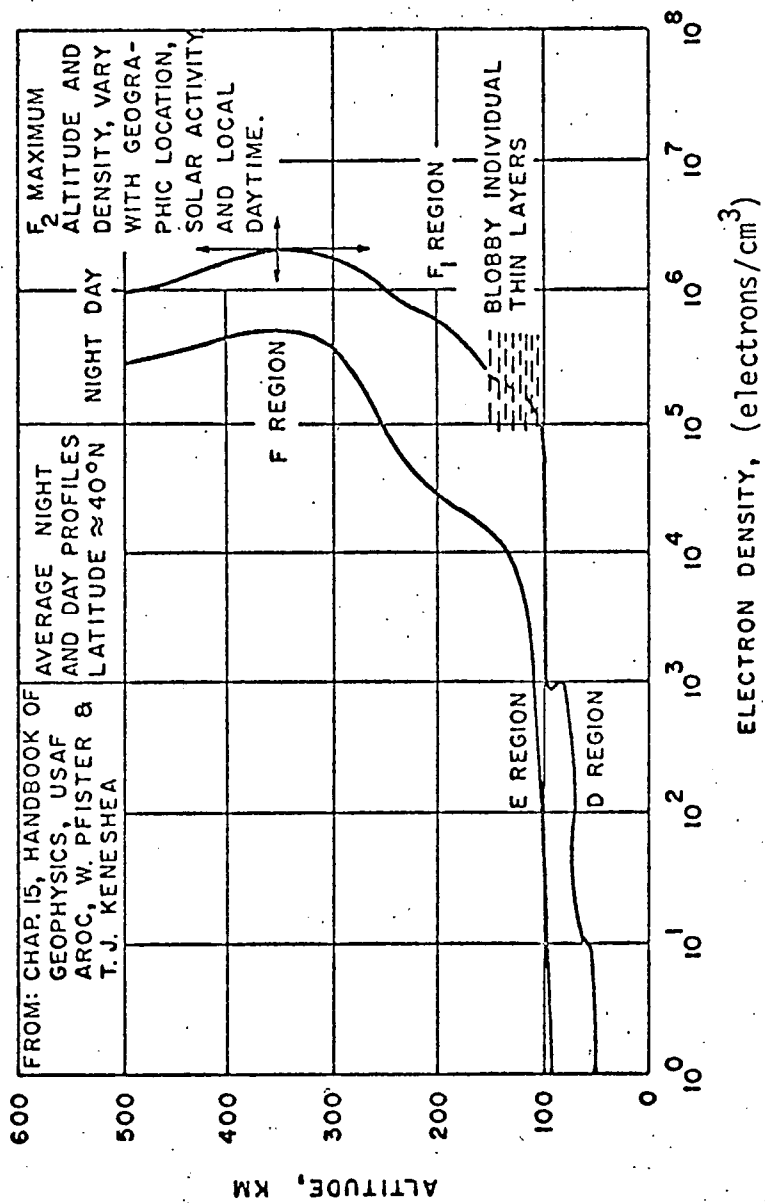


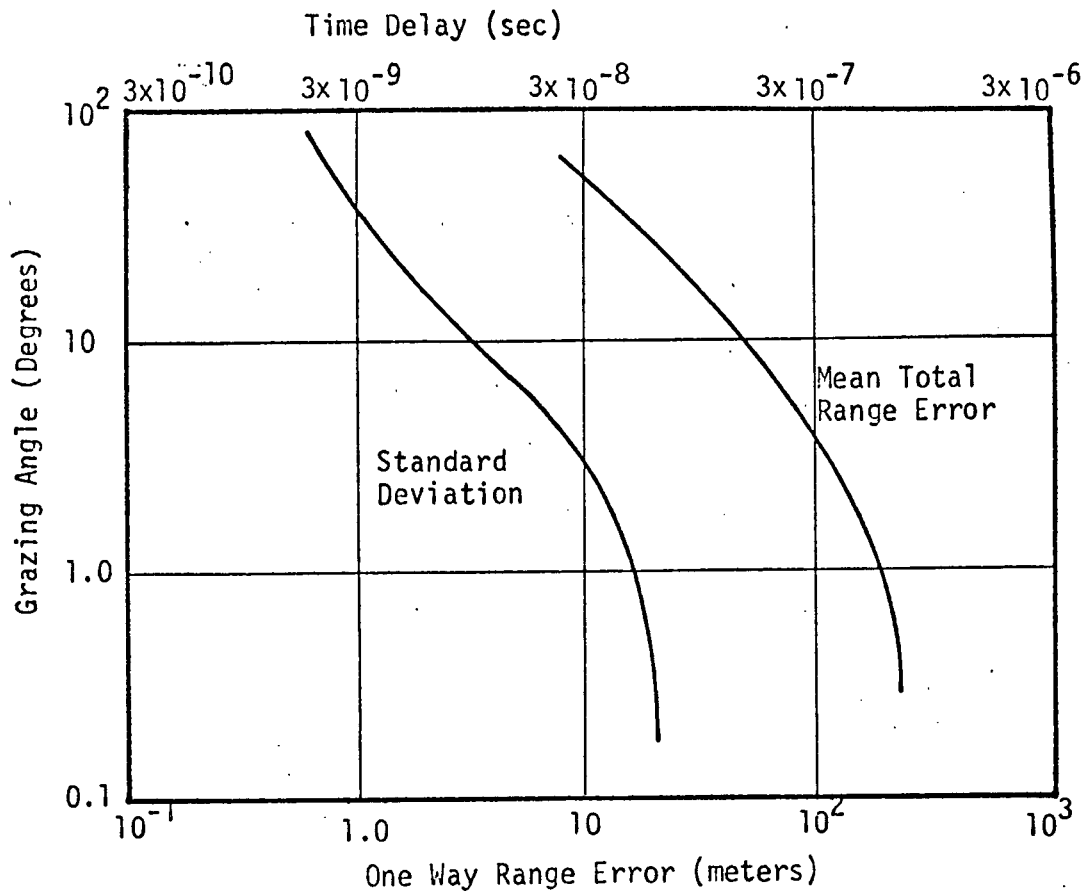
Fig. 2.17 An Electron Density Model in the Ionosphere

delays and range errors for several values of grazing angle are shown in Figure 2.18(a), and a similar set of errors due to ionospheric effects is shown in Figure 2.18(b). The errors imposed by the troposphere are essentially a function of refractive index and grazing angle, and independent of frequency. The curves of these two figures indicate that the troposphere induced time delay will be on the order of 10^{-8} sec for VHF and S-band, and that the ionosphere induced time delays will be on the order of 10^{-6} and 10^{-8} sec for VHF and S-band respectively, either of which, when compared to the multipath time delays is relatively insignificant.

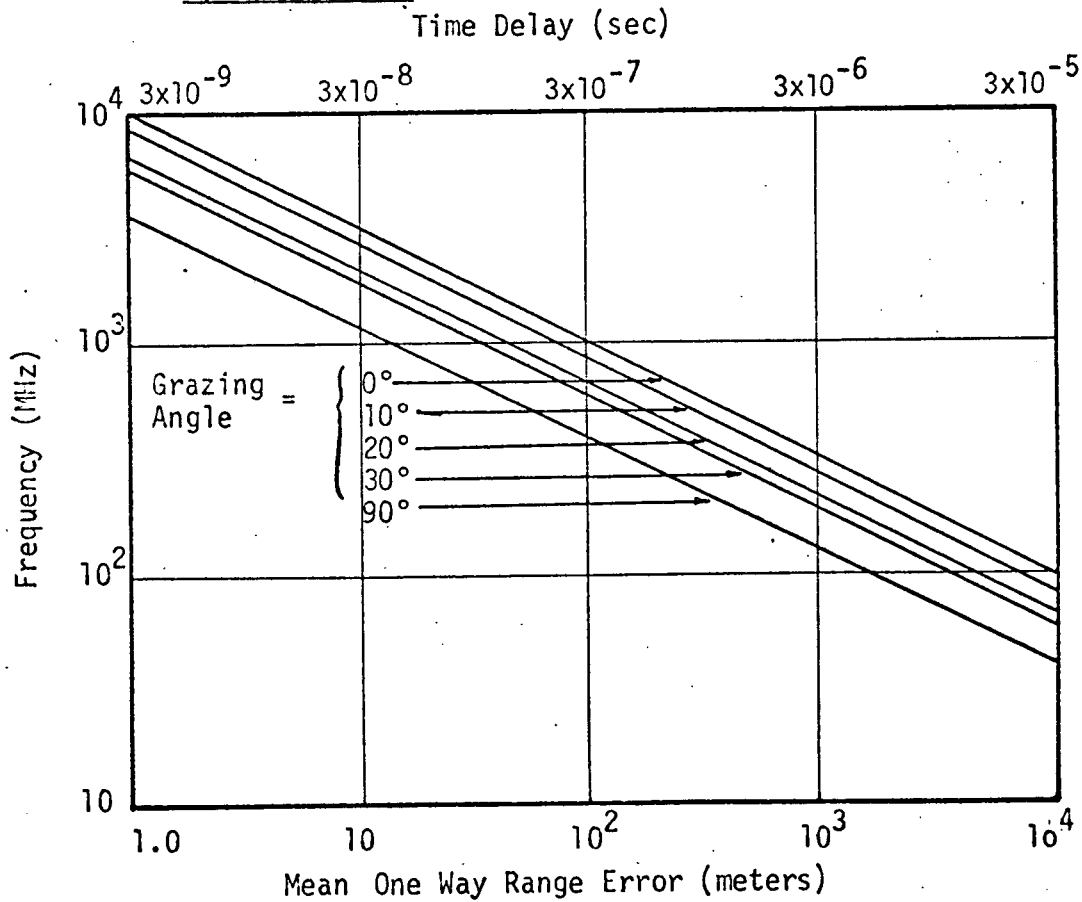
3. Polarization Rotation

a. Faraday Effect

A signal traveling in the ionosphere experiences a force due to the presence of an electromagnetic signal in the earth's permanent magnetic field. Thus, waves traveling in the ionosphere are doubly refracted, and as a consequence, the axis of polarization of linearly polarized waves are continuously rotated as they pass through the medium. The physical properties of the wave emerging from the medium are such that the polarization of the wave is different from the original wave. One obvious problem to be encountered for a system using linearly polarized antennas, is that this effect decouples the transmitter and receiver and manifests itself as an apparent power loss. Since the earth's magnetic field is not constant, this effect can not be circumvented by a simple misalignment of the transmitter and receiver polarization axis. The amount of rotation realized at VHF and S-band is dependent on the path length through the medium and the electron density in the medium.



a) Troposphere



b) Ionosphere

Figure 2.18 Typical One Way Time Delays and Range Errors

The initially polarized wave is rotated through the Faraday rotation angle, ϕ , where

$$\phi = \frac{e^3}{2\pi m^2 c^2 f^2} H \cos \theta \sec \delta \int_{h_1}^{h_2} N dh$$

where

e = electron charge

m = electron mass

c = speed of light

f = propagation frequency

H = magnitude of earth's magnetic field

θ = angle between H and direction of propagation

h_1, h_2 = extremes of propagation path

δ = angle between direction of propagation and zenith

N = electrons/ m^2 between h_1 and h_2 .

The approximate effects of maximum ionospheric activity and frequency on Faraday rotation is shown in Figure 2.19. In general, it can be said that if the system antennas are not circularly polarized, severe distortion below 500 MHz will exist due to Faraday rotation and differential Faraday rotation.

For the case of the TDRS/User link, however, the antennas are circularly polarized, thereby rendering the channel relatively insensitive to this effect.

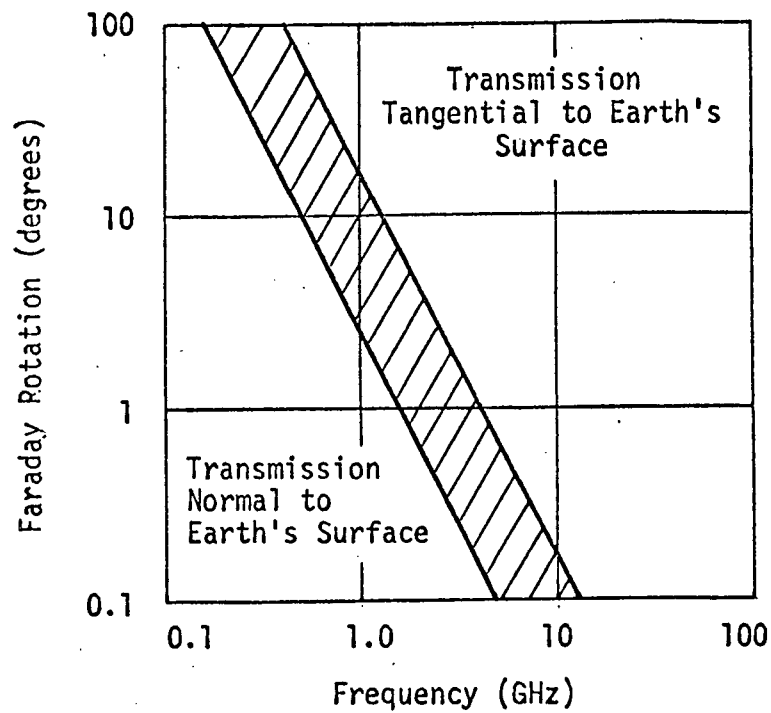


Fig. 2-19 Faraday Rotation Effects

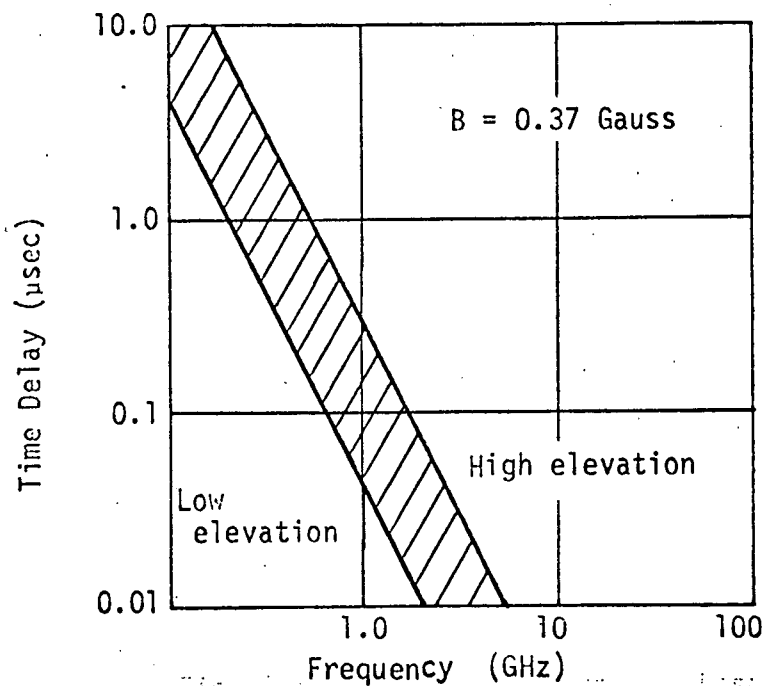


Fig. 2-20 Time Delay Between Phase Fronts of Ordinary and Extraordinary Rays

b. Birefringence

A electromagnetic wave impinging on a plasma in a magnetic field divides into two components called an ordinary ray and an extraordinary ray. These two rays, due to the differences in refractive indices, proceed independently through the ionosphere with different phase velocities.

The refractive index for each ray is given by

$$n = 1 - \left[\frac{N e^2}{m \epsilon_0} \left(\omega_p^2 \pm e \mu_0 H \frac{\omega_p}{m} \right)^{-1} \right]^{\frac{1}{2}}$$

where e , m , ϵ_0 , μ_0 are the electron charge and mass, and the free space permittivity and permeability respectively, and where, N is the number of electrons per cubic meter, ω_p is the radial propagation frequency, and H_0 is the component of the earth's magnetic field in the direction of propagation. The propagation delays which are birefringence induced are directly proportional to the magnetic field strength and inversely proportional to the cube of the propagation frequency. The effect of this delay is to produce a spreading of the energy in the signal being propagated. This spreading is manifested in a decreased signal amplitude and increased duration. The birefringent phenomenon can cause severe distortion of signals below 100 MHz. The time delay between the phase fronts of the ordinary and extraordinary rays is shown in Figure 2.20 as a function of frequency and elevation angle. Over the frequency range of interest the delay is on the order of nanoseconds and therefore has relatively insignificant effect on the channel.

c. Chromatic Aberration

Chromatic aberration may cause severe distortion in signals below 500 MHz. Because of the changing refractive index of the ionosphere, signals possessing many different frequency components will have their phase

relationship changed. This phenomena can cause severe degradation to pulse, type transmissions, and in effect reduce the level of received signal. The phase shift difference between phase components of a signal caused by aberration is inversely proportional to the square of the propagation frequency. The differential phase delay between ordinary and extraordinary rays for the frequency range of interest has a maximum value of less than twenty degrees per MHz of bandwidth. Such phase delay differences will have no apparent effect on the signal over the TDRS/user link.

4. Aurora

If the user satellites are orbiting near the polar regions interference from aurora could be anticipated. The physical effect of aurora is to change the ion density in the geographical area of interest and likewise the effects of most of the ionospheric channel parameters discussed previously. Aurorally associated absorption events occur at the auroral zones and at high magnetic latitudes, and are less frequent as one progresses toward lower geomagnetic latitudes. It has been shown^{*} that at frequencies around 30 MHz typical values of absorption have been measured to be on the order of 6 dB. Therefore, with the degree of absorption decreasing as the square of increasing frequency (i.e., for frequencies greater than 30 MHz), signal absorption due to auroral effects at 136-150 MHz, even for increases in the normal electron densities of from 2 to 3 orders of magnitude, is less than 1 dB and at S-band absorption is less than .1 dB.

D. RADIO FREQUENCY INTERFERENCE AND NOISE

In addition to interference resulting from multipath, the user satellites and the TDRS will be confronted with unintentional upward directed inter-

^{*}Rawer, Karl, "Propagation Problems with Space Radio Communications" Journal of Research of the National Bureau of Standards, Section D, Radio Propagation, Vol. 66D, No. 4, July-August 1962, pp. 375-393.

ference from emitters which are located on the earth and in view of the user satellites and in view of the TDRS. Furthermore, there are sources of noise influencing performance of the link. Each of these parameters will be investigated herein

1. The Effects of RFI

In order to evaluate the expected power levels experienced by the user and TDRS, The Magnavox Company, through the auspices of NASA, has collected printouts of various signal types and their power levels for Region II. This has been done for various frequency bands which have been allocated to space telemetry, command and control, and general exploration. The frequency bands covered in these analyses extend from 136 MC to as high as 33 GC and encompasses most of the available frequency bands allocated to space technology. Region II encompasses North and South America as shown in Figure 2.21.

In Table 2.2 we list the frequency bands investigated by Magnavox for their potential interference sources.

Table 2.2 Frequency Bands Covered by Interference Data for Region II

<u>Frequency Band</u>	<u>Comment</u>
136-138 MHz	good
148-154	looks bad
267-273	looks bad
401-402	looks good
465-466	marginal
2290-2300	good

The table is by no means exhaustive, but is felt to cover the primary frequency bands allocated to space technology in Region II.

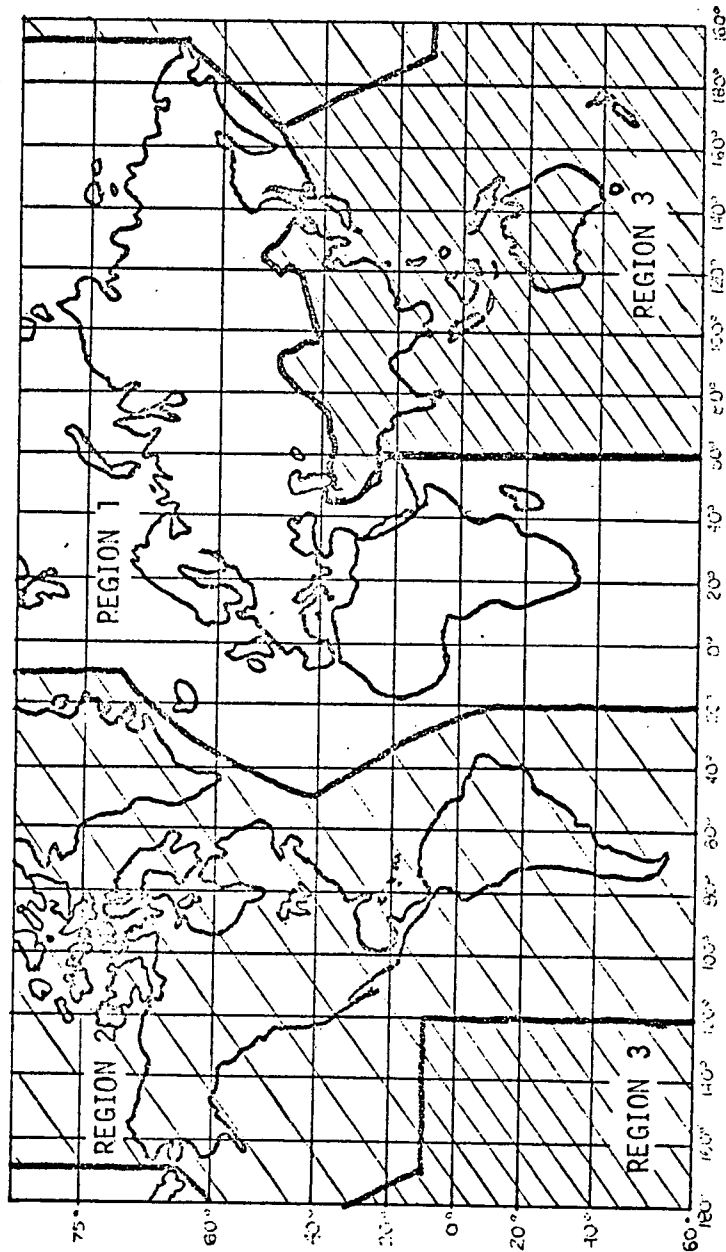


FIGURE 2.21 RFI Regions

John Bryan* of the NASA/GSFC, has catalogued the potential interference sources confronting a data relay satellite located over the west coast of South America in view of North America and South America. It has been indicated that at this time (1968) there was no significant sources of interference located in the 136 to 138 MHz band.

Emitters located just outside the 136 to 138 MHz band are allocated to the FAA and have on numerous occasions presented interference problems for the tracking facility at Rosman. There are over 1038 emitters assigned to the FAA for the frequency band 135.85 and 923 emitters at 135.95. These are typically 5 watt transmitters with essentially an omnidirectional antenna.

The user satellites will receive command information and R and R in the frequency band 148 to 149.9 MC from the data relay satellite. In the receive mode the user will be confronted with two sources of interference, one resulting from multipath and a second source resulting from emitters located on the earth which occupy the band of 148 to 149.9. Bryan has compiled a rather thorough list of emitters which occupy this band for Region II, and this list is presented in Table 2.3. It is obvious from the table

* John W. Bryan, "TDRSS Frequency Interference at VHF," GSFC DRSS TM002, July 31, 1968.

Table 2.3 Effective Radiated Power Per Emitter in Watts

Frequency MHz	Total Emitters	1-9	10-19	20-29	30-39	40-49	50-59	60-69	80	Greater than 100 watts
148.20	6		5				1			
148.21	47		7	32		1	1	6		
148.215	4		3		1					
148.22	37	11		6	16	2	2			
148.23	28	1				12	13	2		
148.24	17				16			1		
148.25	56	4	8	29	11	1	1	1	1	
148.26	3									3
148.29	176	31	18	61	22	4	34	1	4	1
148.51	53	11		35				7		
148.515	18				17		1			
148.52	149	17	53	40	22	3	5	4	5	
148.54	88	21	59	1		1	2	1	3	
148.545	12		11					1		
148.55	316	50	222	8	15	5	11	4	1	
148.56	1									1
148.575	1									1
148.59	16	1				11	4			
148.93	1						1			
148.95	32	17		9			4	2		
148.988	1							1		
149.00	33		1	31				1		
149.01	285	13	32	159	52	3	22	2	1	1
149.47	40	18		22				1		
149.48	229	64	37	14	110	1	1	2		
149.49	15			9			5	1		
149.50	150	60	44	1	34	4	5	1	1	
149.51	347	83	8	77	183	2	1	3		
149.53	40	25	7			4	4			
149.54	39	28	6			3	2			
149.55	13						1	12		
149.56	70	40	5	11	3	3	4	8	1	
149.565	47			47						
149.57	100	23	35	7	9	3	7	8	9	1
154.19	3				1	1	1			

that there are a large number of relatively high power sources which a user satellite, because of its omni-directional antenna, will be able to see when passing over various parts of the world. Needless to say that there will be hot spots and cool spots as viewed by the user satellite.*

2. The Effects of Noise

The noise sources that influence the TDRS/user link can be broken into two general classes: sources either external or internal to the physical system. Noise generated internal to the system are primarily a function of the noise sources from the antenna to the input stages of the receiver (including the transmission line). In discussing the intensity of external noise sources, the concept of equivalent temperature is used. Regardless of the actual nature (with exception of RFI) of the noise, all noise energy is assumed to be thermal radiation from a perfect black body. The noise sources can then be quantitatively modeled by applying familiar expression for thermal noise power $P_N = KT_a B$, where T_a is the effective antenna temperature. The expected carrier-to-noise power density level at the TDRS and user spacecraft for VHF and S-band is shown in Table 2.4.

Table 2.4 Expected Carrier-to-Noise Power Density Levels

Frequency Satellite	VHF	S-band
TDRS	44.6 dB-Hz	33.8 dB-Hz
USER	54.6 dB-Hz	44.9 dB-Hz

*[Intense interference has recently been observed in the 150 MHz command band by the OSO-IV Satellite. (ref: "Command Channel RFI and Its Effect on OSO-IV" X-154-68-413, April 69)]

E. CONCLUSIONS

It was stated at the beginning of Section II that the investigation of factors such as propagation path geometry, multipath, atmospheric effects, radio frequency interference and noise would be made to determine their effect (if any), either collectively or individually, on the performance of the communications link between the TDRS and the user spacecraft. In Table 2.5 is presented a summary comparison of the relative magnitudes of the propagation channel parameters. The data presented is for VHF (136-150 MHz) and for S-band (2.2-2.3 GHz), and provides an indication of the impact of the various parameters on the channel.

Even a cursory interpretation of the table indicates that on a relative basis those parameters which have a pronounced effect on channel performance are the following:

- (1) Free Space Attenuation
- (2) Multipath Time Delay
- (3) Direct Path Doppler
- (4) Differential Doppler (Specular Reflection)
- (5) Fading Bandwidth (Diffuse Reflection)
- (6) System Noise Power Density
- (7) Radio Frequency Interference

It is not implied here that the parameters which have been omitted from simulation are insignificant, but because of the predominating effects of those cited above, and the cost factors involved in simulating the effects of all the parameters even though they may only slightly affect the signals of interest, the aforementioned seven parameters are much stronger candidates for simulation.

In the design of the simulator which is presented in the sections that follow, it is essentially these seven parameters that will be considered.

Table 2.5 Comparison of the Relative Magnitude of the Propagation Channel Parameters for the TDRS/User Link

Description	VHF	S-band
<u>Attenuation Effects:</u>		
Free Space Attenuation		
Direct Path Loss	165-169 dB	189-192 dB
Indirect Path Loss	167-170 dB	191-193 dB
Ionospheric Absorption	<.1 dB	<.001 dB
Tropospheric Absorption	<.05 dB	<.3 dB
Losses due to Aurora	<1 dB	<.1 dB
<u>Refraction:</u>		
Ionospheric Refraction	<10 ⁻³ radians	<10 ⁻⁵ radians
Tropospheric Refraction	negligible	negligible
<u>Signal Phase Delay:</u>		
Ionospheric Effects	≈10 ⁻⁸ sec	≈10 ⁻⁸ sec
Tropospheric Effects	≈10 ⁻⁶ sec	≈10 ⁻⁸ sec
Birefringence	<10 ⁻⁹ sec	<10 ⁻⁹ sec
Multipath Time Delay	.2-30 msec	.2-30 msec
<u>Polarization Rotation:</u>		
Chromatic Aberration	< 2°/MHz	< 2°/MHz
Faraday Rotation*	≈ 200 degrees	≈ 1 degree
<u>Frequency Effects:</u>		
Direct Path Doppler	0-4 KHz	0-68 KHz
Differential Doppler	0-2 KHz	0-34 KHz
Fading Bandwidth	0-2 KHz	0-34 KHz
Coherent Bandwidth	5-30 KHz	5-30 KHz
<u>Carrier-to-Noise Power Density:</u>		
At TDRS	44.6 dB-Hz	33.8 dB-Hz
At User	54.6 dB-Hz	44.9 dB-Hz
Radio Frequency Interference	problem	minimal

* For systems employing circularly polarized antennas such as the TDRS, Faraday rotation effects are not encountered.

III. PRELIMINARY DESIGN OF THE TDRS CHANNEL SIMULATOR

In the sections contained herein, a general evaluation will be made of the basic design requirements of the TDRS channel simulator and a hardware specification presented for the implementation which will approximately realize the channel parameters selected in Section II. A summary of those parameter values is presented in Table 3.1. The values specified in the table cover a range which is actually in excess of what would typically be encountered over the TDRS/user link, thereby permitting modems to be tested under more severe conditions. In arriving at the selected design approach, the following points were considered:

- ° The ease and flexibility with which the simulator parameters could be changed by an external control unit.
- ° The cost of implementation traded off against the accuracy to which parameters could be adjusted.

Throughout this section it has been assumed that the input signal has a 2 MHz bandwidth. Accordingly, the preliminary simulator design presented in this report is based on such a signal. The primary objective of this study is to develop a functional design of a channel simulator with primary consideration given to implementation and cost.

In Section A a discussion of overall simulator block diagram on a functional basis is presented, and the basic simulator operation and control is discussed in Section B. The final portion of the report treats each of the

individual functional blocks in more detail. In some cases alternate techniques are discussed and for major components estimates of cost have been secured from various component manufactures.

Table 3.1
Summary of Simulator Parameters

PARAMETER	VHF (136-139 MHz)	S-BAND (2.3 GHz)
Differential time delay between Direct and Reflected Signals	0-30 ms	0-30 ms
Signalling Bandwidth	2 MHz	2 MHz
Maximum Differential Time Delay of Reflected Signal	256 μ sec	256 μ sec
Fading Bandwidth of Reflected Signal	\sim 0-2 kHz	\sim 0-34 kHz
Direct Path Doppler	\sim 0-4 kHz	\sim 0-68 kHz
Reflected Path Doppler	\sim 0-4 kHz	\sim 0-68 kHz

A. FUNCTIONAL FORM OF THE CHANNEL SIMULATOR

The general model of the channel simulator of Figure 1.3 can be configured to allow an apparent correspondence between the major components of the simulator and the propagation parameters of the TDRS/user channel. To

review the general characteristic of the TDRS/user channel, a characterization of the channel response in the time domain was shown in Figure 2.12(b). The earliest received signal is that of the direct path. After a delay the specular component of the indirect path occurs, followed by the diffuse components scattering from the surface of the earth. The direct and indirect paths are both subject to a doppler shift while the diffuse component is subject to a frequency spreading caused by the time variation of the scattering patch from which the indirect ray is reflected.

Figure 3.1 shows a functional arrangement of the simulator components. In this figure the upper signal line corresponds to the direct path between the repeater satellite and the user. A group of delay paths is provided in the lower section which provide the multiple delays characteristic of the earth scattering on the indirect propagation path between the TDRS and the user satellite. Each delay path is followed by a tap modulation unit which provides the capability of modulating the outputs of each of the delay paths with a complex gain function. The exact parameters of this gain function depend upon the propagation characteristics but in general consist of Rayleigh fading envelope and uniform phase distribution. In keeping with the TDRS channel model, the facility for adding a specular (non-fading) component on to the earliest multipath signal has been provided. This is accomplished with the separate path marked "Specular" in Figure 3.1.

Following the tap modulator unit the outputs of all delay path units are added together after which provision is made for the insertion of a frequency offset on the signal to provide the simulation of doppler effects of the channel. Simulated additive interference and noise can be inserted after the summation point as shown in the figure.

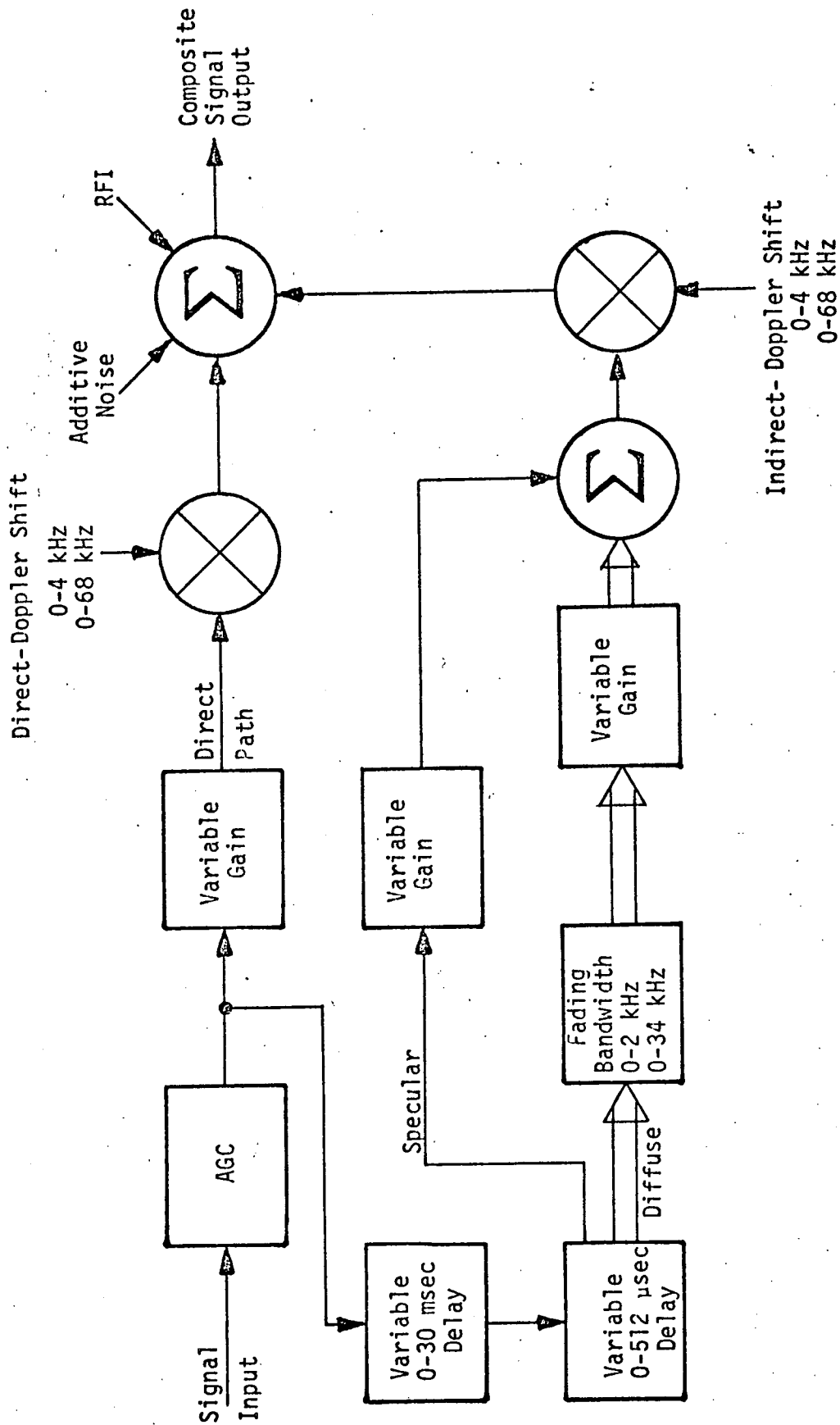


Figure 3.1 Functional Block Diagram of the TDRS Channel Simulator

In the sections which follow a detailed explanation of fundamental channel simulator operation will be presented and in Section III.C. a complete description of the simulator, both functionally and on a hardware basis (including costs), will be discussed.

B. OPERATION AND CONTROL OF THE SIMULATOR

To facilitate a description of the simulator operation we refer to the control panel layout shown in Figure 3.2. (The layout of the panel as shown can probably be simplified somewhat in the final configuration but will serve for the present illustration.) The top left-hand knob marked "SIGNAL" changes the frequency of the local oscillator which mixes the input signal down to baseband. Consequently, it must be set to correspond to the frequency band of the input signal. The function of the MODE knob will be explained in the following paragraphs. A given set of simulation conditions is uniquely determined by the contents of 21 registers, namely:

- ° Two Doppler Registers
- ° Nine Path Gain Registers
- ° Eight Delay Registers
- ° One Additive Noise Register, and
- ° One Fading Bandwidth Register

Detailed descriptions of these register functions are deferred to the end of this section.

When the MODE switch is in its AUTO position, the contents of these 21 registers will be determined by an external control unit and will vary



Figure 3.2 Simulator Control Panel

dynamically at any rate selected by the control unit. This is referred to as the dynamic controlled operation and provides the following:

- 1) Complete Orbit Dynamics
- 2) Preemptive Resume Control
- 3) Preemptive Repeat Control
- 4) On-Line User Interaction
- 5) Programmable Tests
- 6) Real and Virtual Time

Since Figure 3.2 is intended only to show control functions, no attempt is made to show input and output signal jacks, control unit connectors, on-off switch, etc. At some point in the course of a given simulation, however, it is conceivable that one would wish to suddenly "freeze" the changing contents of the parameter registers at their current values. For example, if one were to discover that a given set of conditions gave rise to loss of sync, high error rate, etc., he might wish to freeze the simulated channel conditions in this unfavorable state, make a record of what they were, and perhaps do further investigation before continuing. To do so the operator sets the MODE switch to MANUAL. The contents of the parameter registers would then remain at the last value specified by the control unit prior to the MODE switch being changed, and this binary value appears on the appropriate set of register lights. As long as the MODE switch remains in MANUAL, the parameter registers maintain their fixed value. This is referred to as "Static" stand-alone operation and provides for:

- 1) Independent Operation
- 2) Manual Setting of Controls
- 3) Frozen Orbit Statistics
- 4) Independent Calibration

Under such conditions the only "dynamic" process going on in the simulator is the random variation of the Rayleigh modulated gains (i.e., the FADING BANDWIDTH REGISTER, whose value is now fixed, only specifies the bandwidth of these random processes), and the additive noise process.

With the MODE switch in its MANUAL position the contents of each of the 21 registers can be manually set to any given value by use of the appropriate bank of switches shown on the control panel. For example, to manually enter a particular gain value for, say, the specular path, the GAIN select switch is set to position 9, the ten switches of the path gain register are set to their appropriate positions, and the MANUAL ENTER key is depressed.

The MANUAL MODE position not only allows one to "freeze" the dynamically varying parameters from an external control unit, but in fact allows one to specify these parameters manually without the aid of a control unit. In this latter case, of course, one could get "dynamic" behavior of the registers only in the sense that he could manually change them from time to time. The ability to manually set up a given set of simulation parameters is an extremely important and desirable characteristic. With this feature, the simulator can be used to simulate a given set of fixed channel conditions without the need for an external control unit. In view of the fact that a digital design approach in most cases has proved to be desirable, this feature is obtained with very little additional cost.

Shown on the front panel are five display banks labeled DOPPLER, PATH GAIN, DELAY, FADING BANDWIDTH and ADDITIVE NOISE. Their contents at any time indicate the present value of that parameter. Although the functions of these various registers have been referred to throughout the report, we include a

brief review in the following paragraphs:

DOPPLER REGISTERS. The direct path doppler will vary from 0 to ± 68 kHz in steps of 50 Hz. This corresponds to 2722 discrete frequencies, and can therefore be specified by a 12-bit number. For the reflected path, the maximum doppler is ± 34 kHz (680 discrete frequencies) which requires 11 bits.

PATH GAIN REGISTERS. The implementation of the variable gain introduced into the direct and specular paths (as well as the seven diffuse components of the reflected signal) is described in Section III.C.1-d. For simulation purposes, it will be adequate to provide approximately 50 dB of dynamic range (attenuation) on each of these nine paths. Using the technique described in Section C1-4, this would be done in 256 steps of approximately .19 dB each over a 48.2 dB range. In addition, one register setting will be devoted to removing the path entirely (i.e., infinite attenuation). For a 256 step gain quantization, one can readily determine that a total of 8 bits is required to specify the gain of any path.

DELAY REGISTERS. It has been determined that the 30 msec delay line would consist of 117 taps spaced at 256 μ sec intervals. Hence, the tap on the 30 msec line can be specified by a 7-bit number. This tap feeds a delay line having 4096 taps. Of these 4096 taps, 2048 are addressable as is discussed in Section III.C.4. Consequently 11 bits are necessary to specify the position of any of the seven multipath components.

FADING BANDWIDTH REGISTERS. The fading bandwidth will range anywhere from 20 Hz to 34 kHz. It is envisioned that this will be accomplished using

two separate filters each having a range of less than 50 to 1. For example, filter #1 would cover the full range of VHF variation from 20 to 2000 Hz, while the second would vary from, say, 2 to 34 kHz. Under the assumption that the filter bandwidth will change linearly with the binary control number from the control unit, an 8-bit control word would provide approximately 8 Hz increments for filter #1 and approximately 125 Hz increments for filter #2. It is felt that smaller increments than this are not necessary. One of the 8-bit control words, the all zero word for example, will be reserved to set the fading bandwidth to zero as discussed in Section III.C.5. It should be pointed out that the fading bandwidth of all 7 diffuse components are determined by the contents of the single FADING BANDWIDTH REGISTER, and are therefore identical. This is in keeping with the TDRS channel model in which the average fading bandwidth from all annular reflecting rings of equal delay is the same. If separate control of the fading bandwidth of each component in the diffuse path is desired, we estimate that the total cost of the additional simulator hardware will be increased on the order of 1%.

ADDITIVE NOISE REGISTER. Additive noise is introduced just prior to up-conversion. At this point the signal amplitude is determined by the contents of the nine path gain registers. Knowing the contents of these registers allows any specific signal-to-noise ratio to be set up by properly setting the contents of the ADDITIVE NOISE REGISTER. For purposes of simulation, a 50 dB variation of additive noise is adequate, and will be controlled digitally by means of a switchable ladder attenuator. This attenuator will be similar to the type described in the paragraph on PATH GAIN REGISTERS, and will provide for increments in steps of approximately 0.2 dB. A bandpass filter following the wideband noise source will limit the noise bandwidth to the 0.75 to 2.75 MHz region in which the signal is located.

It is evident that the state of the simulator at any given time is determined uniquely by:

- 1) The contents of the 19 DOPPLER, GAIN and DELAY registers.
- 2) Information to determine which of the two fading bandwidth filters is in use.
- 3) Contents of the FADING BANDWIDTH and ADDITIVE NOISE registers. In the AUTO MODE, items 1, 2 and 3 are determined by an external "control unit" and communicated to the simulator via an appropriate interface. The number of bits necessary to determine a simulator state is easily found to be:

2 Doppler Registers @ 12 bits/register	= 24
9 Gain Registers @ 8 bits/register	= 72
8 Delay Registers @ 11 bits/register	= 88
1 Fading Bandwidth Register @ 8 bits	= 8
Doppler Register Control	= 1
1 Additive Noise Register @ 10 bits	= 10
	<u>203 bits</u>

Since the parameter values specified by these register contents change at a rate determined by the orbital motion of the satellite, it is evident that for real time orbital simulations, an updating of the register contents on the order of every few seconds is quite adequate. For nonreal time simulations, this updating might take place "several" times per second. At any rate it is clear that a maximum data transfer rate between the control unit and the simulator on the order of 1000 bits/sec is adequate.

In view of the relatively low data rate needed to specify the time variation of the simulation parameters it is clear that one does not want to tie up an expensive digital computer for the duration of a simulation. A

more satisfactory alternative appears to be one whereby a mini-computer is programmed to generate the channel parameters from a knowledge of the orbital parameters. For on-line control a PDP-8 (or equivalent) with 4-K of memory appears to be adequate. A mini-computer of this type costs approximately \$5000. These channel parameters values could then be recorded on tape, or fed directly into the simulator. In either case attention will have to be given to proper formatting of these data so that it can be loaded into the simulator parameter registers.

C. FUNCTIONAL DESIGN OF THE SIMULATOR

1. Discussion of Overall System

The overall system block diagram is shown in Figure 3.3. The 2 MHz wide input signal is assumed to be an IF signal at 70 MHz. Throughout the text to follow, when referring to the baseband signal, the 2 MHz signal translated down to occupy a bandwidth from approximately 0.75 to 2.75 MHz is implied.

a. Baseband Frequency Selection

The reason for selecting a baseband of 0.75 to 2.75 MHz is due to the fact that a digital technique was selected for obtaining the delay required for proper simulation. This requires sampling the analog baseband signal (at a rate sufficiently above the Nyquist rate that aliasing spectra can easily be filtered) and converting the sampled level into a binary number. Since binary storage is expensive and increased linearly with the sampling rate, the baseband must be placed as low as possible. Unfortunately, the baseband cannot be located from 0 to 2 MHz because a single sideband operation must be performed later in the system (i.e., doppler spectrum shift as discussed in Section III.C.3 and SSB up conversion as shown in Figure 3.3). This operation could not be performed properly on a baseband spectrum where the lower end approaches DC. The vestigial filtering technique for performing the SSB operation in the doppler spectrum

shift unit has the drawback that, as the low end of the baseband gets closer to DC, the skirt roll-off characteristics of the required vestigial filter become more and more severe. Over the range of 2.75 MHz to 0.75 MHz, however, the problem is not severe. The SSB up conversion to 70 MHz at the simulator output will be performed by a single conversion. By locating the baseband signal in the .75 to 2.75 MHz range, the undesired IF sideband is 1.5 MHz away from the desired one. Vestigial SSB filters (for example, the ITEL Model FBT/2-70/2-9/50-3A/3A) are available which will provide 50 dB of attenuation to this sideband. This filter has adequate inband phase and attenuation characteristics.

b. Low Pass Filtering and AGC

The purpose of the low pass filter (Figure 3.3, Unit #2) is to remove the double frequency component at the filter output (138.5 MHz). Since steep skirt selectivity is not required, a Bessel filter has been selected to provide minimum phase distortion. Since the level of the signal at this point (and throughout the simulator) is relatively large, the noise figure of this filter (or the mixer before it) is not critical. This is evidenced by the fact that for a bandwidth of 3 MHz thermal noise (at room temperature) is on the order of -110 dBm. Hence, even if this filter is built using relatively noisy active devices, its noise figure will not be a significant factor.

The purpose of the AGC unit (Figure 3.3, Unit #2) is to make the average signal power approximately constant regardless of whether it occupies the full 2 MHz bandwidth or not. This insures that the dynamic range of the subsequent A/D converter is efficiently utilized. Since the peaking factor of the signal will change with its bandwidth and type of modulation, the exact level (relative to the maximum quantization range of the A/D converter) set by the AGC is specified by the input signal level. The time constant of this

AGC must be on the order of 10 times the reciprocal of the minimum bandwidth signal that will be processed by the simulator. This of course is to insure that signal modulation will not be removed by the AGC.

c. A/D Converter

The A/D converter operates at an 8 MHz sampling rate, with an 8 bit accuracy. This sampling rate places the lowest aliasing frequency at 5.25 MHz. These aliasing frequencies must, of course, be removed by filtering as discussed in Section III.C.1-f.

Under the assumption that the signal has a Gaussian probability density function, an AGC adjusted to make the rms signal amplitude fall at one-sixth of the total (peak-to-peak) quantization range will cause the signal to fall outside this range only 0.1% of the time. For 8 bits of uniform quantization under these conditions, one can readily show that the signal power to mean square quantization noise is slightly greater than 43 dB. For a uniformly distributed signal, this figure would be 48 dB, enough to provide sufficient accuracy for TDRS simulation.

At this time two companies which manufacture an 8-bit A/D converter operating at this conversion rate have been identified. They are Inter-Computer Electronics, Inc., Landsdale, Pa., and American Astrionics, Inc., Palo Alto, California. These units are rack mounted in a standard 19" relay rack, and cost on the order of \$7000. Due to the present state-of-the-art, these units must be custom-built, and consequently cannot be obtained as an "off-the-shelf" item.

The bit stream from the A/D converter enters a multistage shift register which in essence has 117 taps spaced every 256 μ sec up to a total delay of 30 msec. The details of this 30 msec delay line (Figure 3.3, Unit #4) are discussed further in Section III.C.2.

d. Generation of Direct Path Signal: Variable Gain and Doppler Spectrum Shift Units

The input to the A/D converter (i.e., before conversion) plays the role of the "direct path" between the user and TDRS satellites.

Variation in signal gain along this path as a function of orbital parameters is accomplished by the "Variable Gain" unit (Figure 3.3, Unit #9). This unit is identical to those in the Specular and Diffuse Signal paths shown in Figure 3.3. This unit is envisioned as a standard ladder attenuator having 8 switchable sections. Each section changes the attenuation by a specific power of 2. Hence, a range of $2^8:1$ (i.e., 48.2 dB) of attenuation is possible in steps of approximately .19 dB. The most critical factor in the design of this ladder appears to be the implementation of the switching device. If a solid state switch is used, care must be taken to insure that capacitive coupling across the switch is negligible over the frequency range of interest (up to 2.75 MHz). Furthermore, the on impedance must be low compared to the respective ladder element. Mechanical switching (relays) will avoid these problems at some reduction in hardware reliability. A suggested relay (\$4.50/unit in small quantities) for this purpose is the Struthers Dunn Model MMRIADS (form A contacts). This unit (packaged in a dual-in-line configuration) operates from standard TTL logic levels (0,+5 volts) and will switch 100 MA of current in approximately 2 ms.

The Direct Path signal experiences up to about 4 kHz of frequency offset for the VHF simulation and approximately 17 times this offset (68 kHz) for the 2.3 GHz S-band simulation. This offset is obtained by a straightforward up conversion followed by SSB filtering, and down conversion, to baseband again with a precisely controlled offset frequency. The details of the doppler spectrum

shifting technique are described in Section III.C.3. An identical technique is used to effect doppler shift of the multipath signal (Figure 3.3, Unit #10).

e. Digital Delay Lines for Generation of Multipath Components

Under direction of the control unit, any one of the 117 taps of the 30 msec line can be fed to a short, multitap delay line (Figure 3.3, Unit #5) for purposes of generating the "reflected signal". This short line contains 4096 taps spaced one-eighth μ sec apart over a 512 μ sec interval. Seven taps are used to generate a time "diffuse" component of the reflected wave which can last up to 256 μ sec. The earliest of these seven taps is used to generate the "specular" component of the reflected path. The implementation of the 30 ms delay line is discussed in Section III.C.2. Details of the short delay line are discussed in Section III.C.4.

f. D/A Conversion and Filtering of the Aliasing Frequencies

The seven analog signals which make up the reflected path signal are each obtained by D/A conversion of the appropriate 8-bit digital signal. A suggested D/A converter (Figure 3.3, Unit #5) is Analog Devices Model MDA-8F (\$220/unit in small quantities). This high speed, 8-bit D/A converter will settle to within .05% of full scale within 40 ns. As discussed in Section III.C.1-c, the lowest aliasing frequency resulting from the sampling process occurs at 5.25 MHz. An aliasing filter (Figure 3.3, Unit #6 with at least 35 dB of attenuation at this frequency is recommended. To minimize signal distortion, the pass band ripple (up to 2.75 MHz) should be less than -1 dB (peak-to-valley) and the change in group delay across the pass band should be less than 10%. Discussion with Axel Electronics, Jamaica, New York has indicated that a custom-built filter of this type can be readily built, and will cost on the order of \$100 in small quantities.

g. Fading Bandwidth Modulation

A fading bandwidth specified by the controller unit, as indicated previously, is introduced onto the diffuse multipath components. A fading bandwidth up to 2 kHz can be selected for the VHF simulation, and up to approximately 34 kHz for the S-band simulation. The fading bandwidth modulator (Figure 3.3, Unit #7) is discussed in Section III.C.5.

h. Miscellaneous Considerations

In several cases, the inability to implement the functions as ideally specified in Table 3.1 results in a certain amount of signal distortion, residue noise, etc. Generally, we have required that any implementation technique be good enough that these undesired interfering signals are down by at least 40 dB from the desired signal. In addition, no attempt has been made to have the simulator provide for the total free space path attenuation over the direct and reflected paths. If it is desirable to simulate the actual input signal levels that the receiver would see (in this case at IF), then such control must be provided for by external attenuation. This in itself is not a burdensome task, and can be accomplished with fixed attenuators. The variation in path loss (approximately 4 dB) as a function of grazing angle, however, is provided for by the variable gain control elements in the simulator.

2. 0-30 msec Variable Delay Line

Several techniques for obtaining the necessary variable delay of the 2 MHz signal were considered. The techniques which were considered

could be classified as either analog or digital, according to the following list:

Analog Techniques

Recirculating Quartz Delay Line
Tape (analog)

Digital Techniques

Drum
Core
Disk
Tape (digital)
MOS-LSI Memory

The longest practical quartz delay line can provide 4 msec of delay. Microsonics could provide such a line, having 20 MHz of bandwidth (extending over the range of approximately 20 MHz to 40 MHz) for about \$4000 per unit. Four or five recirculations of the 2 MHz signal could probably be frequency multiplexed into a single 20 MHz line, in which case two lines would be sufficient to achieve the full 30-msec of delay. In such a case, however, the effective "tap spacing" is 4 msec which is considered too coarse for this application. This could be remedied with one additional recirculating 1 msec line whose input could be any one of the coarse 4 msec taps. Using this procedure, one could position a single tap in increments of 1 msec.

General Atronics has used this technique with reasonable success in the past^{*}; however, in such applications the signal being recirculated utilized only a small portion of the available delay line bandwidth, resulting in negligible distortion being introduced as a result of nonlinear phase and/or amplitude characteristics of the line. In the present application, however, this is not the case. Furthermore, the cost of the delay lines, associated

^{*} Zimmerman, M.S., J. H. Horwitz, "A Flexible Transmission Channel Simulator," Paper 17.2, 1967 IEEE International Conference on Communications, Minneapolis, Minn.

amplifiers, multiplexing oscillators, filters and additional hardware is only a small fraction of the engineering costs involved in designing and debugging such a loop. It is for these reasons, the technique is not considered optimum.

Any digital technique requires, of course, that the storage unit be preceded by an A/D converter. As discussed at the beginning of this section, the highest frequency in the baseband signal is 2.75 MHz, and we have chosen to sample this at an 8 MHz rate. As a result, the lowest aliasing frequency falls at 5.25 MHz which can be adequately removed by conventional filtering. Each of these samples is then converted into an 8-bit word, resulting in an effective 64 MHz bit rate. The output of the A/D converter is 8 separate 8 MHz signals representing the 8 bits from LSB to MSB.

In order to obtain 30 msec of delay, the storage unit must have a capacity of approximately 2×10^6 bits. Although this amount of storage can be obtained with a single disk unit, the read/write bit rate is typically limited to about 4 MHz. At a cost of \$4000 per unit, any approach using disk units appears to be impractical.

Drum systems suffer from basically the same drawback. For example, a unit manufactured by Vermont Research Corp. consisting of 64 heads operated in parallel would have provided both the required storage and read/write time. The cost to implement this approach is approximately \$130,000.

The major drawback with a tape system is the limited speed of the tape transport, which typically, for commercially available units, is an order of magnitude slower than that required for this application. In addition, the requirement of varying the delay from nearly zero to 30 msec makes this approach impractical.

A typical 8K-word core stack (32 bits/word) with a 500 nsec cycle time can be obtained for about \$17,000 (including the associated input and output registers, drivers, etc.). Several of these could conceivably be operated in parallel to obtain the required storage but the resulting cost is well over \$100,000.

The most practical (and cost effective) approach is offered by presently available MOS-LSI shift register memories. For example, the INTEL 1403 is a 1024-bit shift register available in a single TO-5 can with taps at 512 and 1024 bits. In the quantity required for this application the cost of these units is less than one cent/bit. Approximately 1900 of these units would be required to provide the 2×10^6 bits of storage necessary. These units can be clocked at a maximum rate of 5 MHz; however, to keep power dissipation to a minimum (approximately 0.15 mw/bit) the units will be operated at approximately 2 MHz. Commutation (x32) provides the required 64 MHz bit rate. The October 1970 price of the INTEL 1403 is \$10.35 per unit in the quantities necessary (1900). As a result the cost for MOS storage is approximately \$20,000.

One can readily determine that the power dissipated by approximately 2000 TO-5 cans (or dual in-line packs) is on the order of 0.3 kw ($0.15 \text{ mw/bit} \times 2 \times 10^6 \text{ bits}$). At the present time we conceive of packaging forty TO-5 cans on a single PC card, ten cards per 19" cage and five cages stacked in a standard 19" relay rack housing.

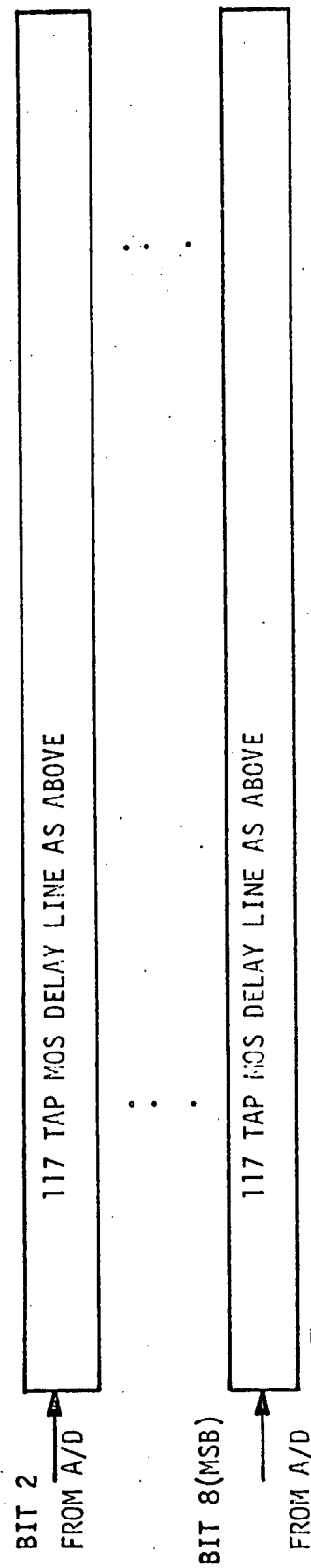
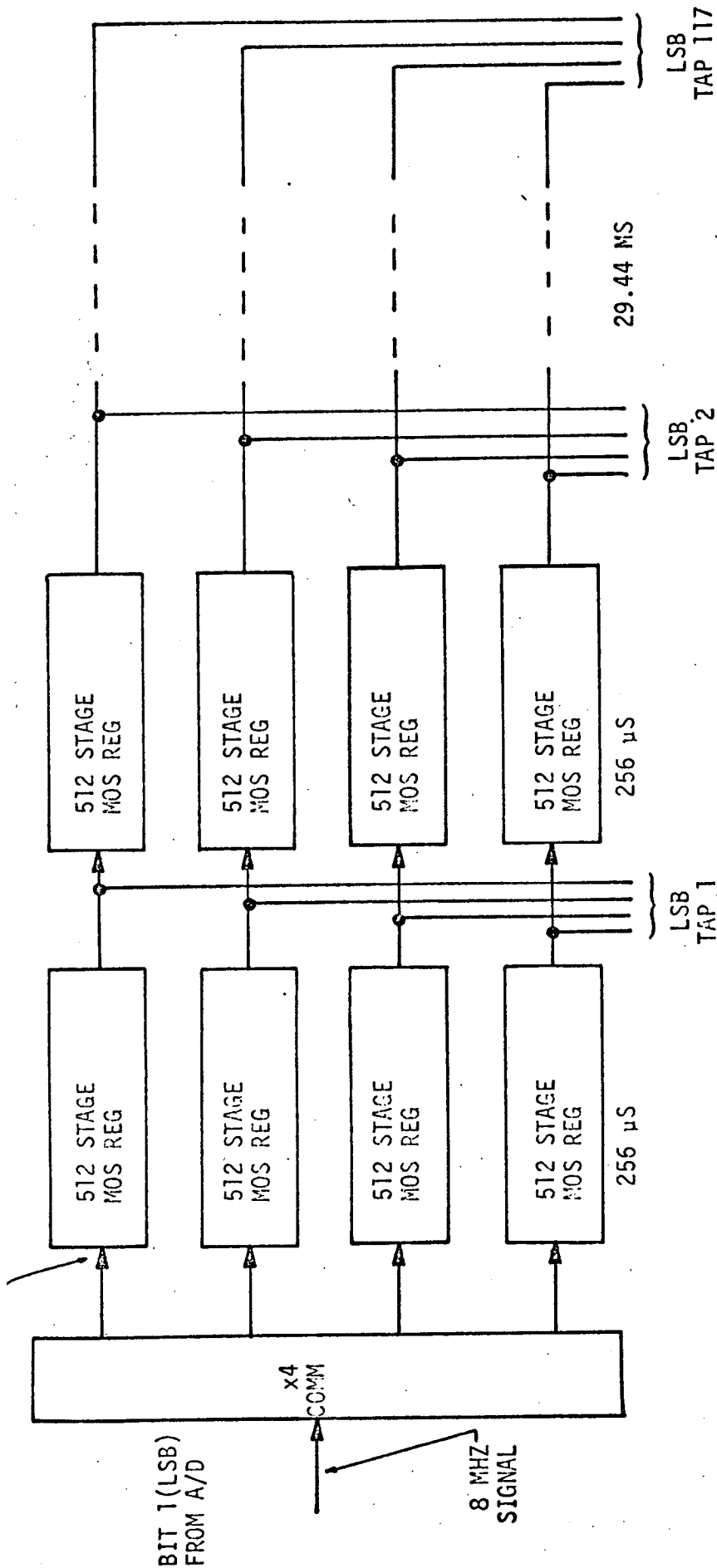
In addition to its relatively inexpensive cost and simplicity from an engineering design point of view, this approach offers considerable flexibility from a control point of view. In particular, since taps are available every 512 bits, and the clock rate is 2 MHz, the effective delay

increment between taps is 256 μ sec. (This can be reduced to 128 μ sec by use of the INTEL 1402 which is somewhat more expensive.) To achieve the desired 30 msec maximum delay 117 taps are required any one of which can be selected by the control unit with a 7-bit address. The basic configuration of the MOS memory is shown in Figure 3.4.

3. Implementation of the Doppler Spectrum Shift Unit

The "direct path" signal between the user and TDRS satellite has no delay (for purpose of simulation) and can, therefore, be taken directly from the output of the AGC unit (before the A/D converter). This signal then passes through a variable gain element whose value is established by the control unit, and which simulates change in power received along the direct path between user and TDRS satellites. At this point the direct path signal spectrum is doppler shifted by an amount which can vary anywhere from 0 Hz to 68 kHz as specified by the control unit. This is done in the unit referred to as the "Doppler Spectrum Shift" unit in Figure 3.3. The doppler spectrum shift unit for the "reflected path" is identical in implementation to the one in the direct path of Figure 3.3 and as such will be discussed as a single unit. When in operation, these two units will be introducing different doppler shifts at any given time under supervision of the control unit. As much as 68 kHz of doppler effect may have to be introduced as indicated in Table 3.1. It is worth observing that the initial translation from 70 MHz down to baseband at the simulator input is performed with the same oscillator which is used to go from baseband back up to 70 MHz at the simulator output. This is done deliberately to insure that these translations will not be a spurious source of doppler shift.

There are a number of ways by which spectrum shifting can be achieved. First, the method which is preferable will be described, then



TOTAL: 1872 INTEL 1403 DUAL
MOS REGISTERS (1024
BITS EACH)

Figure 3.4 MOS DELAY LINE

reasons as to why it has been chosen over some alternate techniques will be presented.

A block diagram of the spectrum shifting technique is shown in Figure 3.5. From this figure it can be seen that the basic technique consists of mixing the baseband signal up by a precise frequency in single sideband fashion, then mixing it back down with a frequency which is offset by the desired doppler shift. It is very important that the offset of the mixdown frequency be both stable (so that doppler shift calibration is accurate) and easily controlled (for interface with the control unit). For this technique a fixed up conversion frequency of 4 MHz has been assumed. The down conversion frequency is determined by the VCO which has a center frequency of 4 MHz and can be varied over approximately $\pm 1.5\%$ (± 68 kHz). If the countdown register is set to $N = 80 \times 10^3$, then phase-lock (at 50 Hz) will occur only when the VCO frequency is equal to the up-converter frequency. If N is then changed to, say $80 \times 10^3 + 1$, then phase-lock will occur when the VCO frequency is 50 Hz greater than the up-converter frequency. Obviously, different integer values of N will result in a doppler offset frequency which is some integer multiple of 50 Hz. It is felt that discrete steps of 50 Hz is adequately small for simulation purposes. Consequently, the countdown register will be a 17-bit register which can be preset to any integer between 78,640 and 81,360 at the discretion of the control unit.*

*In general, the output of a straight countdown chain will not have a 50-50 duty cycle (necessary for phase comparison) unless the final stage is a $\div 2$. This can be arranged by running the VCO at 8 MHz and adding a flip-flop at the output of the countdown chain, and before the down-converter mixer.

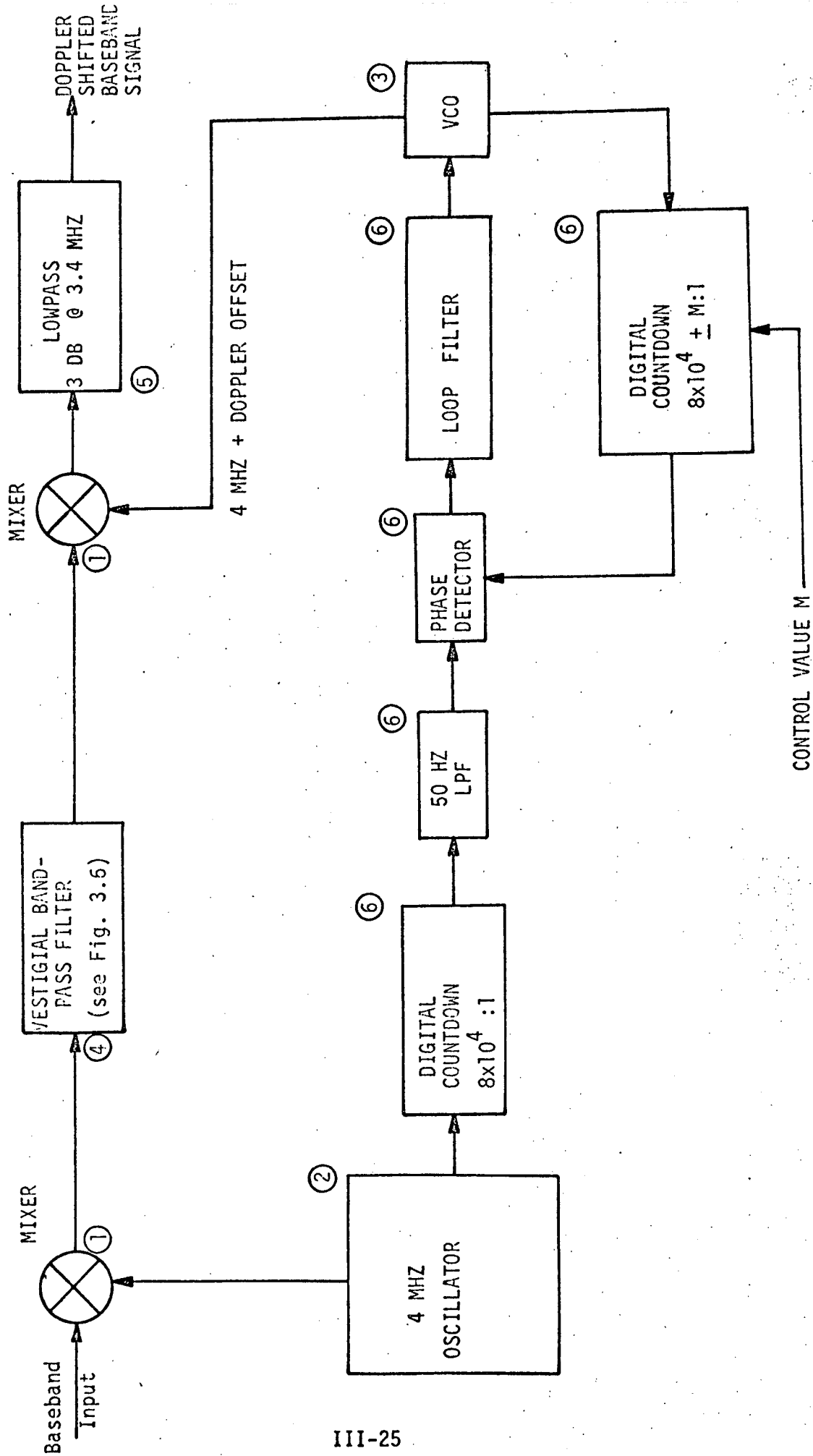
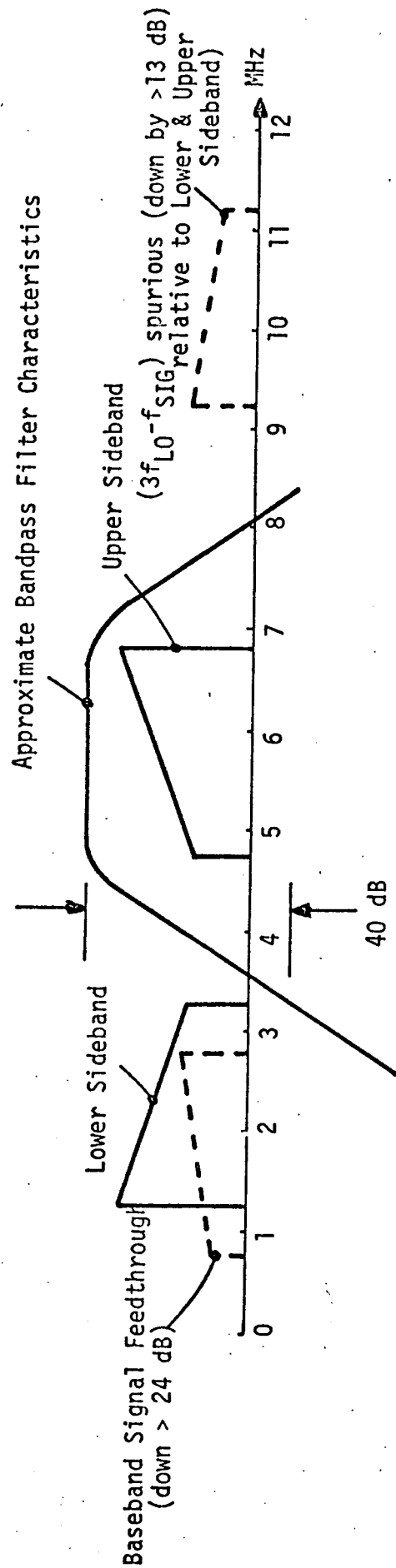


Figure 3.5 DOPPLER SHIFT UNIT

The technique selected for single sideband conversion shown in Figure 3.5 is one of vestigial filtering, and consists of locating a band pass filter between the up-converting and down-converting mixers. The selectivity of this filter is determined by the various spectra produced by the mixing process. In addition to the upper and lower sidebands, the two major spurious mixer responses are direct feed-through of the baseband signal and the intermodulation product of the input signal, f_{SIG} , and the local oscillator, f_{LO} , which is located at a frequency of relative location of these various spectra is shown on Figure 3.6. The 24 and 13 dB levels associated with the spurious responses were obtained from manufacturer's data on the RELCOM Model M1 mixer, and are representative of good commercial balanced mixers. From that figure it is seen that a bandpass filter centered about the upper sideband with skirt attenuation on the order of 40 dB at 3.25 and 9.25 MHz will remove the lower sideband (as required for single sideband conversion), as well as the spurious mixer spectra. Discussion with a filter manufacturer (AXEL Electronics, Jamaica, New York) has indicated that such a filter can be manufactured for about \$125 (in single quantities). The filter would have less than $\pm 1/2$ dB ripple, and less than a 10% change in group delay across the passband from 4.75 to 6.75 MHz.

The purpose of the low pass filter following the down-conversion mixer is to remove the sum frequencies (between 8.25 and 10.25 MHz) from the desired baseband (.75 to 2.75 MHz). This is not a particularly difficult



Note: Up Conversion Frequency - 4 MHz

Figure 3.6 Major Spectra Produced by Mixer Operation

filtering requirement, and can be done, for example with a 5-pole Butterworth having a 3 dB cutoff frequency of approximately 3.7 MHz. This will provide approximately 40 dB of attenuation to the lowest sum frequency.

Consider now the fundamental operation of the phase-locked loop. The phase detector operates as follows: A single shot, generating a 15 ms pulse, is fired on the positive-going zero crossings of the 50 Hz reference sinewave. The first digital transition which occurs at the output of the variable countdown chain is used to trigger a sample-and-hold on the value of the reference sinewave. The sampled value is proportional to the phase error ψ between the 50 Hz reference signal and signal derived countdown generator, and is applied to the loop filter. The loop filter can be a single pole lowpass with a cutoff frequency somewhere on the order of 0.5 to 1 Hz. It can be shown by considering a standard analysis of the phase-locked loop, that the fixed DC offset typically introduced by a sample-and-hold circuit (on the order of a few millivolts) will not introduce any steady state frequency errors. In Figure 3.7 it has been assumed that the phase detector is ideal, the loop filter has a transfer function of $H(s)$, and the gain of the VCO is K Hertz/volt. For a typical 4 MHz VCO that can be pulled by 60 kHz with a 3-volt level, K is found to be 20×10^3 Hz/volt. The effect of the loop count-down circuit (not shown in Figure 3.7) can be accounted for by assuming that the VCO operates at 50 Hz rather than 4 MHz; hence the value of K used in the analysis must be $(20 \times 10^3 / 80 \times 10^3)$ Hz/volt or

$$K = 0.25 \text{ Hz/volt}$$

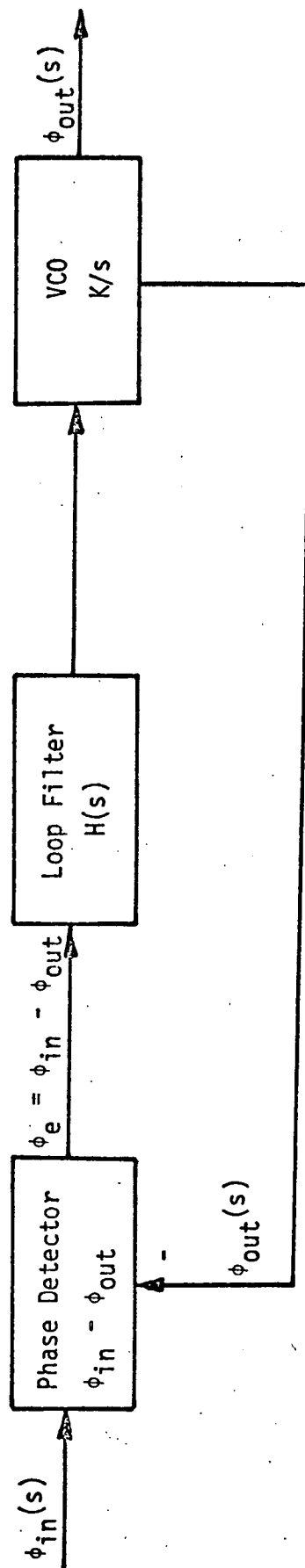


Figure 3.7 Linear Phase Locked Loop Model

Assuming there is no DC offset introduced by the phase detector or the loop filter, then the signal phase at the VCO output is

$$\phi_{out} = \frac{K}{s} H(s) \phi_e \quad (3.1)$$

where ϕ_e is the phase error between the reference and VCO.

A DC offset, Δ_{DC} , appearing at the output of the loop filter would modify the above expression to be

$$\phi'_{out} = \frac{K}{s} H(s) \phi_e + \Delta_{DC} \frac{K}{s} \quad (3.2)$$

Then, (3.2) can be rewritten as

$$\phi'_{out} = \frac{KH(s)}{s+KH(s)} \phi_{in} + \Delta_{DC} \frac{K}{s+KH(s)} \quad (3.3)$$

from which it is evident that in steady state the error term $\Delta_{DC} K/s+KH(s)$ goes to zero.

To obtain some feeling for the response time of this loop the error term in (3.3) is neglected, and it is assumed that the input to the loop is a step in frequency of Δf . Assuming the loop filter is a simple lowpass type with a transfer function of

$$H(s) = a/s+a \quad (3.4)$$

Substitution into Equation (3.3) results in a time response, $f(t)$, of the output frequency of the loop (to a frequency step input) of the form

$$f(t) = \Delta f [1 - e^{-at/2} \{ \cosh[(a/2)^2 - aK]^{1/2} t + \frac{a/2}{[(a/2)^2 - aK]^{1/2}} \cdot \sinh[(a/2)^2 - aK]^{1/2} t \}] \quad (3.5)$$

If we assume that the 3 dB bandwidth of the loop filter is 1 Hz (i.e., $a = 2\pi$), and K is the value given previously (0.25 Hz/v), then $(a/2)^2 \gg aK$ and for t greater than about 1/2 second we can write equation (3.5) as

$$f(t) \approx \Delta f \{1 - e^{-Kt} \left[\frac{1 - K/a}{1 - 2K/a} \right]\} \approx \Delta f \{1 - e^{-Kt}\} \quad (3.6)$$

Hence for all practical purposes, the loop responds like a single pole lowpass filter with a time constant of 4 seconds.

At this point the following observation can be made. In a real time orbital simulation, the doppler changes more or less linearly with time except when the user spacecraft is at low elevation angles. In particular, one can generate the chart (Table 3.2) of maximum doppler rate (which also occurs in the linear region) for various orbits:

Table 3.2 Maximum Doppler Rate as a Function of User Altitude

ORBIT HEIGHT	DOPPLER RATE	
	VHF	S-BAND
4000 km	4.4 Hz/sec	75 Hz/sec
1000 km	8.6	146
250 km	17.2	292

Consider now the case of a 4000 km orbit at VHF. Since the doppler loop as we have configured it can be changed only in increments of 50 Hz, it is evident that it will have to be incremented about once every 11 seconds (in the linear region). Since the loop response is that of a lowpass filter of time constant K, the initial rate of frequency change of the loop to a step of 50 Hz (assuming the loop starts in steady state) is $50 \cdot K \frac{\text{Hz}}{\text{sec}}$ (i.e., 12.5 Hz/sec). This is about a factor of 3 greater than the actual maximum orbital doppler rate, and may in fact be outside the design limits of the unit being tested with the simulator. This problem can be remedied by decreasing the K factor to about 0.09. Under such conditions it is likely that the maximum rate of 4.4 will never be exceeded by very much, but now there will be a time lag of a few seconds between the controller command signal, and the time that the simulator actually generates that doppler value.

Although this lag time should not affect the results of any testing performed with the simulator, some thought has been given to alternate techniques. Any alternate technique must also have the capability of changing the simulator doppler smoothly from one frequency to the next, since discrete steps -- even small ones -- place a burden on the equipment being tested. The technique that we consider to be the best alternate to the previous one is shown in Figure 3.8.

Referring to the block diagram of Figure 3.8, the frequency synthesizer output, Δf , varies over the range of 96.000 kHz to 164.000 kHz. At a setting of 96.0 kHz the effective doppler introduced onto the baseband signal is 0 Hz, while at 164 kHz, the doppler is 68 kHz. The reason this range of frequencies was chosen was to facilitate the SSB conversion. The Pacific Instruments type 1029 synthesizer costs only \$1600 (which is inexpensive by

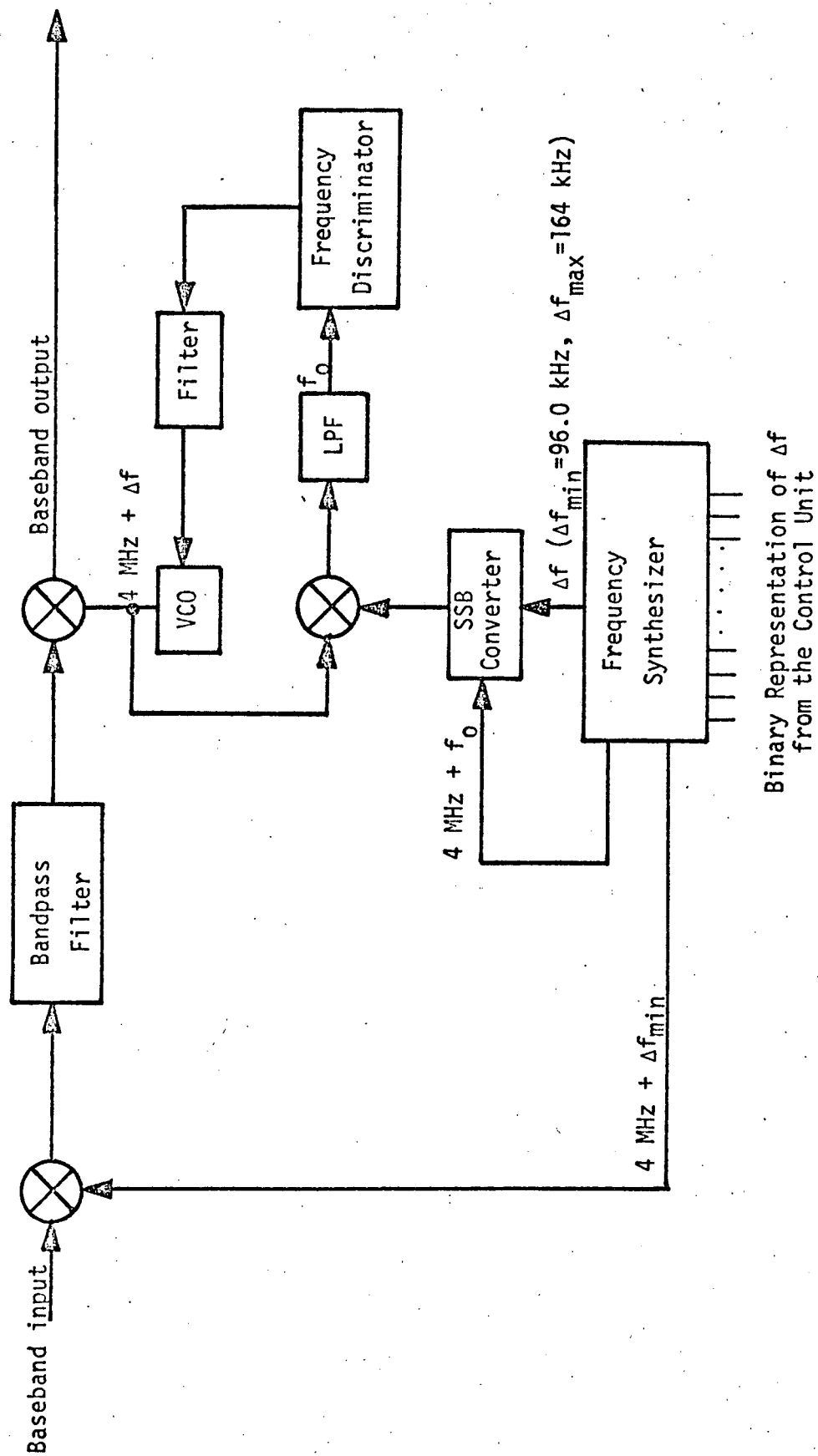


Figure 3.8 Alternative Method of Generating Doppler Spectrum Shift

synthesizer standards by virtue of the fact that it only provides 5-place resolution). A synthesizer of higher frequency would make this conversion easier but the synthesizer selected has only 5-place frequency resolution, hence, for doppler offsets of 0 to 2000 Hz (i.e., $\Delta f = 96.0$ to 100.0 kHz) incremental settings as close as 1 Hz are possible. For doppler offsets between 4000 and 68,000 Hz, 10 Hz increments are possible. This is obviously a much finer frequency resolution than was possible with the previous technique. The remainder of the circuitry shown in Figure 3.8 is simply a frequency-locked loop which "smooths" the discrete frequency increments out of the SSB converter. It should be noted that this frequency-locked loop has been designed so that for the steady state case, the input to the discriminator is always close to its center frequency f_0 , regardless of the doppler offset. Typically f_0 might be on the order of 2 kHz, and the discriminator curve must be approximately linear over a range that is comparable with the largest frequency step that the synthesizer will produce (approximate linearity over the range $f_0 \pm 500$ Hz would be adequate). It can be shown that with a single loop-filter, the frequency-locked loop responds to an input frequency function in a manner similar to a narrowband single pole filter.

The chief advantage of this approach over the previous one is that it provides greater frequency resolution. Hence, the loop can be updated more frequently by the control unit, with the result that the maximum doppler rate can now be made to be very close to the average rate without introducing much lag. Since this approach is more expensive in both hardware and design, it is suggested that the initial approach be given primary consideration, at least on a cost-effective basis.

This section concludes with a short discussion of other techniques for implementing the doppler spectrum shift. However we do not feel that these techniques are as satisfactory as the one initially discussed. Probably the most obvious modification to the block diagram of Figure 3.5 is to replace the phase-locked loop which generates the down-conversion frequency with a simple VCO whose control voltage is specified by the control unit. To get a reasonably stable center frequency, however, one would have to go to a voltage controlled crystal oscillator (VCXO) which can typically be pulled only $\pm 0.1\%$ of center frequency.* Obtaining the desired maximum doppler of 60 kHz would, therefore, require a center frequency on the order of 60 MHz. After appropriate aging (say, in excess of 30 days) one could expect a drift in center frequency on the order of one part in 10^7 per day (6 Hz per day). Such a drift could, of course, be removed by adjustment of the oscillator (i.e., every couple of weeks, or before a critical simulation). In addition to drift, the control voltage vs frequency curve for a VCXO is typically nonlinear, and would have to be compensated for by proper programming of the control unit.

4. Generation of the Time Dispersed Component of the Reflected Signal

As mentioned the reflected path exhibits a gross delay relative to the direct path which varies from 0-30 msec. Using the technique described in Sub-section III.C.2, this delay is achieved in the form of a digital shift register with 117 taps spaced every 256 μ sec. In addition to this gross delay, the reflected path exhibits a time dispersion which results in a coherent bandwidth which can vary over a range of approximately 5 to 30 kHz. This corresponds to a "multipath spread" which varies from approximately 200 μ sec maximum to 30 μ sec minimum. While in reality this time smear is probably more or less continuous, for purposes of simulation, it is reasonable that we approximate this continuum

*VCO's cable of $\pm 1\%$ deviation are available but suffer from a decrease in stability.

with a set of discrete multipath components. In using this approach, a couple of considerations must be made. First, one must arrive at some decision as to the number of multipath components necessary to approximate the continuum, and secondly, any technique selected must have the facility for having the set of tap positions easily changed under direction of the controller. We feel that the number of discrete components necessary to adequately approximate the multipath profile is on the order of 6 to 8, with the exact number to be determined by ease and cost of implementation.

In view of the fact that the signal is already digital as it emerges from the 0-30 msec delay line, a digital approach to generating the dispersive components seems superior. In addition, a digital technique will lend itself to easier interfacing with the control unit. A surface wave type delay line of the sort developed by B. J. Hunsinger of Magnavox (Urbana) was considered for this application. Such a unit would require 50 available taps spaced 5 μ sec apart. Under direction of the control unit, a given subset of these 50 taps would be selected to comprise the dispersive component. For all practical purposes, the elements of this subset could be changed as fast as the control unit will allow. In order to use this surface wave device, the binary data would have to be modulated into a carrier, probably on the order of 60 MHz, and demodulated back down at its output. Cost estimates for this device indicated that it would be considerably more expensive than the recommended technique.

The possibility of using a bank of variable length magnetostrictive lines was also considered. A 2-30 μ sec variable delay line, however, costs over \$100 per unit and has only about 1 MHz of bandwidth. The basic expense of the line itself plus the mechanical and reliability problems which would be involved in coupling the required number together, makes this approach impractical.

Due to the relatively slow rate at which they must be clocked (less than 5 MHz) and the relatively long delay between taps (256 bits or longer), MOS register, similar to those used in the 0-30 msec line cannot be used to obtain the short incremental delays required here. Since they are quite inexpensive, however, (on the order of 1 cent/bit) it was anticipated that they could be used in some redundant fashion to obtain relatively short incremental delays and still be economical. As discussed further at the end of this section, however, this does not appear to be the case.

The technique finally selected consists of using a series of T²L (or possibly MOS) random access memories (RAM). Although the exact configuration is subject to change as less expensive and more flexible RAM's are introduced, the basic implementation will be similar to that shown in Figure 3.9. Here we have shown a configuration of 128 RAM's of 256 bits each (INTEL type 3102 or equivalent). The October 1970 quantity price of the 3102 is \$51.20 per unit resulting in a total cost for RAM's of about \$6,600 (20 cents/bit).

From a functional point of view, any one of the 117 taps from the long delay line can be selected (by the control unit) to feed the RAM array. In effect, a new 8 bit sample is clocked into a given RAM address once every one-eighth μ sec.* Hence, the maximum delay time available is 512 μ sec.

The RAM delay operates in the following manner. A new data bit will be read into a RAM directly on top of the oldest bit already there. This "overlay" technique avoids the necessity of excessive shifting of data which would be necessary if the RAM was used to directly implement a shift register, and as such requires only that a simple technique be employed for updating the addresses within the RAM. As indicated in the figure, the oldest 8-bit word

* Since the long line is being clocked at a 2 MHz rate, the amount of additional commutation necessary to feed the RAM array at a 1 MHz rate is 2:1.

(labeled word i) is shown in address 1 where it has resided for the last 512 μsec . Consequently, the next 8-bit word (from the 30 msec delay line) will overlay the word in address 1. The following word, one-eighth of a μsec later, will overlay address 2 and so on. In actuality, eight consecutive words from the long delay line (i.e., 1 μsec of data) will be buffered in the separate 64-bit register shown in Figure 3.9. Since the access time of the 3102 is 120 nsec, all eight of these words can each be dumped (in parallel) into the appropriate eight consecutive addresses of RAM storage in slightly less than one-eighth μsec . The seven-eighth μsec remaining before new data is dumped into the RAM's provides seven additional "accessing times" which can be used to effect seven "taps". This is done with the aid of seven additional auxiliary 64-bit registers (one for each tap) and is shown in Figure 3.10. During access time #1, any eight consecutive RAM addresses are dumped in parallel into auxiliary register #1. During access time #2, any eight consecutive RAM addresses are dumped in parallel into auxiliary register #2 and so on until auxiliary register #7 is full. The individual auxiliary registers are then clocked out in real time to effect seven continuous data streams. Notice that in this technique any eight consecutive words can be obtained without accessing any RAM more than once. There are effectively 4080 taps spaced one-eighth μsec over a 512 μsec interval. Any seven of these taps can be selected to comprise the time dispersive multipath component. Since RAM addresses expressed in binary form are easily selectable by a digital control unit, the multipath structure may be easily and rapidly changed in any fashion selected by the control unit.

As mentioned earlier, only about 200 μsec is necessary to realize the maximum multipath spread. In actuality, the maximum time differential between any two of the seven taps does not exceed 256 μsec but this

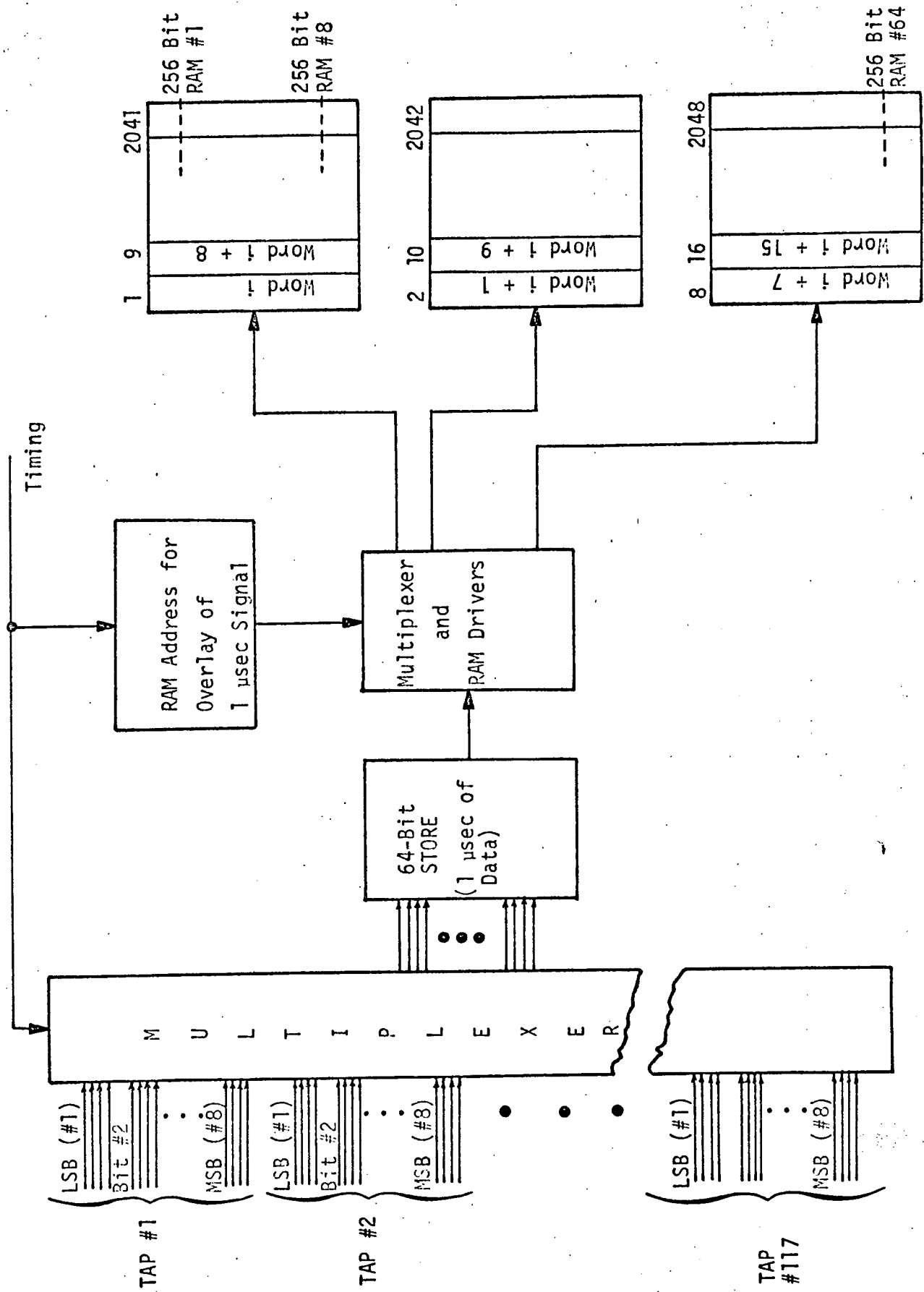
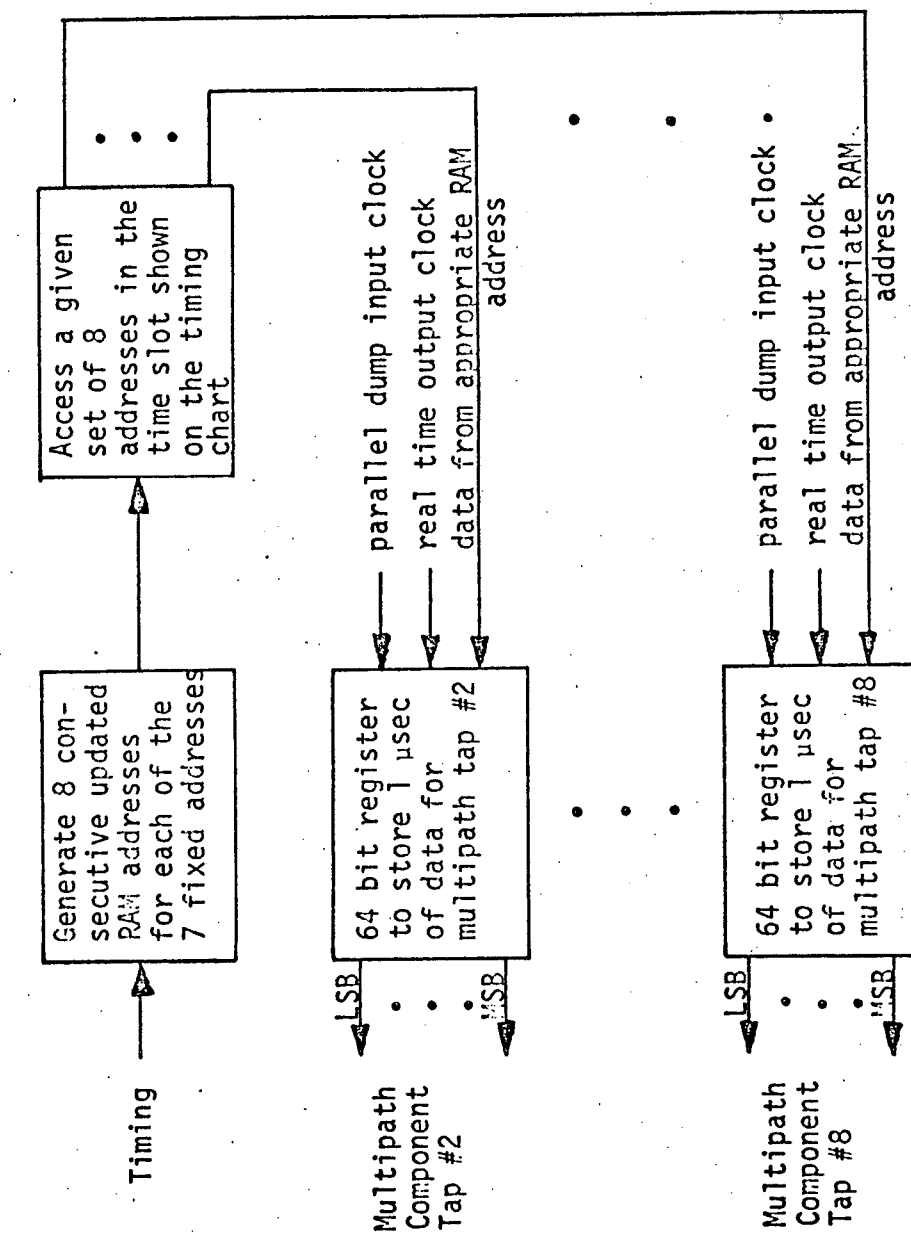


Figure 3.9 RAM CONFIGURATION FOR SHORT (512 μ s) DELAY LINE WITH 1/8 μ s ACCESS INTERVALS

7 fixed addresses
from the control
unit to specify
multipath tap
positions



Timing Chart

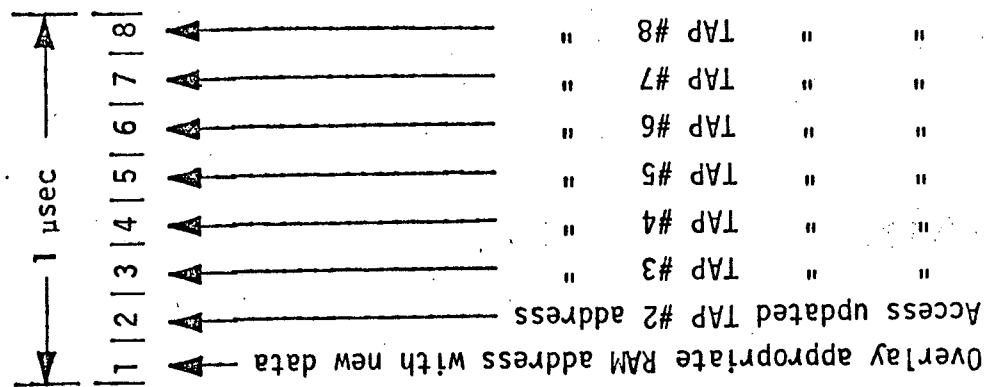


Figure 3.10 RAM Configuration for Short Delay Line
(Accessing Scheme to generate 7 taps)

spread can be located anywhere within a 512 μ sec time frame. In fact, as orbital time increases, the 256 μ sec spread, initially located in the first half of the 512 μ sec window, gradually shifts to the last half. As soon as it is located entirely in the last half, the input to the RAM memory can be stepped to the next output of the 30 msec line, and the RAM addresses of the seven effective taps decremented by 256. Hence it is evident that a 512 μ sec line is necessary to allow one to position the seven-tap multipath spread structure anywhere over the 0-30 msec line, in 125 nanosecond steps.

If access to more than seven taps is desired, one could use the INTEL 3101 (or equivalent) which has an access time of only 60 nsec (with appropriate changes in bookkeeping). Since this is a 64-bit RAM; 512 of these units would be necessary to provide a total of 512 μ sec delay. In this configuration, however, each unit could be clocked at a 1/2 MHz rate resulting in access to over 30 of the 4080 taps. Since the cost per bit for the 3101 is twice that of the 3102, this approach would cost about \$13,000 for RAM's alone.

Since tap spacing of one-eighth μ sec is probably much closer together than one needs for adequate simulation, it seems desirable to seek some trade-off whereby considerably fewer taps are required (spaced every 5 μ sec, for example) at some significant saving in hardware cost. In particular, since the cost per bit for MOS memory is presently a factor of about 20 less than for RAM's, a technique using MOS registers, even in some highly redundant fashion, would be preferable. Considerable thought was given to various MOS configurations in an attempt to realize some cost saving. However, while the MOS memory itself is relatively inexpensive, the amount of additional hardware needed to get the required degree of flexibility in tap positioning pushes the total cost above

that required for RAM's. This problem would be reduced if 256-bit MOS registers were available with taps every 16 bits or so. At present, four taps on a 1024-bit register is about all that is available,* however, this approach warrants reexamination before the simulator is actually built.

5. Technique for Introducing a Fading Bandwidth onto the Time Dispersive Components

In the previous section a technique was described whereby the continuous time dispersive component of the multipath signal would be approximated by a finite number (7) of discrete components. As shown in Figure 3.3, onto each of these discrete components we must now introduce a "fading bandwidth" which ideally is to vary from 0 to 2 kHz for VHF simulation and up to 34 kHz for the S-band simulation. In this section two different techniques for implementing this requirement are discussed. In the first technique the quadrature components of the signal are each multiplied by separate (independent) Gaussian noise processes. Consequently Rayleigh amplitude variation and uniform phase variation is introduced onto each multipath component, simulating the actual physical conditions encountered on the channel. In the second technique, only Rayleigh amplitude variation of each multipath component is introduced. Although the technique is easier to implement (and believed to be adequate for purposes of testing TDRS communication systems) the lack of phase variation may exclude the use of this simulator from other applications. Consequently, it is recommended that the first technique be implemented. For the sake of completeness, a discussion of the second technique is included as well.

a. Technique #1: Amplitude and Phase Modulation

The block diagram describing the implementation of technique #1 is given in Figure 3.11, and must be duplicated for each of the seven components

* The primary reason that so few taps are available is that considerable buffering is required to provide the MOS-TTL interface.

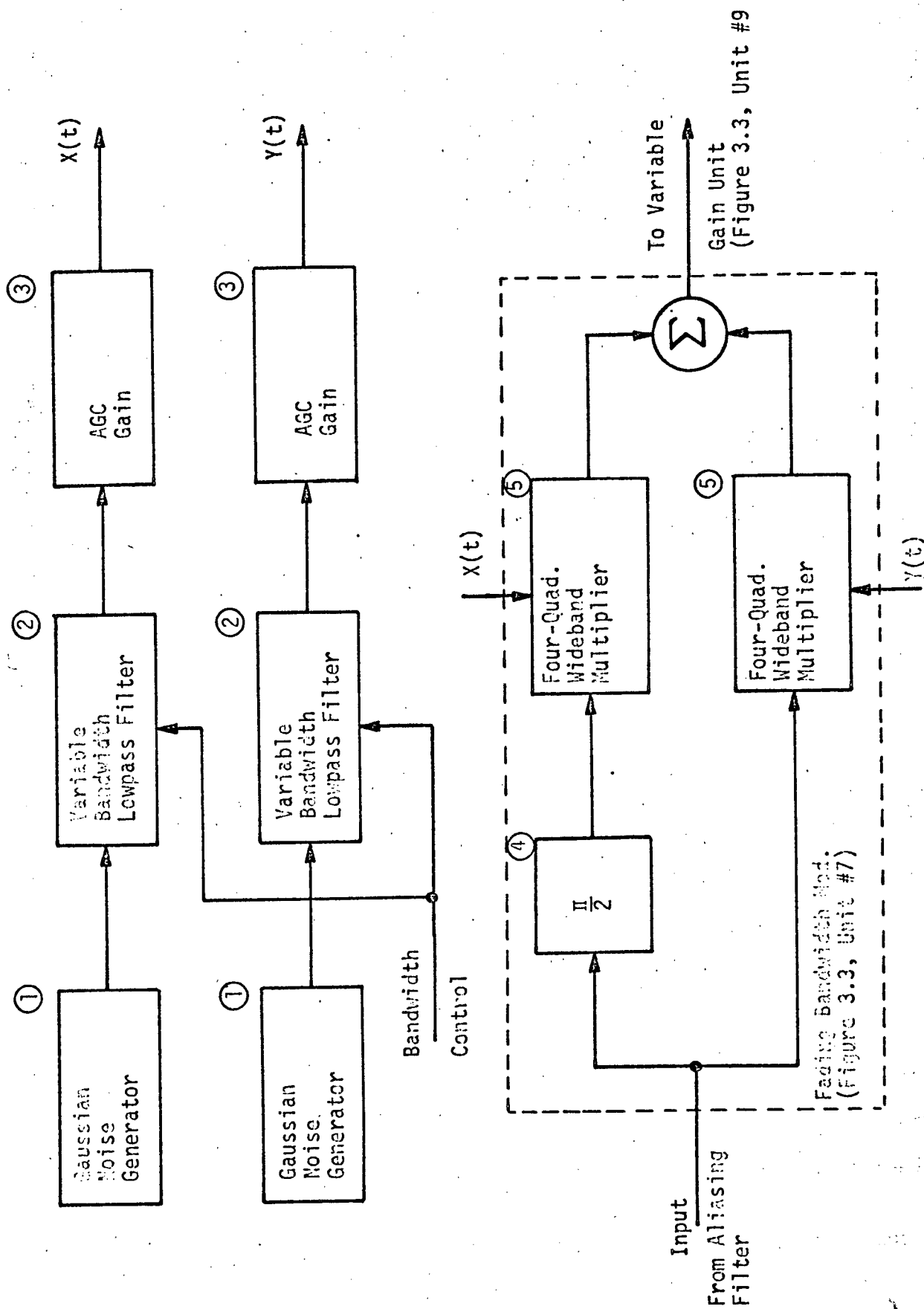


Figure 3.11 Fading Bandwidth Simulation Method #1: Single Sideband Technique

making up the diffuse path. After D/A conversion and filtering of the aliasing frequencies, separate quadrature signals are generated by passing the .75 to 2.75 MHz baseband signal through a 90° phase shifting network. An introductory discussion of 90° phase shifting networks can be found in the text written by Pappenfus.* For purposes of this report it is sufficient to note that over the range of .75 to 2.75 MHz, a simple 90° phase shifting network can be designed to (theoretically) provide less than $\pm 1^\circ$ (peak) phase error. From a practical point of view, a 90° phase shifting network can be built for this application resulting in quadrature crosstalk that will be down by 30 dB or more. Under such conditions, the deviation from the Rayleigh amplitude and uniform phase distribution will be insignificant.

At this point the two quadrature signals are each multiplied by independent Gaussian noise processes. Since both the signal and the Gaussian process can have either positive or negative polarity, each multiplier must be capable of full four-quadrant operation. An investigation was begun of the availability of multipliers which could be used in this application. Included here is a brief discussion of the pertinent properties of some commercially available four-quadrant multipliers.

° Analog Devices Model 422: This unit has a 3 dB bandwidth of 5 MHz, however at 1 MHz the phase response is 1° and is approximately 15° at 5 MHz. This phase shift will introduce substantial quadrature crosstalk unless both multipliers shown in Figure 3.11 have essentially the same phase characteristics. Since the exact phase characteristics are likely to differ by a few degrees from unit to unit, we feel that this device is probably inadequate in this respect. A second parameter of importance is direct signal feedthrough. Direct feedthrough

* Pappenfus, E.W., et al, "Single Sideband Principles and Circuits," McGraw Hill Book Company, New York.

of the Gaussian noise process is of little consequence since it is easily filtered, however, direct feedthrough of one of the quadrature signals results in an undesired "specular" component will be down by approximately 33 dB. Since the desired specular component can, under certain conditions, be down by approximately this amount (see Figure 2.2). It is felt that any undesired specular component from a single multiplier should be down by at least 40 dB. This unit costs \$104 in quantities of 10 to 24.

- ° Motorola MC1595L: This unit has a 3 dB bandwidth of 3 MHz and 3° of phase shift at 750 kHz. Signal feedthrough level is not immediately evident from the specification sheet. This unit cannot be used in the proposal application. Cost is \$27 per unit.

- ° Intronic M510: This unit has a 3 dB bandwidth of 10 MHz and costs \$280 in quantities of 10 to 49. Additional characteristics of this unit were not available at the time of this writing, however it appears to be a good candidate for the proposed application.

C. Watterson* of ESSA has proposed a simple four-quadrant multiplier. We do not know the exact operational characteristics of the proposed unit, but its simplicity makes it worthy of careful consideration. Watterson has made the following comments:

"If a symmetrical field-effect transistor (FET), one whose drain and source terminals are interchangeable, is driven in a balanced manner, with the drain voltage relative to ground, V_d , always equal to the negative of the source voltage relative to ground, V_s , ($V_d = -V_s$), its drain-source current as a function of drain-source voltage, $V_{ds} = V_d - V_s$, will have odd symmetry, as shown in Figure 1 [Figure 3.12 in this report]. Over approximately a ± 1 -volt range, the characteristic will approximate a linear two-quadrant multiplier (a single-balanced modulator).

* Watterson, C.C., "Critique of Preliminary LOS-TDRS Channel Simulator," Private Communication.

If the symmetrical FET is used in the circuit of Figure 2 [Figure 3.13 in this report], where the drain and source are driven by the baseband Gaussian noise, $x(t)$ or $y(t)$, as shown, and the baseband signal (0.75-2.75 MHz) drives the biased gate, the output waveform, $V_o(t)$, will consist of both the desired double-sideband (DSB) noise-modulated signal and the undesired input baseband Gaussian noise, the latter partially suppressed by the low-Q single-pole-filter load. An additional relatively simple bandpass filter (0.75-2.75 MHz) should be used to further suppress the undesired baseband Gaussian noise in $V_o(t)$, ... In the circuit of Figure 2, the unmodulated (specular) input signal ideally does not appear in $V_o(t)$; practically, primarily because the source-gate and drain-gate capacitances are not exactly equal, it appears in $V_o(t)$, but is suppressed by about 80 dB (much more than most multiplier circuits)."

Generation of Gaussian noise processes $x(t)$ and $y(t)$ are shown in Figure 3.11. The Gaussian noise generator shown in this figure can be a diode noise source having flat spectral content out to at least 34 kHz (i.e., the maximum fading bandwidth). Following the noise source is a variable bandwidth lowpass filter whose amplitude response determines the fading spectrum. The location of the variable 3 dB cutoff point of this filter is determined by the control unit. Although the fading bandwidth can vary (ideally) anywhere from zero to 34 kHz, it is felt adequate for simulation purposes to set a limit of 20 Hz as the most narrow fading bandwidth. Consequently, the lowpass filter must be capable of having its 3 dB cutoff point varied from 20 Hz to 34 kHz. It should be pointed out that the facility for providing zero fading bandwidth is provided as well. This can be accomplished by setting either $y(t)$ or $x(t)$ to zero, and the other to unity. A separate FADING BANDWIDTH REGISTER setting is reserved for this situation, however, the resulting switching details are not shown in Figure 3.11

As mentioned previously, the amplitude response of the lowpass filter determines the shape of the fading spectrum. It has been suggested by Watterson* and appears reasonable that a single pole filter probably rolls off too slowly

* Op. cit.

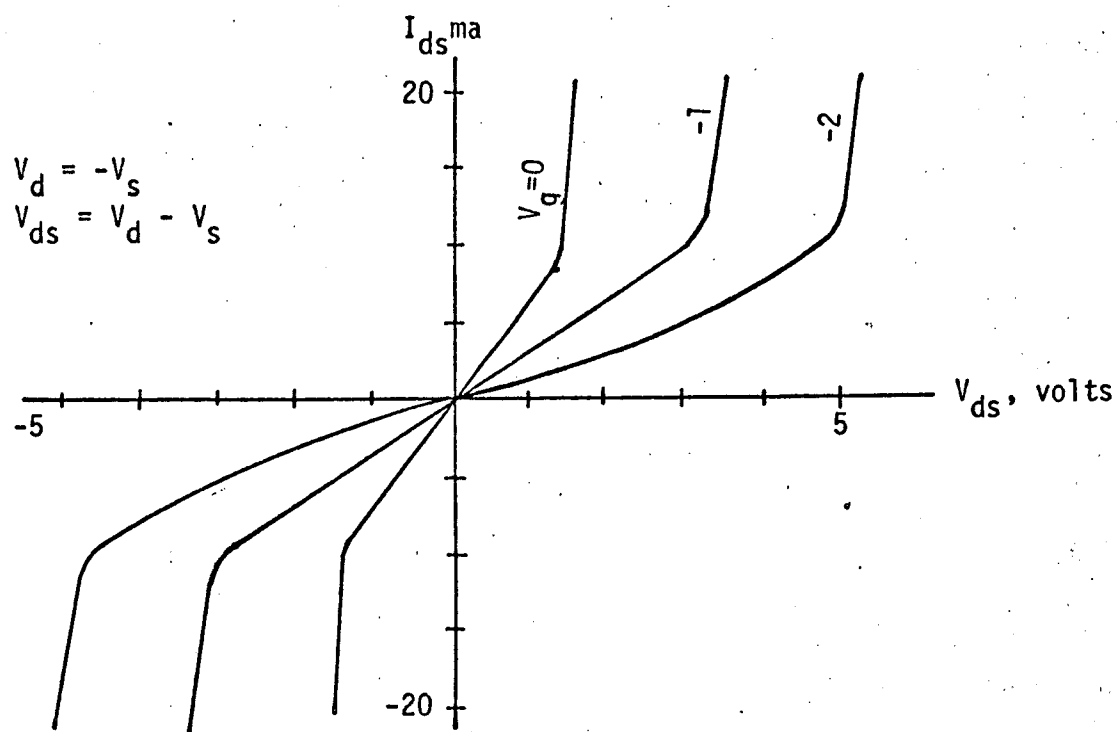


Figure 3.12 Symmetrical FET Characteristic

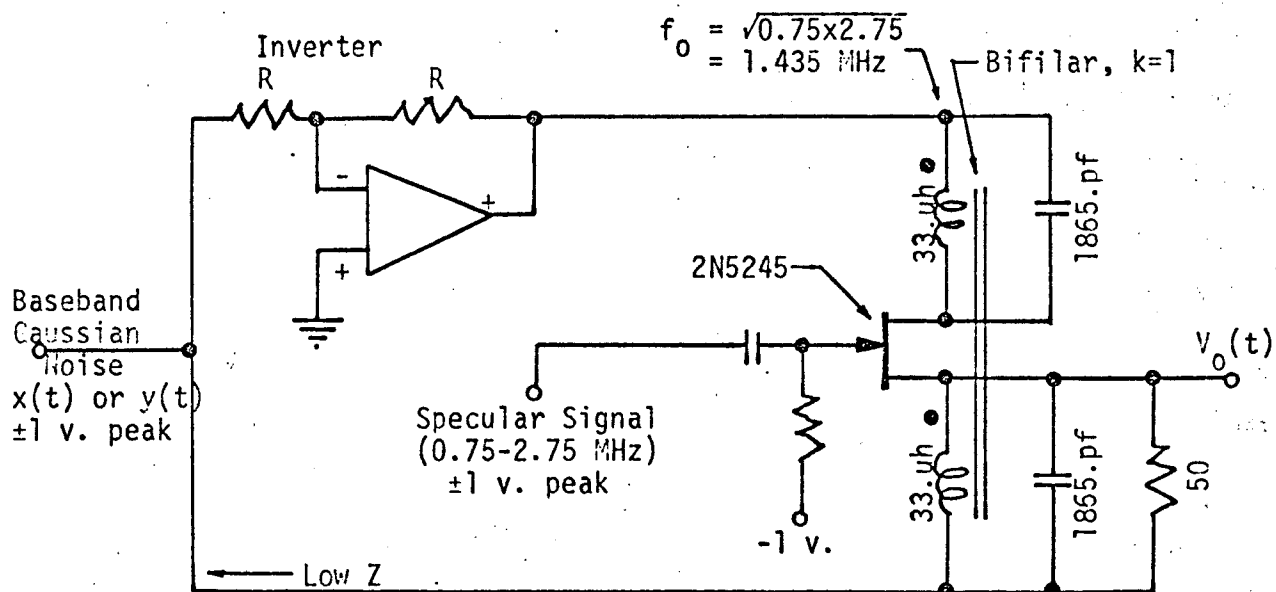


Figure 3.13 Symmetrical Single-Balanced FET Modulator

to be a good approximation to a "typical" fading spectrum. Fortunately the exact roll-off characteristic is only of second order importance in TDRS simulation. It is recommended, therefore, that at least a three-pole configuration be employed. Multi-pole electrically-tunable filters can be obtained commercially from at least one source (ARITECH Corp., Brighton, Mass.), but there may be some difficulty in obtaining the 20 Hz to 34 kHz variation in a single unit. However, obtaining this variation with two separate filters (each varying over a portion of the 20 Hz to 34 kHz range) will not be difficult. Following each filter in Figure 3.11 is an AGC unit which functions to keep the average output power from each filter constant (independent of frequency). In the absence of this AGC, the average power in $x(t)$ or $y(t)$ would change as its bandwidth is changed (i.e., as the fading bandwidth is changed under direction of the control unit, the effective gain of the diffuse components would change).

This AGC unit serves the important secondary purpose of reducing the required dynamic range of the multipliers. The only requirements on the time constant of the AGC amplifier is that it be fast enough to allow the fading bandwidth to change at the fastest rate dictated by the control unit (which will probably be on the order of seconds). On the other hand, of course, the time constant cannot be so fast as to compress the noise function itself. This compression will be avoided if the AGC time constant is at least ten times as long as the reciprocal of the minimum fading bandwidth. Obviously, then, there is plenty of leeway in selecting the AGC time constant. A suggested technique for generating the AGC signal is to "square" the noise process by using the Motorola MC1595L (or equivalent multiplier) mentioned previously. This unit has more than the 34 kHz bandwidth necessary to square the widest

bandwidth noise process. This "squared" signal is then lowpass filtered with a time constant on the order of "several" seconds to provide the AGC signal.

As mentioned, a diode noise source can be used to generate the unfiltered noise processes. A total of 14 sources are necessary for the seven diffuse paths. An alternate technique for noise generation suggested by Watterson* is to replace the diode noise source with a Random Binary Sequence generator. If the generator is keyed at a rate approximately 100 times greater than the filter cutoff frequency, the filter output will be approximately Gaussian. By reducing the duty cycle (or amplitude) of the sequence as the cutoff frequency is increased the average filter output power can be kept constant. The difference in cost between these two techniques is not substantial. In either case care must be taken to insure that any DC component in the noise process is down by at least 60 dB to avoid a spurious specular component in the diffuse path.

Since the value of the fading bandwidth will be determined by the digital control unit described previously, this value will change in finite increments. Some care should be taken to insure that the actual filter bandwidth does not change abruptly as this may introduce undesired transients. This can be avoided by simply filtering the discrete level analog control voltage which varies the filter bandwidth. A time constant on the order of half a second is adequate for this filtering.

*
Op. Cit

b. Technique #2: Amplitude Modulation Only

The technique to be described herein is not recommended at this time in view of the fact that it is a significant departure from the actual TDRS channel.

It is our opinion, however, that this technique will provide an operationally equivalent perturbation of the signals, as far as the modems are concerned. The effect of the diffuse component on the communication system is, to a first order of significance, one of random time dispersion. Random, if not time-varying, phase shifts are introduced by the relative delays of the taps which make up the diffuse component. A variation in the relative location of the seven taps will, in fact, simulate the phase varying effect. From the point of view of cost-effectiveness, it may be worth sacrificing the capability of physical simulation of the channel without reducing the operation simulation of the communication system under test. In such a case, technique #2 could be used.

This technique is simpler to build than technique #1, and it is estimated that it would result in an overall reduction of about 2% of the final system hardware cost. The salient features of this technique are that it provides only Rayleigh fading on the individual diffuse components (i.e., no phase modulation) and that the fading bandwidth is determined by a simple single pole configuration.

In this technique each multipath component is processed separately as before, however the block diagram of Figure 3.11 is replaced by that shown in Figure 3.14. From a functional point of view, the gain of each multipath component is simply varied by a random process, $r(t)$, whose amplitude distribution is Rayleigh, and whose spectral properties are identical to the process $x(t)$, or $y(t)$, shown in Figure 3.11. This is accomplished in the gain modulated amplifier of Figure 3.14.

By utilizing this technique, the circuitry which is to be duplicated can be simplified. In particular, the two wideband four-quadrant multipliers required in technique #1 are replaced with a single amplifier whose gain varies linearly with $r(t)$. This represents some saving in hardware cost in view of the fact that an analog multiplier of the type required here (INTRONICS Type M510, or equivalent) presently costs over \$250. In addition, the hardware complexity required to generate the independent $r(t)$ functions is easier than that required to generate independent sets of $x(t)$ and $y(t)$. Although it is not substantial, the elimination of the 90° phase shifter represents some additional savings.

The suggested technique for generating the seven independent Rayleigh noise processes is evident from Figure 3.14. Here a single wideband Gaussian noise source is passed through a bank of seven narrow bandpass filters (i.e., a comb filter) whose noise bandwidths are all identical, and nonoverlapping. Each filter is then followed by a simple envelope detector. It is well-known that

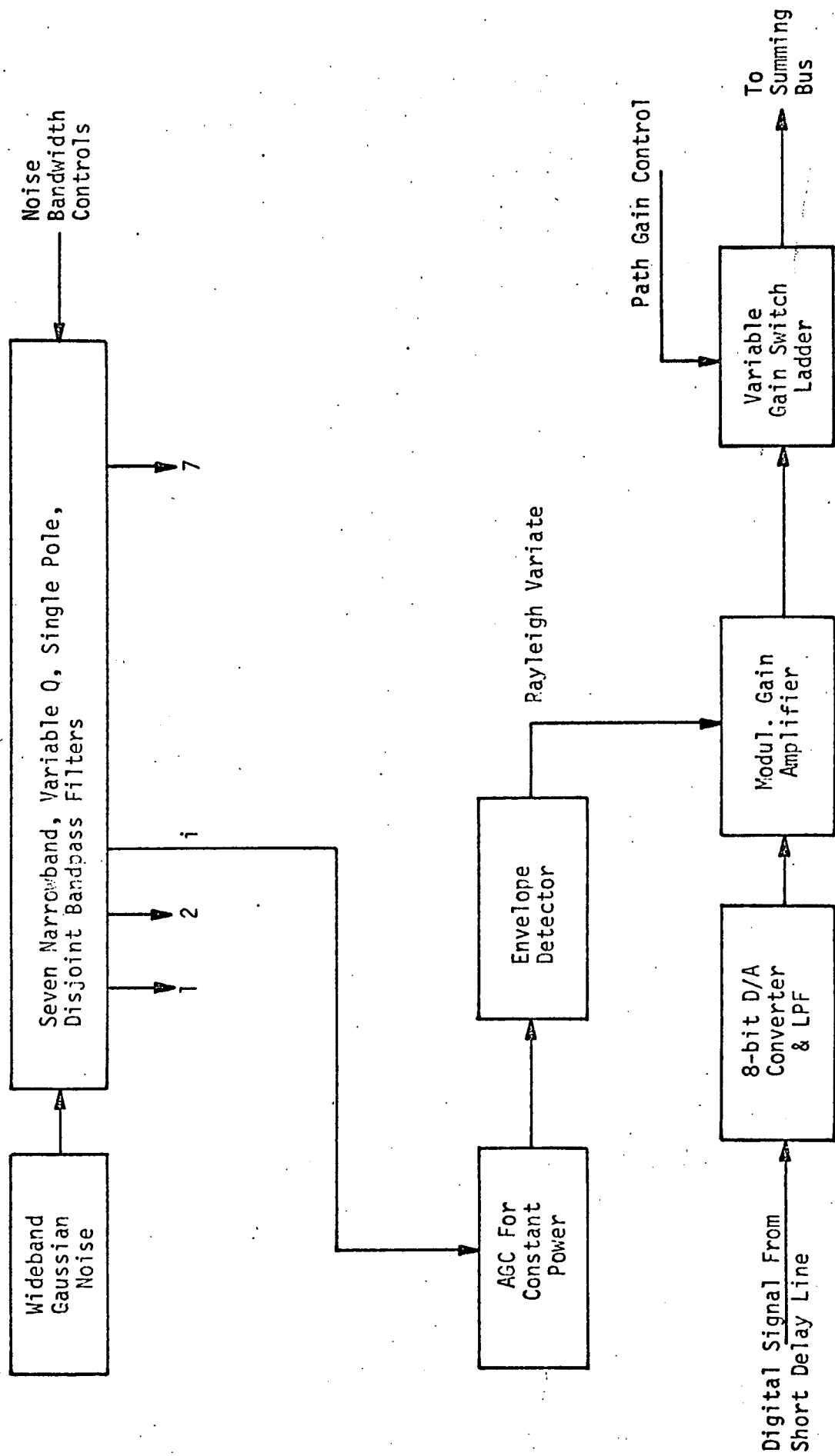


Figure 3.14 Fading Bandwidth Simulation
Method II - Gain Modulation

the various detector outputs are independent and Rayleigh-distributed. The Q of the comb filter is varied to control the fading bandwidth.

Several techniques were considered for implementing the variable bandwidth single pole filters. First to be discussed is what appears to be the best technique, and included at the end of this section two alternate techniques which are considered to be inferior.

As shown in Table 3.1, the maximum fading bandwidth (i.e., maximum bandwidth of $r(t)$) must be 34 kHz as required for S-band simulation. As mentioned previously it is felt that a minimum fading bandwidth of 20 Hz is adequate with the provision for zero Hz fading bandwidth as well. This implies that the fading bandwidth of 20 Hz can change by a factor of 1.7×10^4 . Since the noise process must be narrowband, the minimum Q should not be less than 15. Hence, if a single filter were used to generate the full range of 20 Hz to 34 kHz, its Q would have to vary from 15 to over 25,000! Recommended instead is the use of two separate filters each with a Q which can vary over a range of 41:1 (i.e., 615 to 15). Filter #1, therefore, would have a center frequency of 24.6 kHz (or greater) and cover fading bandwidths which vary from 20 Hz to 820 Hz. Filter #2 would have a center frequency of 1.02 MHz (or greater) and cover the range from 820 Hz to 34 kHz.

To obtain a stable and accurately controllable Q over the range (15 to 615) we propose the simple Q -multiplier circuit shown in Figure 3.15. By selecting R_f to give a Q -multiplication factor of about 4, one need only select a coil with a Q in excess of $(615/4)$ and the 41:1 range of Q can be obtained by varying only R_{in} . The problem one usually encounters with Q -multiplier circuits is that for high Q values, the Q is very sensitive to

the values of the circuit components. This problem is deferred to the end of this section when discussing one of the alternate techniques.

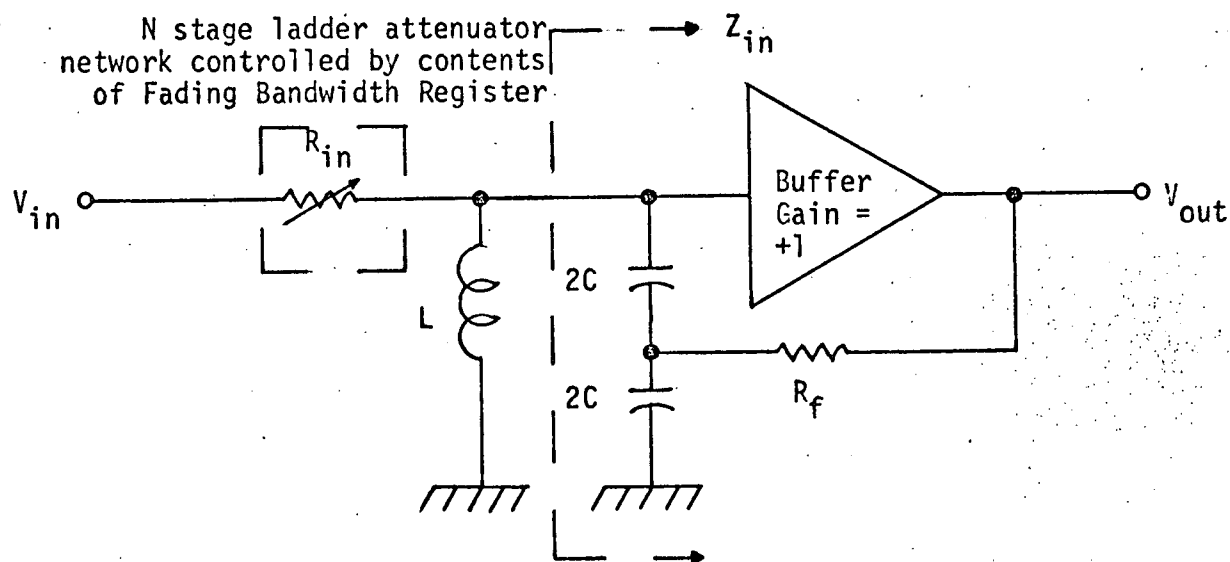


Figure 3.15 Variable Q Multiplier Circuit

In this case, however, the multiplication factor is relatively low (4) and one can show that component variations (temperature, aging, etc.) are not a critical factor. For example, a 1% variation in R_{in} (at the maximum Q setting) will result in only about a 1% variation of the Q.

A total of 14 filters are necessary to obtain the seven independent Rayleigh processes using this approach (seven of filter #1 and seven of filter #2). The center frequencies of the seven filters of a given type can be widely spaced to avoid any possible bandwidth overlap which would result in correlated Rayleigh processes. The chief disadvantage to this technique lies in the fact that two separate filters will have to be used when the signal input is VHF, and the full range of 20 to 2000 Hz of fading bandwidth is desired. Obviously, at some point in the course of such a simulation, it will be necessary to switch from one filter to the other. A certain amount of switching transients can be expected to appear on the resulting signal. With some care in implementation, the transient should not be substantial.

By making R_{in} a ladder with N switchable stages, the Q (i.e., fading bandwidth) can easily and accurately be controlled by an N-bit word supplied by the control unit. Since the Q does not vary linearly with R_{in} , this will have to be accounted for in programming of the control unit.

The envelope detector following the narrowband filter is currently envisioned as being a diode detector followed by a lowpass filter. In view of the fact that the process being rectified is narrowband, the lowpass filter design is straightforward. Some care, however, must be given to the fact that at low levels a diode detector is square law rather than linear. At present this problem has not been investigated; however, (at least) two possible techniques can be considered in an attempt to reduce the effect. First, a DC level could be added to the narrowband process before detection, and subtracted afterward. This would allow the diode to always operate in its linear region, but would require careful subtraction of the DC offset after detection. Another

possibility would be to amplify the narrowband process before detection so that the diode operates in its linear region for all but a negligible portion of the time.

The discussion of technique #2 concludes with a description of two alternate techniques for obtaining the required variable bandwidth Rayleigh process, which are not as satisfactory as the one previously discussed. The first technique was motivated by a desire to cover the entire range of fading bandwidth for a given input signal (VHF or S-band) with a single filter. This would avoid the necessity of ever switching between different filters in the course of a given simulation. The second technique is entirely different in that it attempts to generate a Rayleigh process by taking the square root of the sum of the squares of two independent, lowpass, Gaussian processes.

For simulation purposes, it is reasonable that we restrict ourselves to a 100:1 range in the fading bandwidth (i.e., 20 Hz to 2 kHz for the VHF signal, and 320 to 32 kHz for S-band). Since the noise process must be narrowband to generate Rayleigh statistics, the minimum Q must be no less than about 15. Hence, if two separate filters are used (one for UHF and one for S-band), each must be capable of having its Q varied from 15 to 1500. The center frequency of the VHF filter must be located at

$$\begin{aligned} f_c &= 2Q_{\min}(\text{fading bandwidth})_{\max} \\ &= 30 \times 2 \text{ kHz} = 60 \text{ kHz} \end{aligned}$$

Similarly, for S-band, the center frequency must be located at 960 kHz. In the present application the value of Q would be adjusted by changing the value of the feedback resistor R_f (which changes the Q-multiplication factor) in Figure 3.15. In this fashion, a Q of 1500 can be obtained quite readily.

The primary drawback with this approach is that at high values the Q is very sensitive to the values of certain components in the circuit. One can appreciate this by determining that Z_{in} can be replaced with a parallel RC network, where the resistor is negative. The Q of the total circuit is then determined by the parallel combination of R_{in} with this negative resistance (we assume that the equivalent parallel resistance of the inductor itself is large compared with R_{in}). When these two resistors differ in value by 1%, the Q -multiplication factor is 100. If this difference should drift to 2% due to temperature variation, etc., the multiplication factor drops to 50. Hence at VHF, for example, the fading bandwidth could change from 20 to 40 Hz with only a 1% error in the circuit components.

This problem could be remedied considerably by taking advantage of the fact that very high Q coils (in excess of 300) are available at these frequencies. A variation in Q from 15 to 150 could, therefore, be obtained by padding down the Q of the coil by varying R_{in} , and the variation from 150 to 1500 obtained by the multiplier action. In this case, the maximum Q -multiplication factor is only 10, and a 1% error in component values at high Q will result in only about a 10% error in Q . While this 10% error at narrow fading bandwidth is probably tolerable, it requires that the initial circuit components be accurate to 0.1%. In addition, one must now have the capability for external control of both R_{in} and R_f .

In view of these considerations and the possible stability problems which might be encountered at high Q 's, this approach to generating a variable bandwidth Rayleigh process is considered unsatisfactory. It is worth recalling that the variation in bandwidth must be performed before envelope detection, since passing a Rayleigh process through a narrowband LPF tends to make it Gaussian.

The final approach considered exploits the well-known fact that a Rayleigh process can be made by taking the square root of the sum of the squares of two independent, lowpass, Gaussian processes. Since a total of seven independent Rayleigh processes are required, we must generate 14 independent lowpass Gaussian processes, pass them each through a variable bandwidth lowpass filter, and group them in pairs to form the Rayleigh process. Rather than build 14 separate noise sources, we had envisioned using one wideband diode noise source and a "bank" of 12 heterodyning oscillators of different frequencies. This "band" of oscillators would mix nonoverlapping bandpass portions of the wideband noise down to lowpass. The 12 different heterodyning frequencies would be obtained by various pick-offs from a single, appropriately designed, digital countdown chain.

After heterodyning, one would have 14 Gaussian processes which would be independent if lowpass filtered with a filter whose cut-off frequency did not exceed 32 kHz; a filter whose 3 dB point can be varied from 20 Hz out to 32 kHz would probably have to be implemented in several sections. One technique employed to obtain a simple single-pole lowpass filter whose 3 dB point can be varied over an extremely wide range is shown in Figure 3.16. By electronically switching in and out the resistor R_2 with a variable duty cycle switching function, the resistive portion of the filter time constant can be made to vary from R_1 to $R_1 || R_2$. By making the switching period short compared to the shortest time constant, aliasing spectra can be filtered. Instead of this approach one can employ any one of a number of more conventional variable bandwidth, lowpass filter designs, or can, in fact, purchase similar units (e.g., the advertisement of ARITECH Corp., in September 1970 issue of EEE, vol. 18, p. 82).

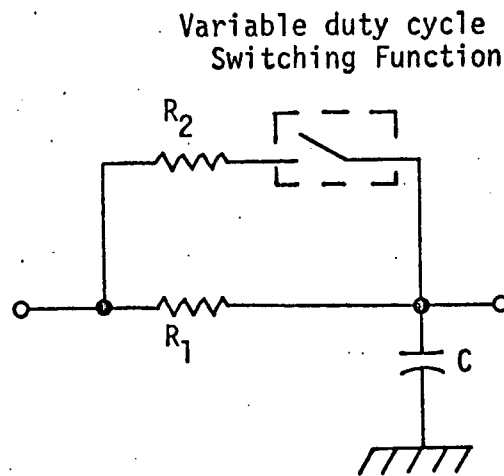


Figure 3.16 Variable Cut-off Lowpass Filter

Techniques for generating $\sqrt{X^2+Y^2}$ by using four-quadrant analog multipliers are available in the application notes of almost any multiplier manufacturer. Unlike the analog multiplier application shown in Figure 3.11 these multipliers need not be wideband (i.e., they are required to operate over 0-32 kHz) or extremely accurate. Consequently, a Motorola type MC-1595L or equivalent (\$27/unit in 1-24 quantity) is adequate. If one prefers, the entire $\sqrt{X^2+Y^2}$ function can be performed with a single module available from INTRONICS (Model VM101) at an October 1970 cost of \$95/module (1 to 9 quantities).

6. Summary of Recommended Major System Components

Magnavox's recommendation for a TDRS channel simulator has been shown, from a functional block diagram viewpoint, in Figure 3.3. Throughout the previous sections several alternative approaches to the design of specific operational functions of the simulator have been investigated with one or more approaches being recommended as optimum. In this section each functional unit of the recommended simulator design will be cataloged and cross-referenced to Figure 3.3 and other figures. This list is presented in Table 3.3.

D. PRELIMINARY COST ANALYSIS OF THE TDRS CHANNEL SIMULATOR

This section discusses preliminary cost estimates of the channel simulator. The objective herein is to establish approximate costs for the major functional components of the simulator as shown in Figure 3.3. No attempt has been made during the program to provide cost down to the circuit level, however, the line-item costs presented reflect the cost for what is felt to be the major portion of the simulator hardware.

For functional units that can be constructed from what is essentially off-the-shelf (e.g., A/D converter, VCO's, mixers, etc.) hardware, manufacturers budgetary estimates have been used; while, for units which require a significant amount of assembly (e.g., delay lines, counters, etc.) typical, catalog prices have been quoted.

The line-item cost breakdown for each of the major functional components of the simulator is presented in Table 3.4 through Table 3.8. The total cost of the simulator as presented herein does not reflect the cost for circuit designing, chassis design, and fabrication.

Table 3.3: Catalog of Principal Components for TDRS Channel Simulator

UNIT DESCRIPTION	REFERENCE		Unit #	DESIGN REQUIREMENT/REMARKS
	Section	Figure		
Down Converter Oscillator	III.C.1-a	3.3	1	Greenray Industries, Inc. Model 74000A Crystal Oscillator @ 69.25 MHz
Down Converter Mixer	III.C.1-a	3.3	1	Relcom Model M1
Low Pass Filter	III.C.1-b	3.3	2	4-pole Bessel with 3 dB frequency at 7.5 MHz
AGC	III.C.1-b	3.3	2	See discussion of Section III.C.1-b
A/D Converter	III.C.1-c	3.3	3	InterComputer Electronics or American Astrionics, Inc. See discussion of Section III.C.1-c
Tapped Delay Line (30 ms)	III.C.1-e III.C.2	3.3	4	See Section III.C.2 for design details
Tapped Delay Line (512 μ sec)	III.C.1-e III.C.4	3.3	5	See Section III.C.4 for design details
D/A Converter	III.C.1-f	3.3	6	Analogue Devices Model MDA-8F
Aliasing Filter	III.C.1-f	3.3	6	Axel Electronics Custom Filter See Section III.C.1-f for design details
Noise Source	III.C.1-f	3.3	11	Diode noise source of standard design may be used here*. Spectrum to be flat out to at least 2.75 MHz. for amplitude control, see ADDITIVE NOISE REGISTER discussion of Section III.B.

* For commercial unit (encapsulated or PC board) see Elgenco, Inc. Model 3607A

Table 3.3: Catalog of Principal Components for TDRS Channel Simulator (continued)

UNIT DESCRIPTION	REFERENCE		Unit #	DESIGN REQUIREMENT/REMARKS
	Section	Figure		
SSB Up Converter	III.C.1-b	3.3	8	Relcom Model M1
Mixer	III.C.1-b	3.3	8	ITEL Model FBT/2-70/2-9/50-3A/3A. Provides 50 dB of attenuation to undesired sideband
Vestigial Filter	III.C.1-b	3.3	8	See Section III.C.1-d for design details
Variable Gain Unit	III.C.1-d	3.3	9	Relcom Model M1
Doppler Spectrum Shift Unit	III.C.1-d	3.3	10	Greenray Model T289
Mixer	III.C.3	3.5	1	Greenray Model T201B
4 MHz Oscillator	III.C.3	3.5	2	Vendor and filter requirements are spelled out in Section III.C.3
VCO	III.C.3	3.5	3	5-pole Butterworth, $f_{3db} = 3.4$ MHz
Bandpass (vestigial) Filter	III.C.3	3.5	4	The design requirements of the PLL are discussed in Section III.C.3.
Low Pass Filter	III.C.3	3.5	5	Detailed electrical design not applicable at this time.
Phase Locked Loop Components	III.C.3	3.5	6	

Table 3.3: Catalog of Principal Components for TDRS Channel Simulator (continued)

UNIT DESCRIPTION	REFERENCE		Unit #	DESIGN REQUIREMENT/REMARKS
	Section	Figure		
Fading Bandwidth Modulator	III.C.1-g	3.3	7	
Gaussian Noise Generator	III.C.4	3.11	1	Diode noise source of standard design may be used here.* Spectrum to be flat out to at least 34 KHz
Variable Bandwidth Filter	III.C.4	3.11	2	4-pole Butterworth. 3 dB point electrically tunable from 20 Hz to 34 KHz. Vendor: AirTech Corp. Brighton, Mass.
AGC Gain	III.C.4	3.11	3	Design requirements for this unit are given in Section III.C.5
$\pi/2$ Phase Shifting Network	III.C.4	3.11	4	Design techniques are available in the literature. See reference in Section III.C.5 for example.
Wideband 4-Quadrant Multiplier	III.C.4	3.11	5	Intronics Model M510 or Watterson design (Section III.C.5).

* For commercial unit (encapsulated or PC board) see Elgenco, Inc. Model 3602A-11154

Table 3.4 Cost Breakdown for Simulator Hardware System Components

Item #	Unit Description	Reference		Type	Quantity	Unit Cost	TOTAL Cost
		Figure	Unit #				
1	Down Converter Oscillator	3.3	1	Greenway Model 74000A	1	\$289	\$289
2	Down Converter Mixer	3.3	1	Relcom, Model M1	1	35	35
3	Low Pass Filter	3.3	2	4-pole Bessel with $f_c = 75$ MHz	1	50	50
4	AGC Amplifier	3.3	2	See Section III.C.1-b	1	100	100
5	A/D Converter	3.3	3	American Astrionics See Section III.C.1-b	1	7,000	7,000
6	Tapped Delay Line (0-30 Msec.)	3.3	4	INTEL Model 1Ho3	1900	10.35	19,655
7	Tapped Delay Line (0-512 μ sec)	3.3	5	(See Table 3.5)	1	7,766	7,766
8	D/A Converter	3.3	6	Analog Devices Model MDR-8F	7	220	1,540
9.	Aliasing Filter	3.3	6	Axel Electronics See Section III.C.1-f	7	100	700
10.	Fading Bandwidth Modulator	3.3	7	See Table 3.6	7	960	6,720
11.	Up-Converter Mixer	3.3	8	Relcom, Model M1	1	35	35
12.	Up-Converter Vestigial Filter	3.3	8	ITEL, Inc. Model F8T/2- 70/2-9/50-3A/3A	1	400	400
13.	Variable Gain Unit	3.3	9	Ladder Attenuator See Section III.C.1-d	9	50	450

Table 3.4 Cost Breakdown for Simulator Hardware System Components (continued)

Item #	Unit Description	Reference		Type	Quantity	Unit Cost	TOTAL Cost
		Figure	Unit #				
14.	Doppler Shift Unit	3.3	10	See Table 3.7	2	\$1,290	\$2,580
15.	Noise Source	3.3	11	Elgenco Inc. Model 3607A	1	40	40
16.	Timing and Book-keeping			See Table 3.8	1	2,100	2,100
TOTAL SIMULATOR HARDWARE COST							<u>\$49,460</u>

Table 3.5 Cost Breakdown for 0-512 μ sec Delay Line
(ref. Figure 3.3, Unit #5; Figure 3.9)

MODULE	REMARKS	QUANTITY	UNIT PRICE	TOTAL PRICE
Random Access Memories	Intel type 3102 256-bit	128	\$51.20	\$6,554
Input 64-bit Buffer	8-bit Registers	1	64	64
Output 64-bit Buffer	8-bit Registers	7	64	448
Hold Register	12-bit Registers	7	12	84
Overlay Register	12-bit Registers	7	12	84
Counting Register	12-bit Registers	1	12	12
RAM Address/Drivers	Intel type 3202	32	16.25	520
TOTAL				<u>\$7,766</u>

Table 3.6 Cost Breakdown for Fading Bandwidth Modulator (7 required)
(ref. Figure 3.3, Unit #7, and Figure 3.11)

MODULE	REMARKS	QUANTITY	UNIT PRICE	TOTAL PRICE
Gaussian Noise Generator	Elgenco 3602A-11154	2	\$ 30	\$ 60
Variable Bandwidth Filters	4-pole Butterworth	2	130	260
AGC	Including MC1959L	2	40	80
4-Quad Multiplier	Intronics (M510	2	280	560
TOTAL				<u>\$960</u>

Table 3.7 Cost Breakdown for Doppler Shift Unit (2 required)
(ref. Figure 3.3, Unit #10; Figure 3.5)

MODULE	REMARKS	QUANTITY	UNIT PRICE	TOTAL PRICE
4 MHz Oscillator	Greenray Model T-289	1	\$175	\$ 290
Band Pass Filter	Axel Electronics	1	125	125
3 MHz Low Pass Filter	5-pole Butterworth ($f_c = 3.4$ MHz)	1	50	50
Count-down Generator	17 stage Register	1	50	50
Variable Count-down Generator	17 stage Presetable Register	1	175	175
VCO	Greenray Type T-201B	1	400	400
Phase Detector	Includes loop filter	1	200	200
Mixers	Relcom Type M1	2	35	70
50 Hz Low Pass Filter	See Section III. C.3	1	50	50
TOTAL				<hr/> \$1,290

Table 3.8 Cost Breakdown for Timing and Bookkeeping Hardware

MODULE	REMARKS	QUANTITY	UNIT PRICE	TOTAL PRICE
Interface	Computer/Control Unit	1	\$800	\$ 800
512 μ sec Line	Includes D/A timing	1	800	800
30 msec Line	Includes D/A timing	1	300	300
System Clock	Greenray T-290	1	200	200
TOTAL				<u>\$2,100</u>

IV. CONCLUSIONS AND RECOMMENDATIONS

A preliminary design of a simulator for the propagation path between the Tracking and Data Relay Satellite (TDRS) and a user spacecraft has been established in this report. We have attempted to arrive at a valid and accurate representation of the actual propagation path characteristics.

The channel parameters which have been investigated include: attenuation, signal delay, differential delay, doppler, doppler spread, ionospheric effects, atmospheric effects, signal phase and amplitude, and interference and noise. It is not economically wise to fabricate a propagation channel simulator to model all the effects of the channel; therefore, the simulator design presented herein represents the results of a trade-off between the system fabrication cost and hardware complexity and the relative effects of the propagation path parameters on the channel. The simulator is designed to provide an accurate representation of essentially seven channel parameters, namely: 1) Free Space Attenuation, 2) Multipath Time Delay, 3) Direct Path Doppler, 4) Differential Doppler, 5) Fading Bandwidth, 6) System Noise Power Density, and 7) Radio Frequency Interference.

The general design arrived at in this report was based on the ease and flexibility with which the simulator parameters could be changed and the cost of implementation traded off against the accuracy to which parameters could be adjusted. Control of the simulator could be maintained by a mini-computer, or computer-generated tapes, or by manual insertion of specific values for channel parameters into the simulator control unit.

/

In general the simulator will operate with any class of input signal regardless of the type of modulation imposed upon it so long as the signal bandwidth is confined to 2 MHz. The simulator subsystem components require, at most, state-of-the-art hardware and as such, are essentially off-the-shelf items.

The estimated cost of hardware for the channel simulator is approximately \$50,000. This cost reflects only the component cost of one simulator system and not the costs associated with design engineering, quality assurance, and fabrication. It is estimated that to completely fabricate the system would require approximately a five man-year effort, distributed over a twelve or eighteen month period. The actual cost of developing such a simulation system requires a detailed set of specifications for the system. Specifications to this level of detail (i.e., to the circuit level) goes beyond the scope of this study effort. Magnavox is of the opinion that such a set of specifications be established prior to any attempt of physical circuit design on the simulator subsystems.